17

A thesis submitted to the University of Cape Town in complete fulfilment of the requirement for the degree Master of Science in Engineering.

The Effect of Welding on the Buckling Behaviour of Spherical Shells: A Review and Some Numerical Results

by

L Grünitz

Department of Civil Engineering

University of Cape Town

July 2001

Declaration

I, Lars Grünitz, hereby declare that this thesis is my own work and it has not been submitted for a degree at any other university.

signature removed

Lars Grünitz

July 2001

Acknowledgements

The bulk of the funding of my postgraduate studies came from a Rotary Foundation International Ambassadorial Scholarship. This scholarship has not only given me the chance to do postgraduate studies, it has furthermore given me the chance to experience another country and society.

I would like to thank the Rotary Club of Signal Hill and especially my counsellor David Lotz for their help and hospitality during my stay in South Africa.

I am deeply grateful to this organisation.

My supervisor, Prof. A Zingoni, was an invaluable source of advice, support and encouragement throughout my postgraduate studies.

I would like to thank Prof. N Marais for helping me editing my thesis.

The software used for the finite element analysis in this thesis was kindly sponsored by the MSC.Software GmbH.

Finally, I would like to express my profound appreciation for all the support from my parents over the past years.

Preface

Shell structures have a wide range of application in engineering construction. Examples include tank closures, roofs and marine structures. Due to the thinness typical of shell structures, buckling is often the governing failure mode.

Buckling analysis of shell structures provides a challenge for engineers. Research in the area of shell stability has been done for nearly one hundred years. Cases where close-form solutions are available are limited to rather simple problems.

Today, the finite element method (FEM) is widely used to determine the critical buckling load. The main problem associated with the use of the FEM is to find an appropriate initial imperfection for this type of analysis in order to obtain a good estimate of the real buckling strength of the structure.

Shell structures made out of steel are frequently constructed by joining curved plates together. Due to the fabrication process, imperfections occur, and these have a significant influence on the buckling behaviour of the shell structure. Welding causes a systematic imperfection due to the shrinkage of the weld during the cooling process. Past research on this effect has investigated cylindrical shell structures under axial loading and conical shell structures under hydrostatic loading.

The purpose of this thesis is to give first a brief review in the area of shell stability with special focus on the effect of imperfections due to the welding process on the buckling behaviour of shell structures. The finite element method is then reviewed with special attention to linear and nonlinear buckling analysis with the finite element method. Finally, the finite element method is used to investigate the effect of a circumferential weld depression on the buckling behaviour of a clamped and hinged spherical cap.

The thesis that has been undertaken consists of the following chapters.

Chapter 1 gives a literature review of the development in the field of shell stability analysis with a special focus on spherical shell structures. Different imperfection shapes due to the manufacturing process and their influence on the buckling behaviour of shell structures are reviewed.

Chapter 2 gives a brief introduction of linear and nonlinear finite element analysis. Special attention is given to the analysis of shell structures with finite element methods. An overview of different types of shell elements is given.

Chapter 3 discusses the analysis of shell stability with the finite element method. Linear (bifurcation) and nonlinear buckling analysis with finite element methods are described and discussed.

A bifurcation analysis with finite element methods of a hinged and clamped spherical shell is carried out in Chapter 4 and the results are compared to the theoretical solution described in Chapter 1.

The effect of a circumferential weld on the buckling behaviour of a hinged and clamped spherical cap is investigated in Chapter 5. A nonlinear finite element analysis is carried out. The modelling of the weld with finite elements is described in detail.

Conclusions and recommendations for further investigation are given in Chapter 6.

Table of Contents

Declaration i

Acknowledgements ii

Preface iii

Table of Contents v

List of Figures viii

Glossary of Symbols x

1 Background and Literature Review

1.1. Introduction 1

1.2. Background, Shell Definition and Thinness Criteria 2

1.3. Buckling of Shell Structures 4

1.3.1. Introduction 4

1.3.2. General Considerations on Buckling 5

1.3.3. Classical Buckling Theory 5

1.3.3.1. The Energy Method 6

1.3.3.2. The Method of Adjacent Equilibrium 7

1.3.4. Linear Buckling of a Spherical Shell Subjected to Radial Uniform Pressure 8

1.3.5. Nonlinear Buckling Theory 15

1.3.5.1. Introduction 15

1.3.5.2. Nonlinear Buckling Theory of Spherical Shells 15

1.4. Buckling of a Spherical Cap 20

1.4.1. Introduction 20

1.4.2. Linear Buckling of a Spherical Cap Subjected to Radial Uniform Pressure 21

1.4.3. Nonlinear Buckling of a Spherical Cap Subjected To Radial Uniform Pressure 22

1.5. Imperfections of Shell Structures 27
1.5.1. Introduction 27
1.5.2. Geometrical Imperfections 28
1.5.3. Previous Studies in Imperfections 29
1.5.3.1. Previous Studies on Imperfections of Spherical Shells 31
1.5.4. Imperfections Due to The Welding Process 32
1.5.4.1. Effect of Welding on the Buckling Behaviour of Shell Structures 34
1.5.5. Methods for The Measurement of Imperfections 37

2 Finite Element Analysis

2.1. Introduction 38
2.2. Linear Static Analysis with FEM 41
2.3. Nonlinear Static Analysis with FEM 46
2.3.1. Introduction 46
2.3.2. Formulation Methods 47
2.3.2.1. The Material Description 47
2.3.2.2. The Referential Description 47
2.3.2.3. The Spatial Description 49
2.3.2.4. The Relative Description 49
2.3.3. Solution Schemes for Nonlinear Static Analysis with FEM 50
2.3.3.1. Introduction 50
2.3.3.2. Conventional and Modified Newton-Raphson Method 50
2.3.3.3. Arc Length Method 53
2.4. Finite Element Analysis of Shell Structures 57
2.4.1. Introduction 57
2.4.2. The Axisymmetric Shell Element 59

3 Buckling Analysis with Finite Element Methods

3.1. Introduction 67

3.2. Eigenvalue Buckling with FEM 67
3.3. Nonlinear Buckling with FEM 70
3.4. Comparison of Linear and Nonlinear Buckling With FEM 71

4 Bifurcation Analysis of a Spherical Cap
4.1. Introduction 72
4.2. Description of the Geometry and Loading 72
4.3. Discretization with FEM and Solution 73
4.4. Results 74
4.4.1. Clamped Spherical Cap 74
4.4.2. Hinged Spherical Cap 75
4.5. Conclusions 76

5 Effect of a Circumferential Weld on the Buckling Behaviour of a Spherical Cap
5.1. Introduction 77
5.2. Description of Geometry and Loading 77
5.2.1. Description of the Circumferential Weld 78
5.3. Discretization with FEM 80
5.4. Solution Procedure with FEM 83
5.5. Results 84
5.4.1. Clamped Spherical Cap 85
5.4.2. Hinged Spherical Cap 88
5.4.3. Comparison of Clamped and Hinged Spherical Cap 92
5.5.4. Discussion of Results 93

6 Conclusion and Recommendations for Further Investigation 94
List of References R1
Appendix A A1
Appendix B B1

List of Figures

1.1	Comparison beam, plate and shell structure	4
1.2	Bifurcation phenomenon	5
1.3	Variation of λ^2	6
1.4	Spherical shell	8
1.5	Shallow shell theory	8
1.6	Reticulated pattern	13
1.7	Spherical cap	17
1.8	Membrane theory support	18
1.9	Clamped spherical cap	19
1.10	Hinged spherical cap	19
1.11	Snapping load of the perfect spherical cap	20
1.12	Change in slope of the bending and buckling deformation	21
1.13	Critical load pertaining to asymmetric buckling (clamped cap)	22
1.14	Critical load pertaining to asymmetric buckling (hinged cap)	23
1.15	Rolling process	25
1.16	Shrinkage of the weld due to cooling	32
1.17	Schematic residual stress distribution during welding process	33
1.18	Radial weld depression	34
1.19	Idealized weld depression according to Rotter and Teng	35
2.1	Sample discretization of a 2D area	39
2.2	Part of a finite element mesh	39
2.3	Geometry of motion	48
2.4	Conventional Newton-Raphson method	52
2.5	Modified Newton-Raphson method	52
2.6	Arc Length solution algorithm	56
2.7	Axisymmetric shell element	59
2.8	Local coordinate system of the element	60
2.9	Membrane strain components	61
2.10	Bending strain component	62

4.1	Geometry of the investigated spherical cap	72
4.2	Axisymmetric model of the spherical cap	73
4.3	Clamped cap, eigenmode 2, critical pressure 0.08775 N/mm	74
4.4	Hinged cap, eigenmode 1, critical pressure 0.08751 N/mm²	75
5.1	Geometry of the investigated spherical cap	77
5.2	Location of the circumferential weld	78
5.3	Microstructure of normal steel	79
5.4	Microstructure of the weld	79
5.5	Change welded material – heat influence zone	80
5.6	Change heat influence zone – normal material	80
5.7	Measurement of $l_{heatinfl.}$	81
5.8	Axisymmetric model of the spherical cap with loading	82
5.9	Assumed imperfection shape after solution step	83
5.10	Buckling deformation for β =10° (clamped cap)	85
5.11	Buckling deformation for β =15° (clamped cap)	86
5.12	Buckling deformation for β =20° (clamped cap)	87
5.13	Buckling deformation for β =10° (hinged cap)	88
5.14	Post-buckling deformation of the hinged cap	89
5.15	Buckling deformation for β =15° (hinged cap)	90
5.16	Buckling deformation for β =20° (hinged cap)	91
5.17	Comparison of the results for different edge conditions	92

Glossary of Symbols

Symbol	Description
$\{a\}$	displacement vector
$\{\overline{a}\}_i^k, \{u\}$	nodal displacement vector
A	area
$B = \frac{Et^3}{12(1-\upsilon^2)}$	bending stiffness of the shell
$\{b\}$	body force vector
$[B]$	strain-displacement matrix
$[D]$	material matrix
E	Young's modulus
$\{f\}$	internal force vector
F	stress function
H	height of the cap
$[K]$	stiffness matrix
$[K]_t$	tangent stiffness matrix
L	diameter at the base of the cap
$N_k(x,y,x)$	displacement shape function
n_{xy}, n_x, n_y	membrane force
p_i	incremental load
p_{cr}	critical buckling pressure
$\{p_c\}$	concentrated force vector
$\{p\}$	load vector
P_r, P_Z, M	local load components
R	radius of the shell, cap
$\{r\}$	reference load
r, z	local coordinates
$[S]$	stress matrix

$T = \frac{Et}{1-\upsilon^2}$	tensile stiffness of the shell
t	shell thickness, time
$\{t\}$	surface traction vector
U	strain energy
$\overline{\{u\}}^c$	displacement vector to concentrated forces $\{p_c\}$
$\underline{u}$, $\underline{w}$	global displacement components
V	potential energy of the applied loads, Volume
x, y, z	Cartesian co-ordinates
Δa	variation of a
$\delta\{a\}$	virtual displacement vector
$\{\varepsilon\}$	strain tensor
φ	meridial angle
λ	variation factor, load factor
υ	Poisson's ratio
$\{\sigma\}$	stress tensor
σ_0	pre-stress
$\sigma_{y,c}$	characteristic yield stress
τ	time variable
ξ	shape function

Chapter 1
Literature Review

1.1. Introduction

Shell structures find wide applications in many different branches of engineering. Examples include cooling tower, steel silos, roofs, pressure vessels and steel tanks [Flügge (1973), Calladine (1983), Zingoni (1997)].

Most shell structures are thin. Hence buckling is often the controlling failure mode. Shell structures often have a complex post-buckling behaviour. It is therefore important that their buckling behaviour is properly understood.

Shell structures made out of steel are frequently constructed by welding curved plates together. This welding constitutes an imperfection in the otherwise smooth surface of the shell, and attracts additional stresses, which greatly influences the buckling behaviour of the shell structure. Investigations on the effect of welding on the buckling behaviour of shell structures has so far only been done on cylindrical and conical shells and research in this area is still ongoing.

As exact analytical solutions for buckling problems are limited to rather simple cases, numerical methods (e.g. the finite element method) are generally adopted.

1.2. Background, Shell Definition and Thinness Criteria

Shell structures have a wide range of applications in engineering. For example, Architecture and Building. The construction of domes for temples, cathedrals and other buildings were the earliest form of shell structures. Historical examples include the Pantheon of ancient Rome, built around 2000 years ago, and the Hagia Sophia of Constantinople, which is approximately 1500 years old [Zingoni (1997)].

Many objects were constructed long before there were any theoretical investigations on shell structures. The early engineers built small-scale models and did overload tests. From these investigations they could see the advantage of shell constructions is their high strength-to-weight ratio.

Shell structures have been theoretically studied for more than one hundred years. Starting with Aron (1874) and Love (1888) [Timoshenko (1953)].

The essential geometric property of shell structures that distinguishes them from other structural forms is the possession of both *surface* and *curvature* [e.g. Calladine (1983)]. This combination gives shell structures their characteristic strength and stiffness.

A shell may be considered as a relatively thin structural element in which the material of the element is bound between two curved surfaces, which are a relatively small distance apart. The behaviour of a shell structure is usually modelled on the basis of its middle surface, which is the locus of interior points equidistant from the two bounded surfaces of the shell.

The theory for the analysis of shell structures is divided into two sections; *thin-shell theory* and *thick-shell theory*. The criteria which classifies a particular shell structure as either thin shell or thick shell is its t/r-ratio, where t is the thickness of the shell and r the minimum radius of curvature of the middle surface of the shell. The cut-off point between thin and thick shell varies in literature between $t/r=1/10$ [Goldberg *et al.* (1974)] and $t/r=1/30$ [Vlasow (1944)].

Most of the shell structures in practical applications have a t/r -ratio between 1/2000 and 1/50 and can therefore be regarded as thin shells. Hence buckling is often the controlling failure mode.

In this chapter a literature review of the development in the stability analysis of shell structures, with a special focus on spherical shells and the influence of imperfections due to the manufacturing process, is given.

1.3. Buckling of Shell Structures

1.3.1. Introduction

Compared to the postbuckling behaviour of beams and plates, most shell structures have a "bad" post-buckling behaviour. "Bad" post-buckling behaviour implies that shell structures collapse totally if the critical load is reached (Figure 1.1). Hence it is necessary to determine the critical buckling load.

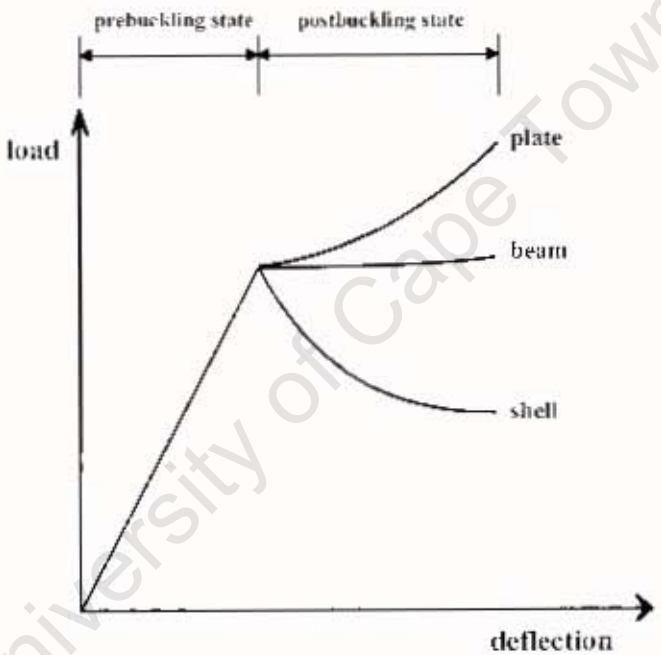

Fig. 1.1: Comparison beam, plate and shell structure

The first shell buckling problem solved was a cylindrical shell under axial loading [Lorenz (1908)]. Robertson (1929), Flügge (1932) and Lundquist (1933) did tests on the buckling behaviour of cylindrical shells. They found that the real buckling loads of cylinders, under axial load, are much lower than the classical buckling loads. Experimental buckling loads as low as 30 % of the classical load are not uncommon.

The investigation of factors (e.g. imperfections, plasticity) responsible for this discrepancy between the theoretical and the experimental buckling load led to an enormous amount of research into shell buckling during the later part of the 20th century.

1.3.2. General Considerations on Buckling

The objective of a buckling analysis is to estimate the maximum load that a structure can support in compression before it becomes unstable or before it collapses.

There are two different types of buckling analysis:

- classical (linear) buckling analysis
- nonlinear buckling analysis

1.3.3. Classical Buckling Theory

Classical buckling analysis is also known as "bifurcation" analysis. It calculates the load under which the structure's primary load deflection path, which is a straight line for linear-elastic static analysis, is bifurcated by a secondary load deflection path (Figure 1.2).

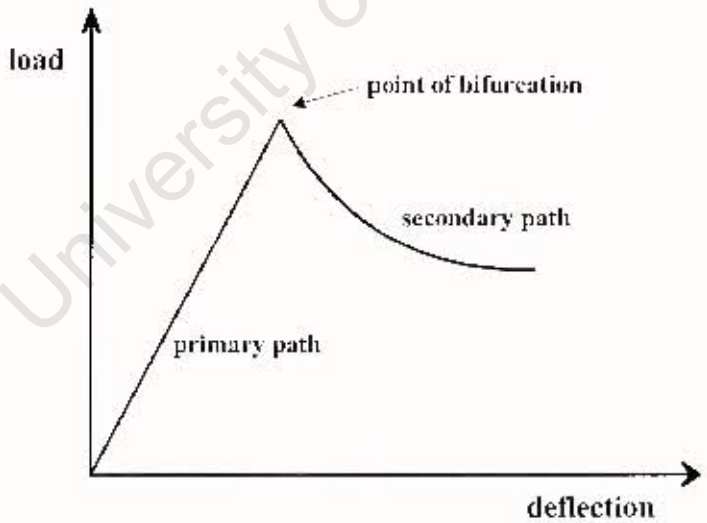

Fig. 1.2: Bifurcation phenomenon

Within the classical buckling theory, there are two different ways to find out whether the structure is stable or not [e.g. Flügge (1973)]:

- the energy method
- the method of adjacent equilibrium

1.3.3.1. The Energy Method

A structure is loaded and has therefore a basic deformation and a basic stress system. Then an additional small deformation is applied which results in additional strain and therefore with additional stress in the structure. For applying an additional deformation energy is needed. This energy can be divided into two parts:

- the work that must be done against the external force
- increase in strain energy due to additional strain

The additional deformation function is varied by multiplying it with a factor (e.g. λ) . Then the variation of the potential energy $\Delta\Pi$ is written as a power series in terms of this factor. The linear term must always be zero because of the "principle of virtual displacement". Otherwise the stress and the strain would not be in equilibrium.

The next term of the power series is the quadratic term (λ^2). This term of the variation of the potential energy is always positive, if the basic load is small enough. Only additional force, which can do work can then supply the required energy. Hence no other deviation can occur. The structure is **stable**. If the critical basic load is reached, the term is vanishing and displacements can occur spontaneously. The structure is **indifferent** (neutral stability). If the load is increased beyond the critical load, the term is negative. Energy will be set free as kinetic energy. The structure is **unstable**.

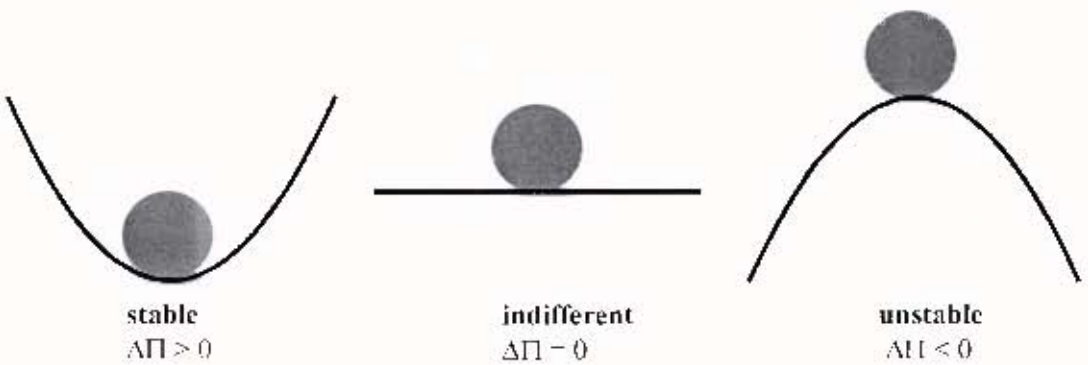

Fig. 1.3: Variation of λ^2

1.3.3.2. The Method of Adjacent Equilibrium

Applying the method of adjacent equilibrium starts with the same initial conditions as applying the energy method: the structure is loaded and has therefore a basic stress system and a basic deformation.

The elastic equilibrium is then again disturbed by a small deformation. A force is needed to produce this deformation. If the additional force is removed and the deformation produced by this force diminishes, the structure is **stable**.

If the additional deformation produced by the additional force remains the same after removing the additional force, then the structure is **indifferent**.

If the deformation increases without applying additional force, then the structure is **unstable**.

The elastic equilibrium always remains stable if the basic load is small enough [v. Mises (1923)]. The smallest value with which the equilibrium stays stable is called the *critical buckling load*.

In order to find the critical buckling load, the differential equations are formulated for the disturbed equilibrium without a disturbing load. The differential equations contain also the terms for the undisturbed equilibrium and the terms with the additional stress due to disturbed shell structure. The applied disturbance is infinitesimal small, hence the additional terms are small. Additional terms result from the fact that the basic forces are now acting on a deformed system. Both groups of additional terms are proportional to the disturbance. These terms must add up to zero since the condition of the equilibrium is satisfied without these terms. The buckling problem can now be described as a set of *homogeneous linear* differential equations, since Hooke's law expresses a linear relationship between the stress and the displacement. These homogeneous linear differential equations can be solved by finding the *eigenvalues* of these equations. Therefore the classical buckling theory is often called *eigenvalue buckling* theory.

1.3.4. Linear Buckling of a Spherical Shell Subjected to Radial Uniform Pressure

The buckling problem of a complete spherical shell (Figure 1.4) was first solved by Zoelly (1915). He used the exact equations [e.g. Flügge (1973)] and did not make use of the *shallowness* [Marguerre (1938)] of the shell.

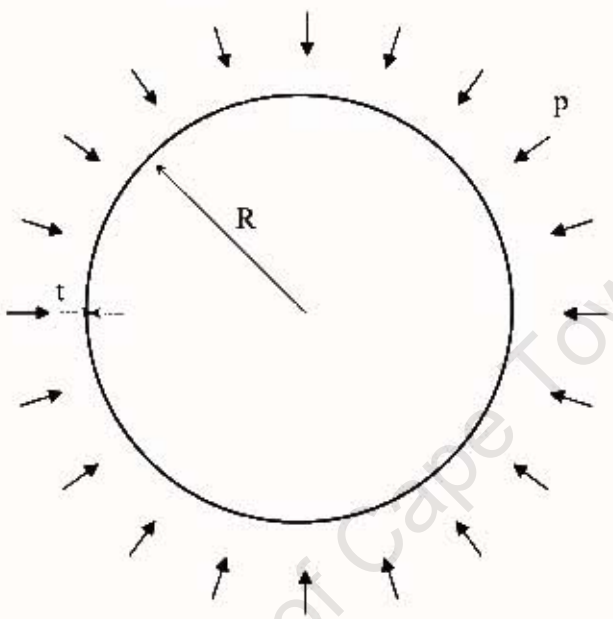

Fig. 1.4: Spherical shell

Even if a spherical shell cannot be regarded as a classical shallow shell (e.g. in the case of a complete shell), the shallow-shell theory can still be applied. A spherical shell may be defined as shallow if the ratio of the rise H to the diameter D is less than 1/5 [Zingoni (1997)].

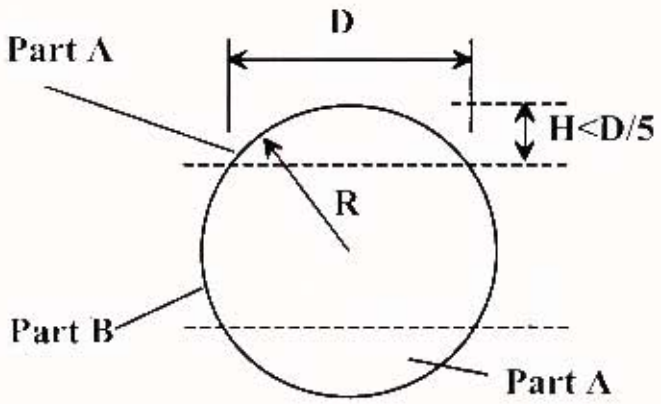

Fig. 1.5: Shallow shell theory

The complete spherical shell can be divided into two shallow caps (Parts A) and a non-shallow frustum (Part B) as shown in Figure 1.5. Assuming that only the shallow parts buckle while the non-shallow part remains stable, then shallow-shell theory can be applied.

Using the shallow shell theory, the critical buckling load can be calculated as follows [Kollár and Dulácska (1984)]:

The equilibrium and compatibility equations of a general shallow shell in the x,y,z- Cartesian coordinate system are [Wlassow (1958)]:

$$B\Delta\Delta w - L_p F = p \qquad (1.1)$$

$$\Delta\Delta F + T(1-\upsilon^2)L_p w = 0 \qquad (1.2)$$

with:

$$\Delta = \frac{\partial^2}{\partial x^2} + \frac{\partial^2}{\partial y^2}$$

and the *Laplace and Pucher* differential operator:

$$L_p = \frac{\partial^2 z}{\partial y^2}\frac{\partial^2}{\partial x^2} - 2\frac{\partial^2 z}{\partial x \partial y}\frac{\partial^2}{\partial x \partial y} - \frac{\partial^2 z}{\partial x^2}\frac{\partial^2}{\partial y^2}$$

where:

w = buckling deformation perpendicular to the shell surface

F = stress function

$B = \frac{Et^3}{12(1-\upsilon^2)}$ = bending stiffness of the shell

$T = \frac{Et}{1-\upsilon^2}$ = tensile stiffness of the shell

E = Young's modulus

υ = Poisson's ratio

t = shell thickness

p = uniform pressure

The membrane forces are the second derivatives of the stress function F:

$$\frac{\partial^2 F}{\partial y^2} = n_x \tag{1.3}$$

$$\frac{\partial^2 F}{\partial x^2} = n_y \tag{1.4}$$

$$\frac{\partial^2 F}{\partial x \partial y} = -n_{xy} \tag{1.5}$$

In the case of a spherical shell with the z-axis pointing toward the center of the spherical shell, the membrane forces of the pre-buckling state are [Pflüger (1981)]:

$$n_{xy} = 0 \tag{1.6}$$

$$n_x = n_y = -\frac{pR}{2} \tag{1.7}$$

where:

p = radial uniform pressure

R = radius of the shell (Figure 1.4)

Eliminating F from equations (1.1) and (1.2) leads to the following equation:

$$B\Lambda^4 w + T(1-\upsilon^2)L_p^2 w = \Lambda p_i^2 \tag{1.8}$$

where:

p_i = incremental load arising during buckling perpendicular to the shell surface

In the case of a spherical shell:

$$\frac{\partial^2 z}{\partial x^2} = \frac{\partial^2 z}{\partial y^2} = \frac{1}{R} \tag{1.9}$$

$$\frac{\partial^2 z}{\partial x \partial y} = 0 \tag{1.10}$$

hence:

$$L_n = \frac{1}{R}\left(\frac{\partial^2}{\partial x^2} + \frac{\partial^2}{\partial y^2}\right) = \frac{1}{R}\Delta \tag{1.11}$$

The incremental load p_i arising during buckling is the product of the change in curvature Δw and the internal force (1.7):

$$p_i = -\frac{pR}{2}\left(\frac{\partial^2 w}{\partial x^2} + \frac{\partial^2 w}{\partial y^2}\right) = -\frac{pR}{2}\Delta w \tag{1.12}$$

Substituting all expressions into equation (1.8) gives the following expression:

$$B\Delta^4 w - \frac{T(1-\upsilon^2)}{R^2}\Delta^2 w = -\frac{pR}{2}\Delta^3 w \tag{1.13}$$

Assuming for a simple reticulated pattern for w as shown in Figure 1.6

$$w = w_1 \sin\frac{\pi}{l_x} x \sin\frac{\pi}{l_y} y \tag{1.14}$$

where l_x and l_y are half of the wavelength in the x and y direction respectively, the equation for the critical pressure p_{cr} is obtained as follows:

$$p_{cr}\frac{R}{2} = B\pi^2 C + \frac{T(1-\upsilon^2)}{R^2\pi^2 C} \tag{1.15}$$

where: $C = \left(\frac{1}{l_x^2} + \frac{1}{l_y^2}\right)$

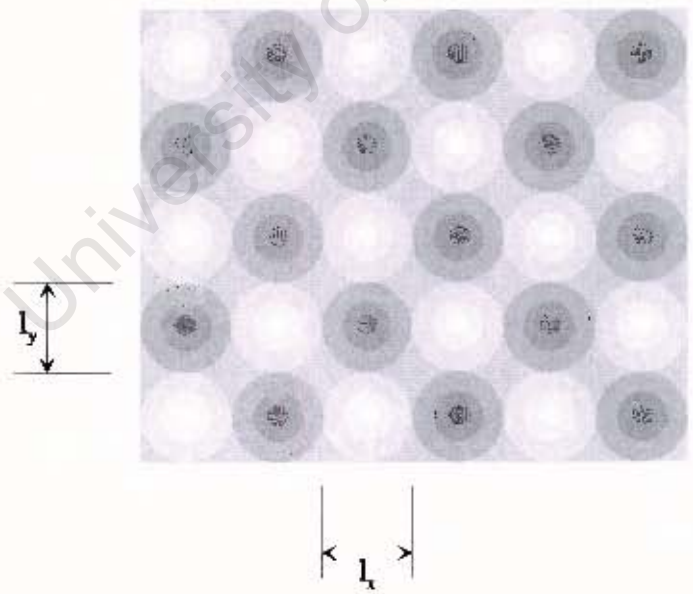

Fig. 1.6: Reticulated pattern

Differentiating p_{cr} with respect to C and equating the derivation to zero results in:

$$C = \frac{1}{\pi^2}\sqrt{\frac{T(1-\upsilon^2)}{BR^2}} \tag{1.16}$$

The buckling shape is **indeterminate** since the equation (1.16) is not dependant on the assumed pattern w. This buckling behaviour is similar to that of a cylindrical shell under axial load and is called *compound-buckling* or *multi-mode buckling* behaviour.

Substituting equation (1.16) into (1.15) gives the well-known expression the linear critical buckling pressure p_{cr} of an entire spherical shell:

$$p_{cr}^{lin} = \frac{2}{\sqrt{3(1-\upsilon^2)}} E\frac{t^2}{R^2} \tag{1.17}$$

Assuming an asymmetric buckling pattern leads to the same result [van der Neut (1932)].

1.3.5. Nonlinear Buckling Theory

1.3.5.1. Introduction

Experiments on the buckling behaviour of spherical shells have shown lower loads for the critical buckling load compared to the classical buckling theory. Krenz and Kiernan (1963) have investigated "near-perfect" spherical shells and found a critical buckling of 80% - 86% of the linear buckling load. To explain this discrepancy between the linear and experimental critical buckling load the nonlinear buckling theory was developed.

1.3.5.2. Nonlinear Buckling Theory of Spherical Shells

The nonlinear buckling theory takes *large deformations* into account. The method is based on the *energy method* described in 1.3.3.1.. It is possible to describe the buckling process from the undeformed state up to several of the shell thickness by taking also the second powers of the first derivation of the displacement w, perpendicular to the shell surface into account.

This calculation for a complete spherical shell was first performed by Kármán and Tsien (1939). They assumed the shape of the buckling pattern, characterising its extension by a free parameter, with respect to which they minimised the load at every loading step. The lowest point of the post-critical load-displacement curve for a complete spherical shell was found to be:

$$p_{cr}^{lower} = 0.365E\frac{t^2}{R^2} \quad \text{for } \upsilon = 0 \qquad (1.18)$$

This is 0.31 times the linear critical buckling load described in 1.3.4..

Later Tsien (1941) improved the accuracy of the calculation by refining the solution procedure and found:

$$p_{cr}^{lower} = 0.312E\frac{t^2}{R^2} \qquad \text{for } \upsilon = 0 \tag{1.19}$$

which is 0.27 times the linear critical buckling load.

A more general theory for nonlinear buckling of shell structures was given by Koiter (1945, 1963). He applied a variational principle of potential energy to obtain equations characterising equilibrium in the prebuckling and initial postbuckling regimes of a shell structure with a multiplicity of buckling modes associated with the critical buckling load. These equations are in the form of simultaneous nonlinear, algebraic equations relating the magnitude of the externally applied load to the deflections in the various buckling modes. The magnitude of assumed geometrical imperfections also appear.

Koiter's theory for multimode buckling can be formulated as follows:

Generalised stress, strain and displacement fields are denoted by σ, ε and u respectively. The magnitude of the applied load system is taken to be directly proportional to the load parameter λ.

The potential energy expression for the structure is conveniently written in the compact form

$$\Pi = \frac{1}{2}\{\sigma', \varepsilon''\} - \lambda B_1(u) \tag{1.20}$$

where the stresses and strains are calculated form the kinematically admissible displacement field u. Here $\{\sigma', \varepsilon''\}$ donates the internal virtual work of the stress field σ'

trough the strain field ε^* and $\lambda B_1(u)$ is the work of the applied force field of intensity λ through a displacement u of the structure.

Considering only structures which can be adequately described by nonlinear strain-displacement relations of the form

$$\varepsilon = L_1(u) + \frac{1}{2} L_2(u) \tag{1.21}$$

where L_1 and L_2 are homogeneous functions which are linear and quadratic, respectively, in u. The stress-strain relations are assumed to be linear and are written symbolically as

$$\sigma = H_1(\varepsilon) \tag{1.22}$$

where H_1 is a linear, homogeneous function of the strain components.

An initial deviation $\bar{u}$ of the unloaded structure from the perfect form is called the *initial imperfection*. In the presence of such imperfection, the strain arising from an additional displacement u is

$$\varepsilon = L_1(u) + \frac{1}{2} L_2(u) + L_{11}(u, \bar{u}) \tag{1.23}$$

where $L_{11}(u, \bar{u}) = L_{11}(\bar{u}, u)$ is the bilinear, homogeneous function of u and u which appears in the identity $L_2(u + \bar{u}) = L_2(u) + 2L_{11}(u, \bar{u}) + L_2(\bar{u})$.

It is assumed that there are several linearly dependent buckling modes $u_c^{(1)}, u_c^{(2)}, \ldots, u_c^{(s)}$ associated with the critical value of the load parameter λ_c. The complete displacement of the structure is written quite generally as

$$u = \lambda u_c - \sum_s \xi_s u_c^{(s)} + \bar{u} \tag{1.24}$$

where λu_c is the prebuckling displacement of the perfect structure subject to the external load intensity corresponding to λ. For the spherical shell under radial uniform pressure, this is just a uniform radial displacement. Each of the modes $u_c^{(i)}$ is taken orthogonal to one another and each is orthogonal to $\tilde{u}$.

The orthogonality condition is

$$\left\{\sigma_0, L_{11}\left(u_c^{(i)}, u_c^{(j)}\right)\right\} = 0 \qquad i \neq j \tag{1.25}$$

where $\sigma_0 = H_2\left[I_1\left(u_0\right)\right]$. Imperfections in the form of the buckling mode may result in significant reduction of the buckling strength of the structure; thus

$$\bar{u} = \sum_n \bar{\xi}_n u_c^{(n)} \tag{1.26}$$

is taken as initial imperfection.

Now, the potential energy is evaluated using the expressions for u and $\bar{u}$ with equation (1.22) to (1.24) and the orthogonality conditions (1.25). The result is:

$$\begin{aligned}\Pi = const + \frac{1}{2}(\lambda \quad \lambda_c)\sum \xi_i^2 \left\{\sigma_0, L_2\left(u_c^{(n)}\right)\right\} \\ + \frac{1}{2}\left\{\sum \xi_i s_c^{(i)}, L_2\left(\sum \xi_i u_c^{(i)}\right)\right\} + \sum \xi_i \bar{\xi}_i \lambda \left\{\sigma_0, L_2\left(u_c^{(i)}\right)\right\} \\ - \text{terms of order } \xi^2, \xi\bar{\xi}^2, \ldots\end{aligned} \tag{1.27}$$

where $s_c^{(i)} = H_1\left[I_1\left(u_c^{(i)}\right)\right]$. Only terms up to and including the third powers of the ξ and imperfection terms such as $\xi\bar{\xi}$ are displayed. This expression for a "quadratic structure" is given by Koiter (1963). It is noted that $\tilde{u}$ does not appear in the formulation of the potential energy since it contributes to quadratic but not cubic terms in ξ.

The potential energy formulation in the truncated form given here can provide an accurate description of the structure's response only so long as the ξ_i and imperfections $\overline{\xi}_i$ are sufficiently small to ensure that the terms neglected are small compared to those retained.

Equilibrium equations relating to the ξ_i to the load parameter λ are obtained from the requirement that the first variations of the potential energy with respect to the ξ_i vanish.

The resulting equations are

$$\xi_i\left(1-\frac{\lambda}{\lambda_c}\right)+\frac{\left\{\sum^{*}\xi_r s_c^{(s)}, L_1\left(\sum \xi_n u_c^{(n)}, u_c^{(t)}\right)\right\}+\frac{1}{2}\left\{s_c^{(t)}, L_2\left(\sum \xi_n u_c^{(n)}\right)\right\}}{-\lambda_c\left\{\sigma_0, L_2\left(u_c^{(t)}\right)\right\}}$$

$$\left(\frac{\lambda}{\lambda_c}\right)\overline{\xi}_i \qquad \text{for } i=1,2,3,\ldots \tag{1.28}$$

Finally, the generalised load-deflection relation for a perfect multimode structure can be obtained from general theory:

$$\frac{B_i(u)}{B_i(u_{0,c})}=\frac{\lambda}{\lambda_c}-\frac{1}{2}\sum_r \xi_r^{\,2}\,\frac{\lambda_c\left\{\sigma_r, L_2\left(u_c^{(rr)}\right)\right\}}{\lambda_c^{\,2}\left\{\sigma_0, L_1\left(u_0\right)\right\}} \tag{1.29}$$

where, from equation (1.20), $B_i(u)$ represents the generalised displacement through which the external loading system acts, and where $u_{0,c}=\lambda_c u_0$.

1.4. Buckling of a Spherical Cap

1.4.1. Introduction

Spherical caps have a wide range of applications in engineering. Examples include roofs, tank closures, pressure vessels and submarine structures. The geometry of a spherical cap is described as a part of a full sphere (Figure 1.7).

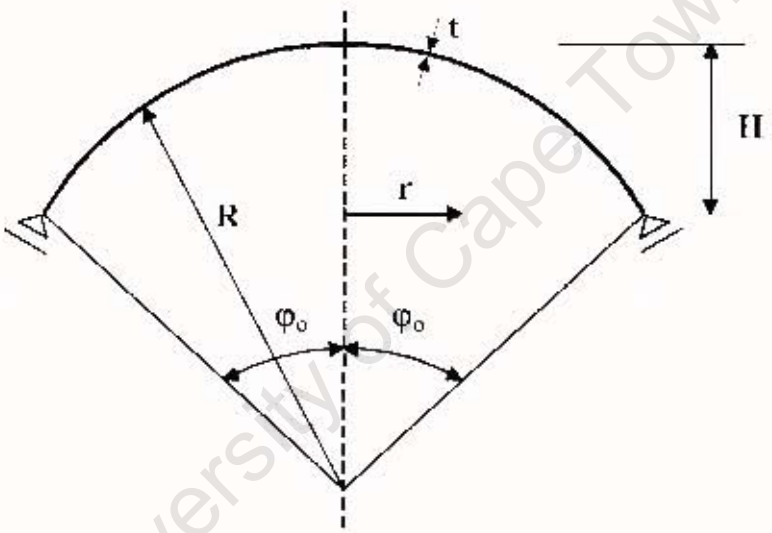

Fig. 1.7: Spherical cap

With H being the height, R the radius, r the base radius, t the thickness of the spherical cap and φ_o is the value of the meridial angle φ at the edge.

1.4.2. Linear Buckling of a Spherical Cap Subjected to Radial Uniform Pressure

The buckling behaviour of a spherical cap depends on the boundary conditions of its edge. Considering a cap which is supported in accordance to the *membrane theory* (Figure 1.7 and 1.8) the shell can only undergo compression without bending.

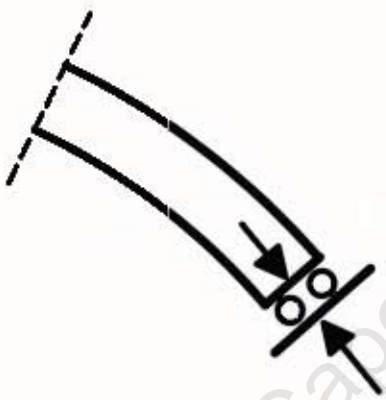

Fig. 1.8: Membrane theory support

The shell behaves like a full spherical shell (see 1.3.4.). In this case, the linear critical buckling load is:

$$P_{cr,cap}^{lin} = \frac{2}{\sqrt{3(1-\upsilon^2)}} E \frac{t^2}{R^2} \qquad (1.30)$$

R = radius of the cap (Figure 1.7)

t – shell thickness

1.4.3. Nonlinear Buckling of a Spherical Cap Subjected to Radial Uniform Pressure

In engineering applications, it is usually impractical to provide a membrane-theory compliant support. Most caps have either hinged or clamped edges. If the edge of the cap is clamped (Figure 1.9) or hinged (Figure 1.10) the shell undergoes bending deformation before buckling, even if the shell is perfect.

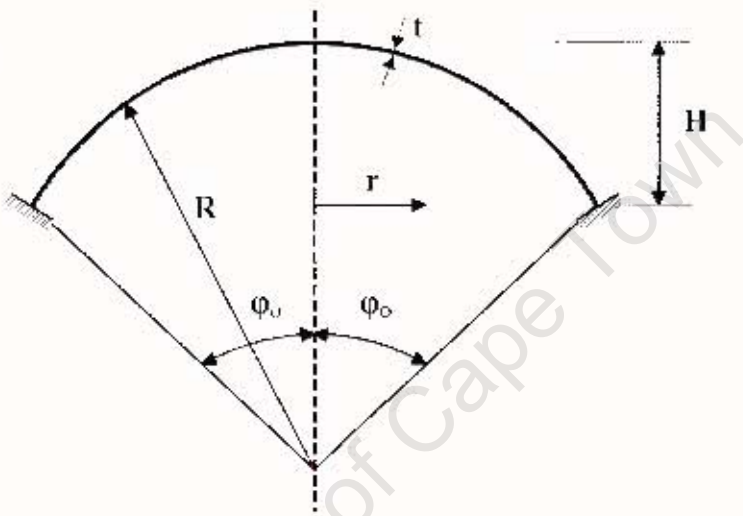

Fig. 1.9: Clamped spherical cap

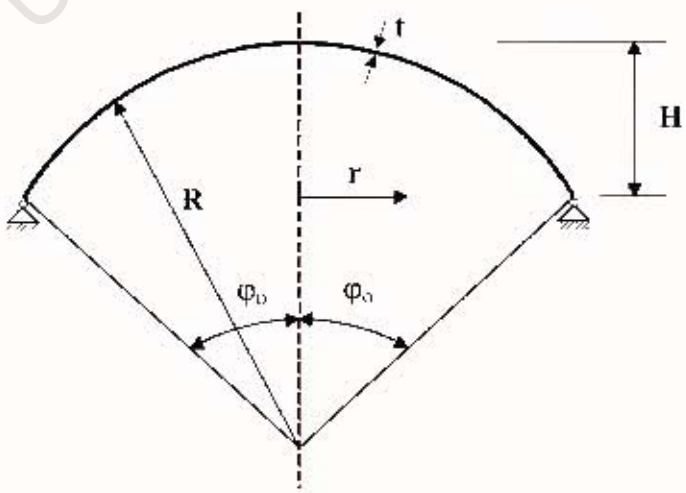

Fig. 1.10: Hinged spherical cap

In some cases the bending deformation has the same character as the buckling deformation. Hence the shell buckles at a lower critical buckling load compared to the linear critical buckling load. In other cases the bending deformation is opposite to the buckling deformation. Hence the shell buckles at a higher critical buckling load compared to the linear critical buckling load (Figure 1.11 and 1.12).

The behaviour depends on the following expression [Kollár and Dulácska (1984)]:

$$\lambda = 2\sqrt[4]{3(1-\nu^2)}\sqrt{\frac{H}{t}} \qquad (1.31)$$

with:

H = height of the cap (Figure 1.7)

Plotting the snapping load of the perfect spherical cap based on the numerical results from Thurston (1961) against the parameter λ leads to the following graph:

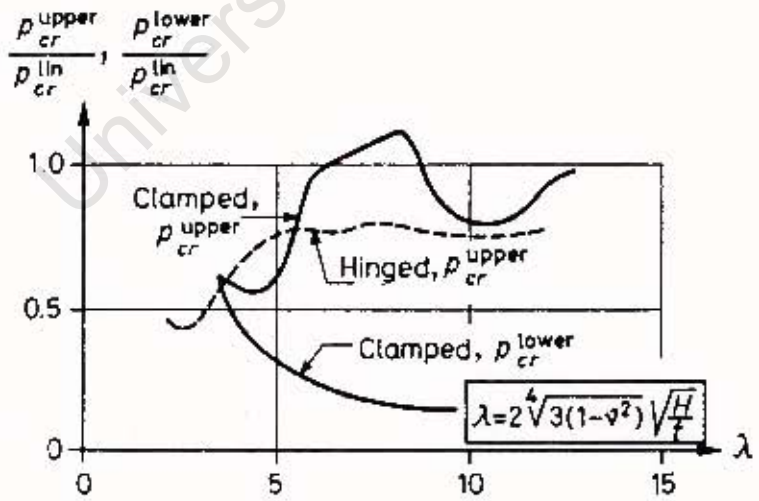

Fig. 1.11: Snapping load of the perfect spherical cap [Kollár and Dulácska (1984)]

The curve of p_{cr}^{upper} for the clamped cap is oscillating. The curve is lower then 1 when the bending deformation and the buckling deformation have the same character. If the bending

deformation and the buckling deformation have opposite characters the curve can be higher than 1. The curve for the hinged cap lies lower than 1, but shows the same characteristics (Figure 1.11 and 1.12).

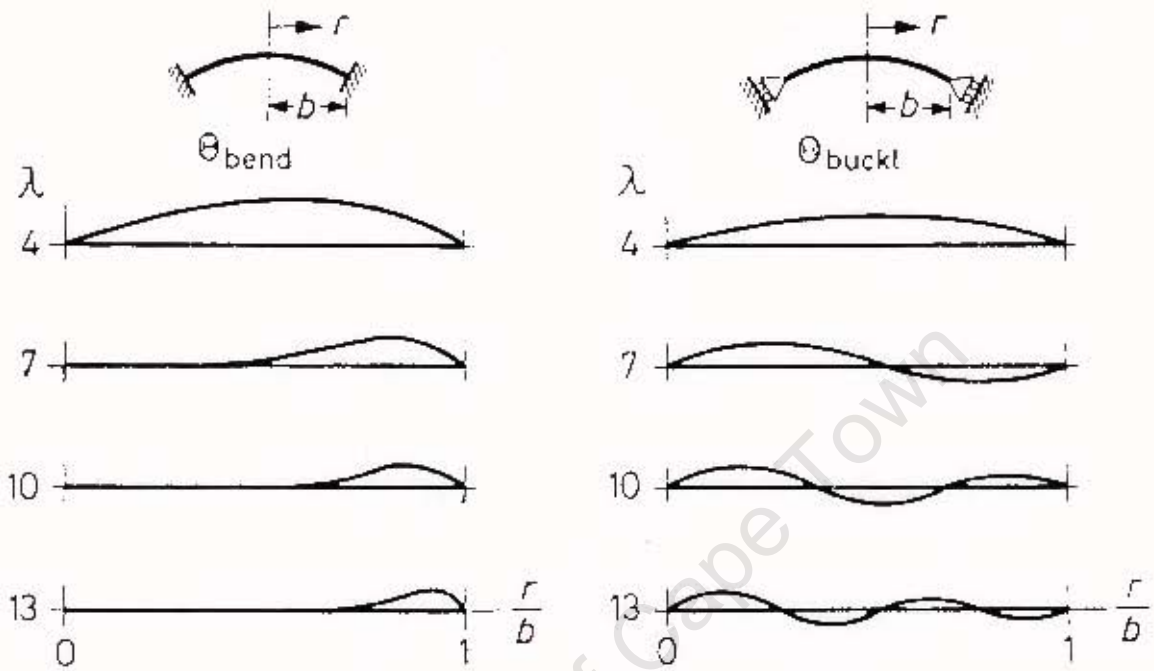

Fig. 1.12: Change in slope of the bending and buckling deformation [Kollár and Dulácska (1984)]

Even if the spherical shell has a perfect geometry, it still behaves like an imperfect shell, because of its boundary condition. When calculating the linear critical buckling load (see 1.3.1) a *membrane state of stress* is assumed. In a clamped or hinged cap bending stress also occurs. Therefore the results from the linear buckling theory do not correlate with the results from numerical nonlinear solutions where the bending deformation is also taken into account.

However, these investigations give still higher values for the critical buckling load than experimental results on "near-perfect" spherical caps. In order to explain this discrepancy between the theoretical and experimental results Budiansky (1960) and later Thurston and Penning (1966) have taken an initial imperfection into account. They described the deformation of the spherical cap by the nonlinear theory and assumed an axisymmetric buckling mode.

These investigations were only based on axisymmetric buckling shapes, although experimental investigations showed that the spherical cap often buckles asymmetrically [Schmidt (1986)]. Hence, theoretical investigations were done to find out when the axisymmetric deformation bifurcates into an asymmetric mode. This problem was first solved by Huang (1964) and later by Weinitschke (1965). They have combined the nonlinear axisymmetric deformation theory with the linear eigenvalue buckling theory. The results from these investigations are plotted against λ for the clamped spherical shell in Figure 1.13 and for the hinged spherical shell in Figure 1.14. In this case n is the circumferential full-wave number of the asymmetric mode. The axisymmetric results (Figure 1.11) are plotted in dashed lines to facilitate better comparison.

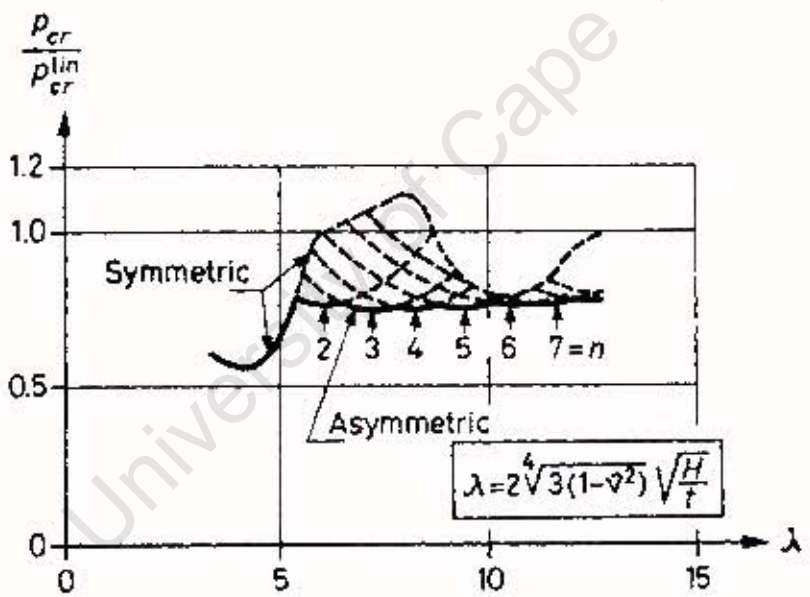

Fig. 1.13: Critical load pertaining to asymmetric buckling (clamped cap) [Kollár and Dulácska (1984)]

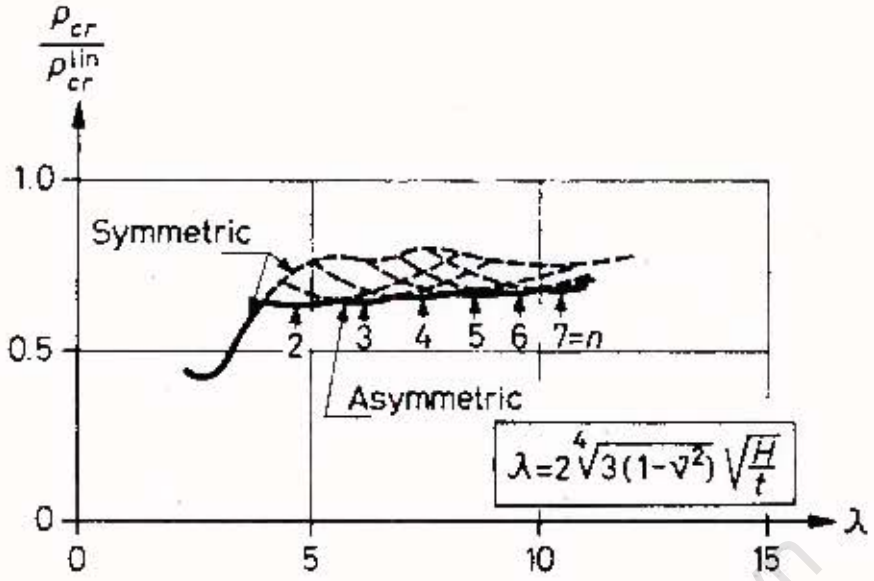

Fig. 1.14: Critical load pertaining to asymmetric buckling (hinged cap)

The characteristic feature of the asymmetric curves in contrast to those describing the axisymmetric buckling of perfect spherical caps (Figure 1.11) is that they do not oscillate, appearing constant and practically independent of λ. The bending deformation of the cap before buckling has no significant effect on the critical buckling load because the cap can bifurcate into an asymmetric buckling shape.

1.5. Imperfections of Shell Structures

1.5.1. Introduction

Shell structures such as metal tanks or silos are frequently constructed by joining curved metal plates together. As a result of the construction process the shape of the shell is not *perfect*. These *geometrical imperfections* have an important effect on the buckling strength of shell structures.

Several design recommendations (e.g. DIN 18800 T4) take these imperfections into account by introducing a "knockdown" factor. The classical critical buckling load of a perfect shell is multiplied in order to render a "practical" buckling load. These knockdown factors are chosen to be small enough to ensure a safe estimate of the practical buckling load. In some cases this knockdown factor is too conservative and therefore the structure is uneconomical.

Several investigations have been done on different imperfection forms to calculate the influence of imperfections more accurately. Idealized forms were used for these investigations. However, the measured imperfection forms are much more complex [Ding, Coleman and Rotter (1996)]. A general stochastic study based on measurement from real shell structures would solve this problem. Nevertheless, the study of idealized imperfection forms provides a good opportunity to understand the influence of these different forms on the buckling behaviour of shell structures.

1.5.2. Geometrical Imperfections

Geometrical imperfections can be divided into *global geometrical imperfections* and *local geometrical imperfections*.

Global geometrical imperfection means that the shell structure does not have the shape that was assumed for the analysis of the buckling strength (e.g. the shell is more hyperbolic than spherical). Hence, the shell structure buckles at a different critical load.

The simplest local imperfection would be a "spot" imperfection that can be caused by a small impact. Former work by the author has investigated the effect of a spot imperfection of half of the shell thickness on a cylindrical shell subjected to axial loading. The numerical results have shown a decrease in the buckling strength.

"Systematic" local geometrical imperfections are caused during the process in which the metal plates are curved [Lacher and Haspel (1980)]. The flat plates are curved by feeding them through a set of rollers (Figure 1.15).

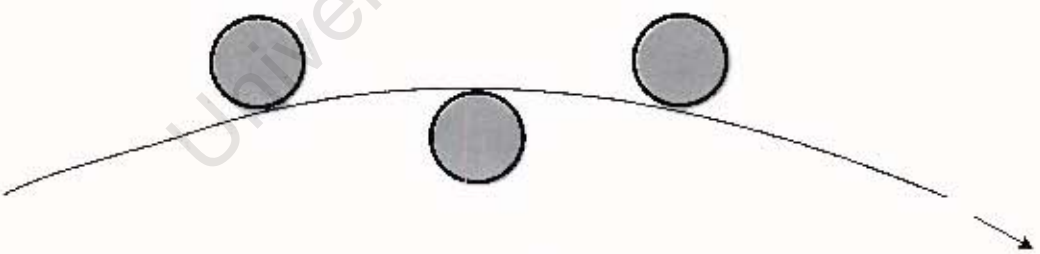

Fig. 1.15: Rolling process

Due to this process, small sections of both sides of the plate remain flat. While in high precision applications (e.g. aeronautical constructions) these flat sections are removed they are normally not removed in civil engineering application. These sections constitute lines of discontinuity in the otherwise smooth surface. Even if this imperfection is in the value of one shell thickness it leads to additional stress and strain in the shell, which influences the buckling behaviour [Mark, Holst and Calladine (1999)].

1.5.3. Previous Studies on the Effect of Imperfections

The effect of imperfections on the buckling behaviour of shells of revolution is very important because of their sensitivity to such initial imperfection. This subject has been the object of much research and many reviews in the last 60 years. It is even difficult to review the reviews since so many have been written. Rather than doing this, a brief history of the subject is given in this paragraph and a number of reviews will be pointed out.

Elastic postbuckling behaviour of shell structures was introduced by Kármán, Tsien and Dunn [Kármán and Tsien (1939),(1941); Kármán and Dunn (1940)] trough strict postbuckling analysis of the perfect structure. Some investigators [e.g. Legget and Jones (1942), Michielsen (1948) and Kemper (1954)] explained that the minimum postbuckling equilibrium is a measure of the load carrying capacity of the system. This latter thinking came to an end when Hoff, Madsen and Mayers (1966) concluded from their calculations that the minimum postbuckling load tends towards zero with increasing the number of terms in the series expansion of the transverse displacement component and with diminishing thickness. In this limiting case the Yoshimura (1955) buckling pattern can be achieved.

Another approach for imperfection sensitivity studies is to deal directly with the imperfect configuration and employ nonlinear kinematic relations. Donnel (1934) first and later other investigators used this approach but had varied success [e.g. Loo (1954), Narasimhan and Hoff (1971)]. Koiter (see 1.3.5.2) was the first to question the use of the minimum postbuckling load as a measure of the load carrying capacity of the structure. He was able to connect the initial postbuckling behavior with the imperfections sensitivity of the structure. His theory is limited to the neighborhood of the classical bifurcation load (immediate postbuckling) and therefore to small imperfections. This type of analysis has been used for a large number of problems. Survey articles have been written by Hutchison and Koiter (1970), Budiansky and Hutchison (1966), Tvergaard (1976) and Citerley (1982). The four survey papers referenced in the forgoing contain almost 800 references which indicates the extend of work on this subject and the impossibility of adequately reviewing the work.

Most early research on imperfection sensitivity was concerned with idealized imperfection forms and imperfections in small-scale laboratory models, but it has now been recognized that these are generally not representative of real imperfections in full scale structures. Babcock, Arbocz, Singer *et al* Arbrocz (1982), (1991); Arbrocz and Babcock (1981), Arbocz and Hol (1991); Elishakoff *et al* (1987); Singer (1982)| have pioneered in the precise measurement of imperfections in laboratory and full scale shells in the area of aeronautical engineering and have developed statistically based design methods, based on the measurement of imperfections in the last 20 years. An International Imperfection Database Bank was established with branches in Delf and Hatfia for the evaluation of imperfection measurements and correlation studies [Arbocz (1982) and Singer (1982)]. Their work has also demonstrated that the form and amplitude of imperfections are dependent on the fabrication process and quality.

Calladine (1995) added a new dimension to imperfection sensitivity research by suggesting that in addition to the assumed-to-be-stress-free geometric imperfections, locked-in stresses likely to occur in shells with fixed boundary conditions may also be important in reducing the load carrying capacity of shell structures. He also presented a thought-provoking review of the ideas deployed in understanding imperfection sensitivity of axially compressed cylindrical shells in the same article.

1.5.3.1. Previous Studies on Imperfections of Spherical Shells

Budiansky (1960) first studied the effect of a small axisymmetric imperfection on the buckling behaviour of a spherical cap. He found little effect on the critical buckling pressure. He concluded that asymmetric imperfections must be considered; however, his conclusion was based on only one investigated imperfection shape, which varied smoothly over the surface.

Later Thurston and Penning (1966) studied the effect of imperfections on the buckling behaviour of spherical shells (see also 1.4.3). They did a combined theoretical and experimental study on the instability of clamped spherical cap under uniform pressure. An axisymmetric imperfection in the form of an inward dimple was applied to the test specimens. They than measured the shapes of the imperfect shells and used these shapes for an input into a computer program based on the numerical solution of Reissner's (1950) finite deflection equations for general shells of revolution under axisymmetric loads. They found a reduction in the buckling strength in the area of 30% when compared to the classical buckling load.

Hutchison (1967) used Koiter's nonlinear shell buckling theory (see 1.3.5.2) to study the effect of imperfections. He showed that small imperfections on complete spherical shells and spherical caps have a severe effect in reducing the buckling strength. He found that an imperfection in the form of a classical buckling mode causes the greatest reduction in the buckling strength.

Tillman (1970) investigated theoretically and experimentally clamped spherical cap. He investigated caps with and without initial axisymmetric imperfection. The applied imperfection consisted of axisymmetrical circular flats of various diameter at the top of the cap. Marguerre's nonlinear shallow shell theory [Marguerre (1938)] was used for the theoretical part of the work. A relatively small imperfection was found to lead to a great decrease in the buckling strength. Good agreement between the theoretical and experimental results was found.

1.5.4. Imperfections Due to The Welding Process

Welding the curved plates together causes another "systematic" imperfection. Due to the cooling process after welding, shrinkage occurs parallel and perpendicular to the weld (Figure 1.16).

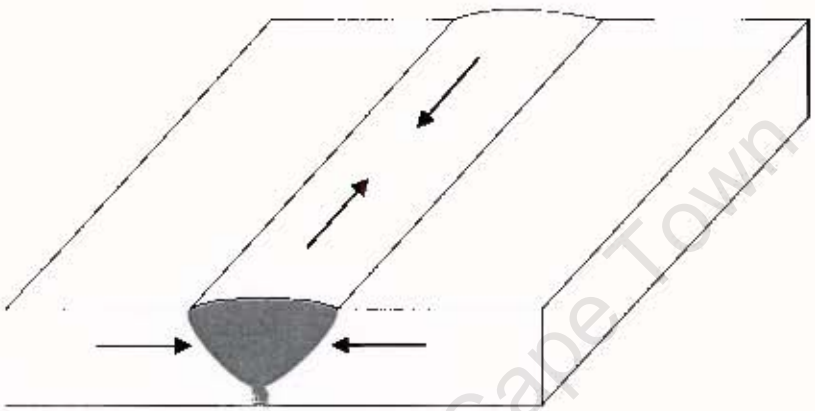

Fig. 1.16: Shrinkage of the weld due to cooling

The amount of shrinkage depends on the following factors:

- temperature during welding process
- method of welding (MIG, etc.)
- material of the weld
- material of the welded plate
- thickness of the plates
- type of weld (K-weld, V-weld, etc.)

The shrinkage in the material during the cooling process also leads to residual stress in the material. A schematic distribution of the residual stress that arises during and after the welding process can be seen in Figure 1.17.

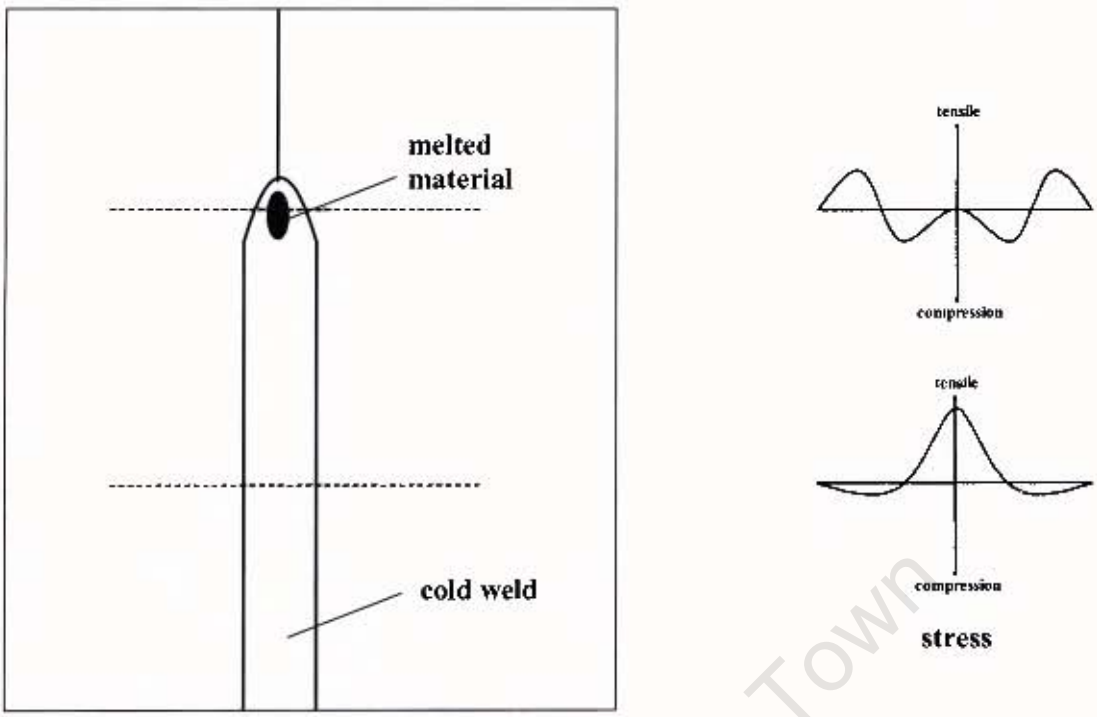

Fig. 1.17: Schematic residual stress distribution during welding process

1.5.4.1. Effect of Welding on the Buckling Behaviour of Shell Structures

Bornscheuer, Hafner and Ramm (1983) first investigated the effect of circumferential weld joint depressions on the buckling behaviour of cylindrical shells, under axial load, by using a nonlinear finite element program. Their investigation was motivated by a buckling phenomena in an arrangement of carbide silos built at the beginning of the 1950's. The areas around the circumferential welds of the cylindrical silos of 7 m diameter have shown buckling deformations up to 10 cm.

They have examined axisymmetric imperfections with an amplitude of either t /2 or t based on measured and idealized imperfection shapes and have also taken the residual stress due to welding into account. Their investigation on cylindrical shells with a r/t-ratio of 500 has shown a decrease of 50% in the buckling strength due to the geometrical imperfection. The residual stress had only limiting effect in the range of 2% to 10% (mean 5%) on the buckling strength and was therefore disregarded.

Later Rotter and Teng (1989) did a parametric study on cylindrical shells with a radius-to-thickness ratio between r/t=100 and r/t=2000 under axial loading conditions. They examined the effects of the weld joint amplitude, the shell r/t-ratio, a change of the shell plate thickness at the joint and also included internal pressure.

They defined two different imperfection shapes for the circumferential weld joint depression. The shrinkage of the cooling weld imposes an inward radial force on the shell (Figure 1.18).

Fig.1.18: Radial weld depression

The final shape of the weld depends on the extent to which bending yielding occurs during the cooling of the weld. For the first shape (Type A)(Figure 1.19) the weld was assumed to resist flexural yielding completely during cooling and for the second shape (Type B)(Figure 1.19) the weld was assumed to be completely flexible during cooling. Measurements by Clarke (1988) on silos have shown that the true shape is between Type A and B.

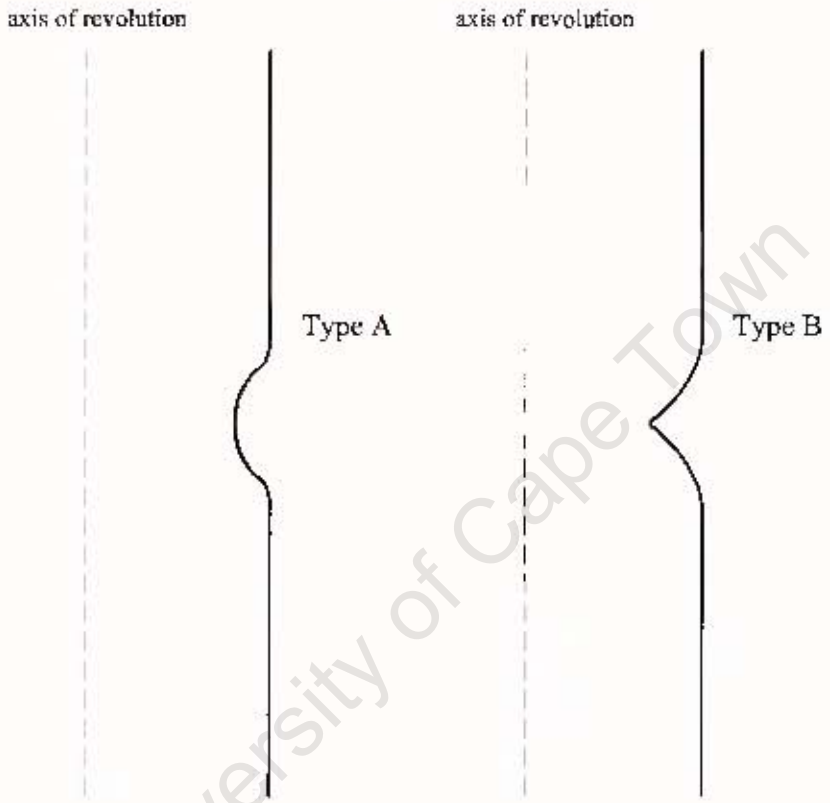

Fig. 1.19: Idealized weld depression according to Rotter and Teng

Their investigation shows that the effect of a circumferential weld depression on the buckling behaviour is independent of the r/t-ratio of the cylindrical shell. The effect of the amplitude of the weld depression on the buckling strength is approximately 60% of the classical buckling load for an amplitude of 0.25 times the wall-thickness and drops down to 30% for 2 times the wall-thickness.

Rammerstorfer *et.al.* (1991) did numerical studies on thin and thick cylindrical shells with circumferential weld depressions under axial and thermal loading conditions.

They have taken the geometric imperfection and the residual stress due to welding into account. The residual stress was assumed to be known or measured. The influence of the welding stress was simulated either directly by initial stresses introduced into the governing equations or by a fictitious temperature field which leads to a thermal stress field similar in nature to the residual stress field.

They established that residual stress has an important influence on the buckling strength of thicker cylindrical shells because of early plastification.

Pircher and Bridge (2001) have investigated the effect of circumferential weld depressions on the buckling behavior of a cylindrical shell under axial loading. They included the effect of neighboring welds on the buckling strength and found that the interaction between the welds leads to a further reduction in the buckling strength.

Numerical investigations using nonlinear finite element techniques were carried out including and excluding the effect residual stress. They found a decrease in the buckling strength for a cylindrical shell with a R/t-ratio of 1000 in the area of 75%. Residual stress was regarded as less imported.

The influence of welding stress and distortion on conical shells under hydrostatic load was investigated by Dammatty, Korol and Mirza (1997). Their work was motivated by the collapse of an elevated conical shaped water tower structure in Canada in 1990. They used nonlinear finite element methods for the evaluation of conical shells. The sensitivity of hydrostatically loaded conical shells to geometric imperfections and residual stress was investigated by analyzing three different cases: (a) perfect shell, (b) perfect shell, but with axisymmetric geometric imperfections in the order of one wall-thickness and (c) same case as b, but with the addition of residual stress due to welding.

They found that circumferential weld depressions lead to a reduction of 40%-45% of the buckling strength, while longitudinal weld depressions have no appreciable effect on the buckling strength.

1.5.5. Methods for The Measurement of Imperfections

A precise measurement of a shell structure's imperfections is required for reassessment of the strength of an existing shell structure and to develop new calculation methods based on a statistical model of different fabrication techniques and kinds of shell structures.

Comprehensive measurement of imperfections in shell structures is very difficult. In order to determine imperfections in zones of a short wavelength many sample points are required. High-accuracy data is necessary to define the precise form of the imperfections.

Several techniques have been developed in order to measure imperfections in shell structures. Bornscheuer and Hafner (1983), Krysik and Schmidt (1990) have used a simple measuring rod. Close-range photogrammetry was used by Shmutter and Ethrog (1971), Papo and Shmutter (1978) and Ethrog (1986). Fischer (1989) and Moss (1990) have used laser instrumentation. All these techniques are used in the measurement of small-scale structures. A technique for large shell structures was developed by Ding (1995) who has used standard survey techniques together with a special profile-measurement system. This technique has been successfully used to measure a 10,000 t grain silo [Ding, Coleman and Rotter (1996)].

Chapter 2
Finite Element Analysis

2.1. Introduction

In this chapter the finite element method will be briefly reviewed. Linear and nonlinear static analysis are explained and discussed. The interested reader is referred to the books of Zienkiewicz and Taylor (1991) for a more detailed treatment of the subject.

Finite element analysis (FEA) is a method of solving, usually approximately, certain problems in engineering and science. It is used for problems where no exact solution is available. As such, it is a numerical method. Methods of this type are needed because analytical methods cannot deal with all engineering problems that are encountered. For example, the analytical mathematical theory of elasticity can be used to calculate the stress and strain in a bent beam, but neither will it be very successful in finding out what happens during an impact of a car against a wall.

The development of the finite element method (FEM) was dependent on the development of fast computers. Applying the finite element method to a realistic engineering problem requires an enormous accumulation of data and calculation.

Finite element analysis was first used to calculate the stress and strain in complex engineering applications. Now it can be used for a wide field of applications, including fluid mechanics, vibration analysis, heat conduction and electrostatics.

Finite element analysis is essentially a piece-wise process. It can be applied to one-dimensional, two-dimensional and three-dimensional problems. The geometry is divided into smaller lines, areas or volumes, which are called *finite elements*. This process is called *discretization*. All finite elements together form an assembly called *finite element mesh*. Finite elements can have many different shapes. An example of a simple discretization of an area is shown in Figure 2.1.

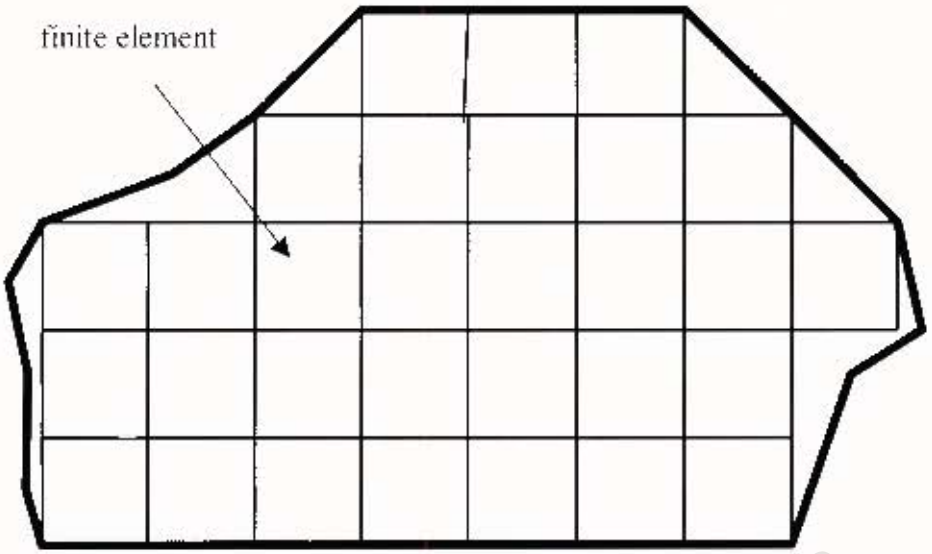

Fig. 2.1: Sample discretization of a 2D area

Here the area is divided into quadratic elements. It can be seen that these elements are only approximating the area because the elements have a given shape. The difference between the real geometry and the shape of the finite element mesh is called *discretization error*.

Every element contains a set of *nodes* that are located at the corner and, depending on the element type, possibly at the midsides of the element. Nodes on the boundaries of adjacent elements are also part of the adjoining elements.

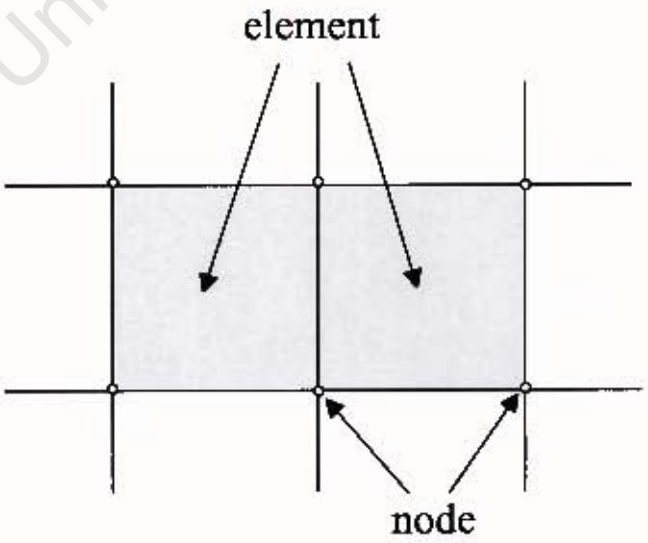

Fig. 2.2: Part of a finite element mesh

Figure 2.2 shows a part of a finite element mesh formed by simple 2D-elements with nodes at the corner of the element.

The analysis of a finite element model calculates the displacement at the node for a certain load applied. Since the displacement of each point within an element is fixed by the values of the displacement of the nodes that belong to the element, the displacement of the element is a function of the *nodal displacement*. Hence, the problem of finding the displacement in the real structure is replaced by finding the displacement of every node. Assuming a 2D-element, the displacement of each node consists of two components, one parallel to the referring x-axis and one parallel to the referring y-axis. These are called *degrees of freedom* (DOF). If the nodal displacement is known, the corresponding strain and then the stress can be computed.

2.2. Linear Static Analysis with FEM

The total potential energy Π of an elastic body under general loading can be defined by [e.g. Washizu (1982)]:

$$\Pi = U + V \tag{2.1}$$

where U is the strain energy of the body and V is the potential energy of the applied loads.

The principle of *minimum potential energy* states that among all the admissible displacement fields $\{a\}$ which satisfies the prescribed kinematic boundary conditions, the actual displacement is the one that makes the total potential energy stationary.
Hence, the derivation of equation (2.1) gives:

$$\delta\Pi = \delta U + \delta V \overset{!}{=} 0 \tag{2.2}$$

where,

$$\delta U = \int_V \{\sigma\}^T \cdot \delta\{\varepsilon\} \cdot dV \tag{2.3}$$

and,

$$-\delta V = \int_V \delta\{a\}^T \cdot \{b\} \cdot dV + \int_A \delta\{a\}^T \cdot \{t\} \cdot dA + \sum \delta\{u^c\}^T \cdot \{p_c\} \tag{2.4}$$

with $\{\varepsilon\}$ being the strain tensor:

$$\{\varepsilon\}^T = \begin{bmatrix} \varepsilon_{xx} & \varepsilon_{yy} & \varepsilon_{zz} & \gamma_{xy} & \gamma_{yz} & \gamma_{zx} \end{bmatrix} \tag{2.5}$$

and $\{\sigma\}$ being the stress tensor:

$$\{\sigma\}^T = \begin{bmatrix} \sigma_{xx} & \sigma_{yy} & \sigma_{zz} & \sigma_{xy} & \sigma_{yz} & \sigma_{zx} \end{bmatrix} \tag{2.6}$$

$\{b\}$ and $\{t\}$ are the body force and surface traction vectors:

$$\{b\}^T = \begin{bmatrix} b_x & b_y & b_z \end{bmatrix} \tag{2.7}$$

$$\{t\}^T = \begin{bmatrix} t_x & t_y & t_z \end{bmatrix} \tag{2.8}$$

$\{a\}$ is the displacement vector given by:

$$\{a\}^T = \begin{bmatrix} a_x & a_y & a_z \end{bmatrix} \tag{2.9}$$

and $\overleftarrow{\{u\}}^c$ is a vector listing the displacement components to concentrated forces $\{p_c\}$.

Equations (2.2) through (2.4) indicate that for an arbitrary virtual displacement $\delta\{a\}$ satisfying the prescribed kinematic boundary conditions, the virtual work done by the force is equal to the virtual work done by the external force (principle of virtual work).

The principle of virtual work holds for any kinematically admissible virtual displacement and is independent of the material stress-strain relationship.

In finite element analysis (FEA), a continuum is discretized by a number of suitable elements, which are interconnected through nodal points on the boundaries of the element (see 2.1). The total potential of the continuum Π may be considered as the sum of the individual element contribution Π^e, so that:

$$\Pi = \sum_{e=1}^{m} \Pi^e \qquad (2.10)$$

where m is the number of the element.

The integrals in equation (2.3) and (2.4) are thus performed for each element individually and summed over all elements.

For finite element formulations based on the principle of *minimum potential energy*, the displacement within the element $\{a\}^e$, are assumed to be a function of the element nodal displacement $\{\overset{e}{a}\}_i^k$:

$$\{a\}_i^e(x,y,z) = \sum_{k=1}^{n} N_k(x,y,z) \cdot \{\overset{e}{a}\}_i^k \qquad (2.11)$$

or

$$\{a\}^e = [N] \cdot \{\overset{e}{a}\}^k \qquad (2.12)$$

where $N_k(x,y,x)$ is the displacement *shape function* or interpolation function, and $\{\overset{e}{a}\}_i^k$ is the vector of nodal displacement components of a typical element:

$$\{\overset{e}{a}\}_i^{k\,e} \quad \left[\overset{e}{a}_i \quad \overset{e}{a}_i^2 \quad \overset{e}{a}_i^3 \quad \ldots \quad \overset{e}{a}_i^n\right] \qquad (2.13)$$

Element strains $\{\varepsilon\}^e(x,y,z)$ are then calculated by differentiating the appropriate displacement components in equation (2.11):

$$\{\varepsilon\}^e(x,y,z) = [B](x,y,z)\cdot\{a\}^e \qquad (2.14)$$

where $[B]$ is the appropriate strain-displacement matrix, and $\{a\}^e$ is the element displacement vector:

$$\{a\}^e = \begin{bmatrix} u_1 & v_1 & w_1 & u_2 & v_2 & w_2 & \dots & u_n & v_n & w_n \end{bmatrix} \qquad (2.15)$$

For a linear elastic material, the stress-strain relationship can be expressed in the form:

$$\{\sigma\} = [D]\cdot\{\varepsilon\} \qquad (2.16)$$

where $[D]$ is the elasticity or material matrix.

Substituting equations (2.3) through to (2.16) into equation (2.2) and considering arbitrary virtual displacement leads to the equilibrium equations of element assemblage in the form:

$$[K]\cdot\{a\} = \{P\}_b + \{P\}_s + \{P\}_c \qquad (2.17)$$

where $\{a\}$ is the global nodal displacement vector, and the matrix $[K]$ is the global stiffness matrix of element assemblage:

$$[K] = \sum_{e=1}^{m}[K]^e = \sum_{e=1}^{m}\int_v [B]^T\cdot[D]\cdot[B]\cdot dv \qquad (2.18)$$

The total load vector $\{p\}$ includes the effect of the body forces $\{p\}_b$, the effect of the element surface tractions $\{p\}_s$, and the concentrated forces $\{p\}_c$, where:

$$p_b = \sum_{e=1}^{m} \iiint_V [N]^T \cdot \{b\} \cdot dV \tag{2.19}$$

$$p_s = \sum_{e=1}^{m} \iint_A [N]^T \cdot \{t\} \cdot dA \tag{2.20}$$

Note that in equations (2.18) through (2.20), the summation sign is symbolic and should be interpreted as an assembly operator, for example:

$$[K] = \sum_{e=1}^{m} [J]_e^T \cdot [K]^e \cdot [J]_e \tag{2.21}$$

where $[J_e]$ is the Jacobian (transform) matrix that relates the element displacement vector to the global displacement vector of the entire system.

2.3. Nonlinear Static Analysis with FEM

2.3.1. Introduction

Nonlinear static analysis deals with nonlinear behaviour of structures under static loading.

The nonlinearities may be:

- material
- geometric
- combined nonlinearity (material and geometric)
- boundary nonlinearity (e.g. contact)

In material nonlinearities, the material constitutive, or stress-strain relations may be dependent on stresses, strains and/ or displacement. Examples include elastoplastic material behaviour and creep.

The second type of nonlinearity behaviour is the geometric nonlinearity. In this case the classical theory of infinitesimal strains does not hold, and the strains are obtained from the displacement via a nonlinear differential operator. This type of nonlinearity may involve large displacement and large rotation, which may be necessary to describe large displacement that occurs during shell buckling.

The third type of nonlinearity is the boundary nonlinearity. In this case, the material and strains remain linear in behaviour. The only nonlinear behaviour comes from changes in the boundary conditions (e.g. contact problems).

In geometric nonlinearity, or combined geometric and material nonlinearity, a relationship has to be established between the original (undeformed) and deformed configuration of the structure, and the equilibrium or energy balance equations must be written in terms of the deformed configuration. Hence, various types of formulation exist for this problem and are described in 2.3.2..

2.3.2. Formulation Methods

In describing the motion of a body, four different methods of formulation exist, [e.g. Truesdell (1977)]:

- material description
- referential description
- spatial description
- relative description

All four methods of formulation are equivalent for any smooth motion of a body.

2.3.2.1. The Material Description

In the material description, the independent variables are the particle or body-point P, and the time t. The description is conceptually the most natural one and is the one exclusively used in analytical dynamics where the individual lumped masses are labelled in a discretized lumped mass system. As it is rarely used in finite element application, it will not be mentioned or explained here.

2.3.2.2. The Referential Description

In the referential description, the independent variables are the position x of a particle P in an arbitrarily chosen reference configuration (C), and the time t. The choice of the reference is arbitrary and would not affect the final results. A particular referential description was introduced by Euler where the position ${}^{0}x$ of the body-point at the particular time $t=0$ is used to describe the motion (Figure 2.3). This particular description is called the *Lagrangian formulation*.

The use of the Lagrangian description is particularly appealing because of the simplicity with which material rates of change can be calculated. Another advantage of the Lagrangian description arises in the treatment of boundary conditions on the surface of the body, which are continuously changing during deformation. The boundary conditions on the deformed surface become nonlinear because the boundary surface is dependant on the unknown displacement. Using the Lagrangian description, which refers the motion to a fixed reference configuration, makes it possible to treat most of the kinematic questions in a relatively simple manner. The same advantage arises for all integrated quantities since integration in the Lagrangian description will be taken over the original known configuration rather than the current unknown configuration.

However, the use of the Lagrangian description also entails some disadvantages, which arise from the requirement that the stress acting in the instantaneous current configuration has to be referred to the initial reference configuration in a way that is physically artificial through mathematical equations and Cauchy's axioms of motion. Another point that is difficult to handle in the Lagrangian description is the requirement for a continuous update of boundary conditions. Excessive deformations of a body might cause a great deal of distortion in the original finite element mesh, and such distortions might affect the accuracy and reliability of the solution.

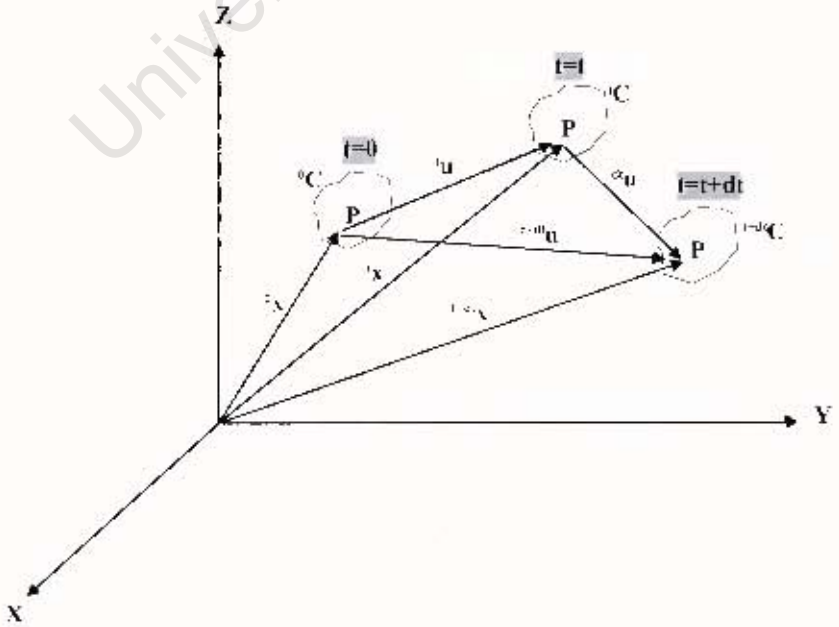

Figure 2.3: Geometry of motion

2.3.2.3. The Spatial Description

In the spatial description, the independent variables are the current location ${}^{t}x$ of the particle P, and the time t. This description was introduced by Bernoulli and D'Alembert and it is often called the Eulerian description. The spatial description is concerned with what is happening in a fixed region of space with regards to time, a description that seems to be ideally suitable for the study of fluids. For the same reason the spatial description cannot be used for soil mechanics, since the law of continuum mechanics refers to what is happening to the body, and not to the region of space which the body momentarily occupies. In all such laws of mechanics, referring to the material of the body, the independent spatial variable ${}^{t}x$ becomes a function of position ${}^{0}x$ in the Lagrangian reference configuration and the time t. Hence, all material rates will be much more difficult to handle in the spatial description.

2.3.2.4. The Relative Description

In the relative description, the independent variables are the position ${}^{\tau}x$ in the current configuration and the variable time τ. The current configuration is taken as the reference configuration, and the variable time τ is the time relative to the present when the particle P occupied a place ξ, where $\xi = \xi({}^{\tau}x, \tau)$. The relative description is a Lagrangian description in nature, in the sense that the reference position is now denoted by ${}^{\tau}x$ at time $t = \tau$ rather than ${}^{0}x$ at time $t=0$. This is called *update Lagrangian formulation*, which is a special case of relative description. Owing the nature of each formulation and its reference configuration, the relative description has some advantages over the referential description. As an example, the question of boundary condition updating and mesh distortion, which may for example occur during shell buckling due to large displacements, may be easier to handle in the updated Lagrangian description. If a nonlinear discretized displacement field is assumed, the choice of an updated reference configuration may result in vanishing nonlinear contributions of the discretized field.

2.3.3. Solution Schemes for Nonlinear Static Analysis with FEM

2.3.3.1. Introduction

In nonlinear static analysis with finite element methods the entire load history is typically divided into *events*. Generally, an event should be defined when new load types are introduced or when solution strategy changes. Each event may have one or more load steps (*increments*). The nonlinear problem is then solved in a step-by-step manner until the full loads are applied. For this procedure several solution methods exist. The most often used methods are:

- conventional Newton-Raphson Method
- modified Newton-Raphson Method
- Arc Length Method

2.3.3.2. Conventional and Modified Newton-Raphson Method

When solving the nonlinear equilibrium equations with the Newton-Raphson method, an incremental-iterative scheme is applied, for which at a time t, the equilibrium equations can be written as follows:

$$[K]_{t}^{i-1} \cdot \Delta\{u\}^{i} = {}^{t+\Delta t}\{p\} - {}^{t+\Delta t}\{f\}^{i-1} \qquad (2.22)$$

and:

$${}^{t+\Delta t}\{u\}^{i} = {}^{t+\Delta t}\{u\}^{i-1} + \Delta\{u\}^{i} \qquad (2.23)$$

where:

$[K]_t$ = tangent stiffness matrix at time t

$\Delta\{u\}^i$ = iterative increment of nodal displacement in interation i

${}^{t+\Delta t}\{u\}^i$, ${}^{t+\Delta t}\{u\}^{i-1}$ – vectors of nodal displacement at time $\Delta t - t$ corresponding to interations i and $i+1$, respectively

${}^{t+\Delta t}\{p\}$ = vector of externally applied nodal force at the time $\Delta t + t$

${}^{t+\Delta t}\{f\}^{i-1}$ = vector of internal nodal force, equivalent to the element stress, at the time $\Delta t + t$ and interation i-1

The incremental solution is performed in a step-by-step manner until the total loads are applied. In each increment, the above iterative scheme is performed until convergence is achieved or the number of maximum iterations is reached. During each interation, the tangent stiffness matrix $[K]_t$ may be updated for each interation (conventional Newton-Raphson method), or kept constant in all iterations of the increment (modified Newton-Raphson method).

Although the use of the modified Newton-Raphson method may be more economical in specific material nonlinearity applications, the use of the method in general material and geometrical nonlinearities is not always successful. Both methods are compared graphically in Figure 2.4 and 2.5 respectively.

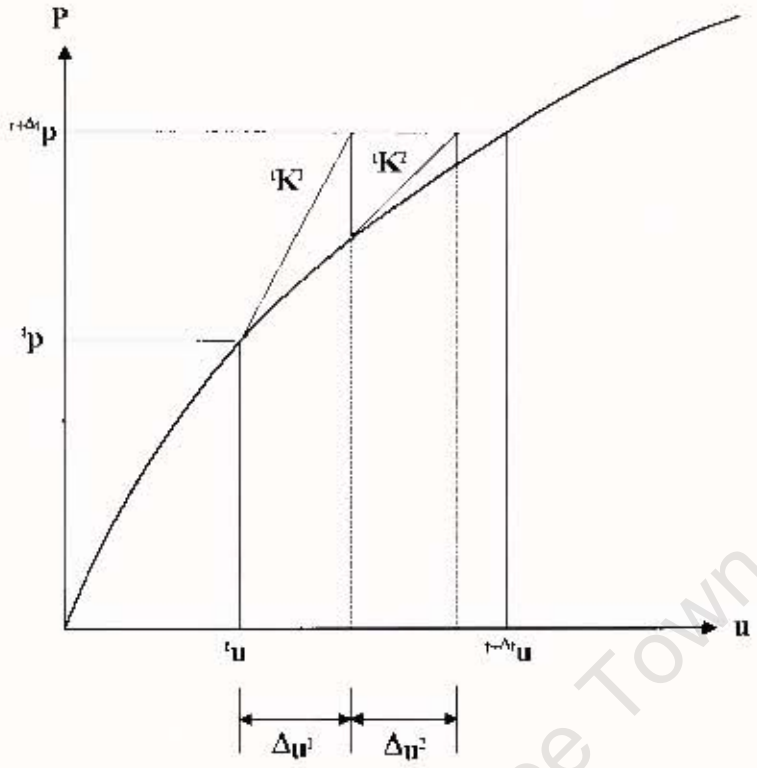

Fig. 2.4: Conventional Newton-Raphson method

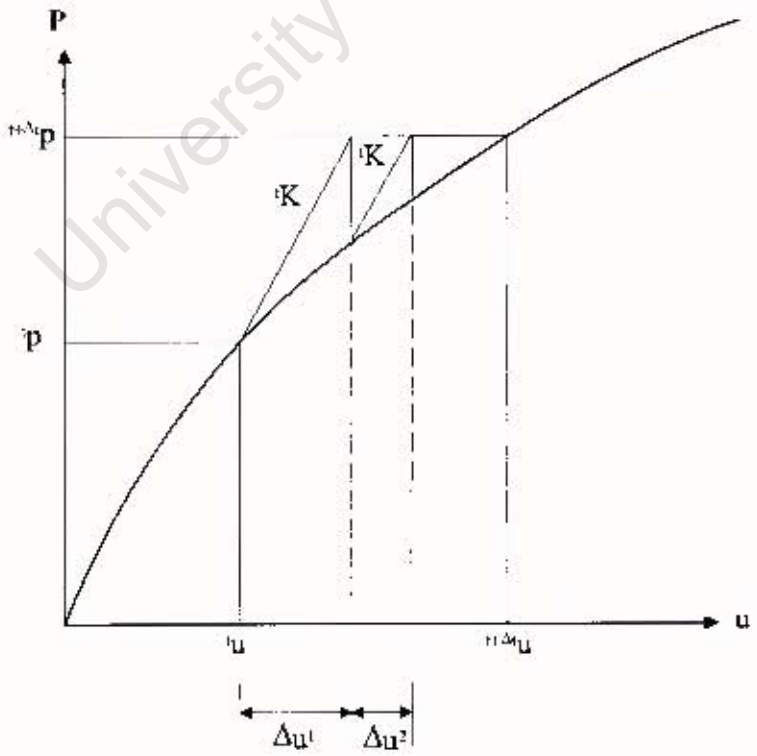

Fig. 2.5: Modified Newton-Raphson method

2.3.3.3. Arc Length Method

To follow the structural response beyond the critical point is very difficult with FEM. The major difficulty is to overcome the singularity of the incremental tangent stiffness matrix when the structure reaches its stability limit. In addition, snap-through and snap-back buckling phenomena pose some of the most difficult problems in nonlinear structural analysis.

A method called "arc length automatic stepping", is a scheme, which can be applied to overcome the problem of stiffness singularity and post-buckling.

The general goal of the arc length procedure is to control the iteration of the numerical solution of complex nonlinear problems. The main idea of this method is based on the concept of constraining the length of the incremental displacement. The incremental length of each successive iteration is constrained by the length of the previous iteration. Correspondingly, the load is adjusted in order to satisfy the global equilibrium requirements of the system.

Procedures of this nature require a reformulation of the traditional mathematical problem into a different form. The standard equilibrium equation for proportional loading is:

$$\lambda \cdot \{r\} - \{f\} = 0 \qquad (2.24)$$

where {r} is a reference load vector and {f} is the vector of the internal force.

The proportional loading factor λ in incremental form yields a general formulation as:

$$K^{i-1} \cdot \{\delta\}^{i} = \lambda^{i-1} \cdot \{r\} - {}^{t+\Delta t}\{f\}^{i-1} \quad i=0,1,2,... \qquad (2.25)$$

$$= {}^{t+\Delta t}\{p\}^{i-1} - {}^{t+\Delta t}\{f\}^{i-1}$$

with:

$$\lambda^{i+1} = \lambda^i + \Delta\lambda^i \qquad (2.26)$$

$${}^{t+\Delta t}\{f\}^0 = {}^t\{P\}$$

where:

$[K]^i$ = the tangent stiffness matrix at the i^{th} iteration

$\Delta\{u\}^i$ = incremental displacement vector from the beginning of the step to the end of current iteration cycle (i^{th} interation)

$\{\delta\}^i$ = incremental displacement vector of current iteration

λ^i = load parameter (scale) for the i^{th} iteration

It can be written:

$$\Delta\{u\}^{i+1} = \Delta\{u\}^i + \{\delta\}^i \quad i = 1,2,\ldots \qquad (2.27)$$

$${}^{t+\Delta t}\{u\}^{i+1} = {}^t\{u\} + \Delta\{u\}^{i+1} \qquad (2.28)$$

and:

$$\Delta\{u\}^0 = 0 \qquad (2.29)$$

In order to find $\{\delta\}^i$ equation (2.25) can be rewritten into two parts:

$$[K]^i \cdot \{\overline{\delta}\}^i = \lambda^i \cdot \{r\} - {}^{i-1}\{f\}^i \tag{2.30}$$

$$[K]^i \cdot \{\delta_r\}^i = \{r\} \tag{2.31}$$

therefore:

$$\{\delta\}^i = \{\overline{\delta}\}^i + \Delta\lambda^i \cdot \{\delta_r\}^i \tag{2.32}$$

where $\{\delta_r\}^i$ is the displacement due to a unit load factor multiplied by the incremental variation in the load level λ^i and $\{\overline{\delta}\}^i$ is the displacement update for a conventional "load controlled" Newton procedure due to the unbalanced load.

It is seen that in order to completely define $\{\delta\}^i$, one must find $\Delta\lambda^i$.

Thus, consider a constrained arc length:

$$\begin{aligned}\left(\Delta l^{i-1}\right)^2 &= \left(\Delta l^i\right)^2 \\ &= \left(\Delta\{u\}^{T^{i-1}} \cdot \Delta\{u\}^{i-1}\right) - \left(\lambda^{i-1} - \lambda^0\right)^2 \\ &= \left(\Delta\{u\}^{T^i} \cdot \Delta\{u\}^i\right) - \left(\lambda^i - \lambda^0\right)^2\end{aligned} \tag{2.33}$$

Based on the above equation, $\Delta\lambda^i$ and $\{\delta\}^i$ can be solved.

This procedure can be applied with either a modified or full (conventional) Newton-Raphson interation scheme. The relationship between these components in the load-displacement space is displayed as shown in Figure 2.6.

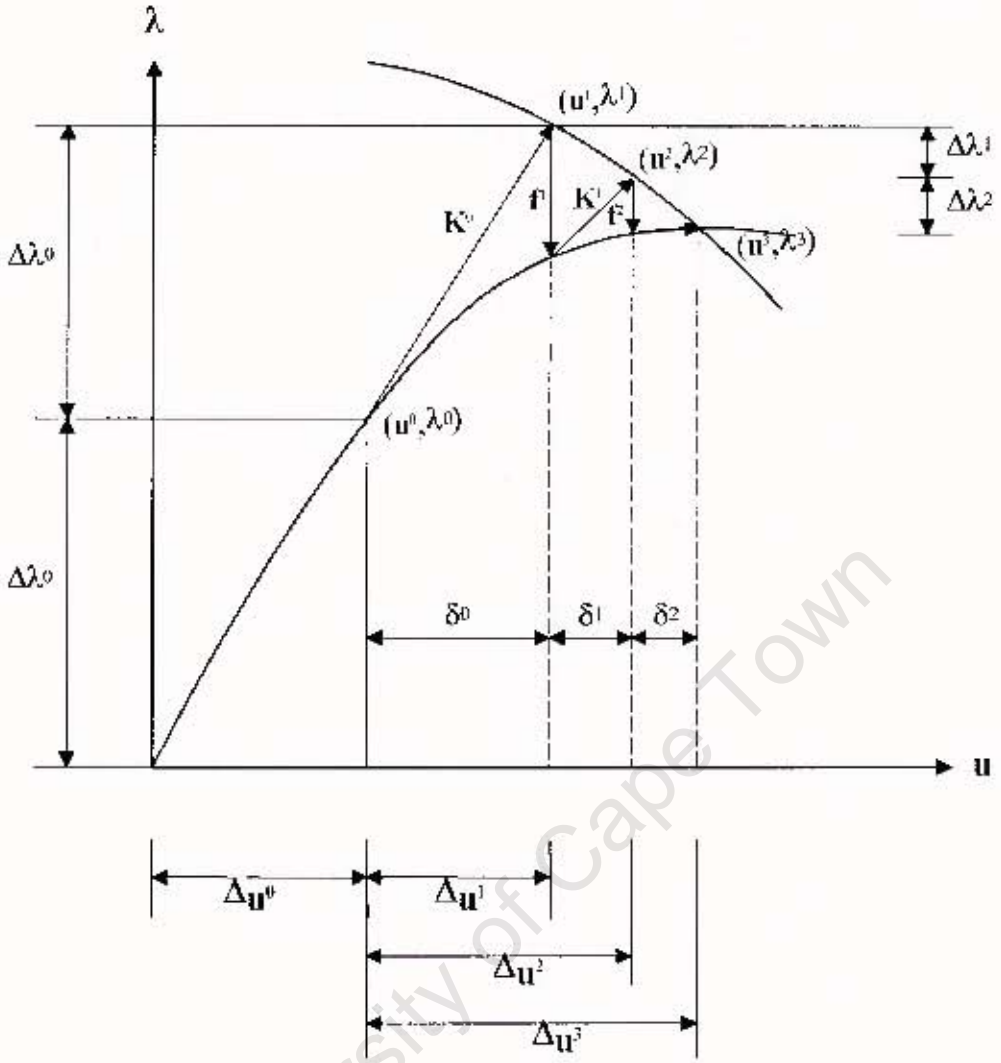

Fig. 2.6: Arc Length solution algorithm

2.4. Finite Element Analysis of Shell Structures

2.4.1. Introduction

The analysis of shell structures with FEM was mainly developed in the area of aeronautical engineering. Several types of shell elements have been developed and development of new shell elements is still in process. Shell elements can be divided into four different groups:

- Facet shell elements
- Solid shell elements
- Curved shell elements
- Axisymmetric shell elements

The facet shell element is a flat shell element, which approximates the curved surface of the shell by a series of facets. Quadratic and triangular elements exist. The facet shell element is formulated by combining a *Kirchhoff* or *Mindlin* plate bending element with a plane stress element. The facet shell element is not very accurate as dicretization errors occur by approximating the curved shell surface with plane elements. The approximated surface is discontinuous which can lead to a large error in the analysis. However, the use of facet shell elements is still very attractive because of its simple geometry and low degree of freedom. The accuracy can be greatly improved by e.g. assumed stress interpolation [Pian (1964)] or the inclusion of drilling degrees of freedom in the membrane component.

Solid shell elements are formulated by using second order 3D solid elements. The curved shell surface can be approximated more accurate by using second order elements. As the shell thickness is rather small compared with the other dimensions a problem of aspect ratio error occurs. This problem is solved by removing the mid-side nodes through the thickness. Hence, no direct strain can occur through the thickness. This element type is therefore often called a *degenerate* solid element and is included in most FEM packages. It is mainly used for thick shells. Transverse shear deformation is included within this element as the displacement is calculated on the top and bottom surface of the element. A problems associated with this element is the large number of degrees of freedom (DOF) which leads to large memory and

computing requirements. The results from these types of elements can be regarded as acceptable, although not as accurate as from the curved shell elements.

The formulation of curved shell elements is rather complex and development in this area is still continuing. The curved shell element was mainly developed to overcome the inaccuracy of the other shell element types. One of the simplest curved shell elements would be the Ahmad Element, which is mainly used for the analysis of thick shells. The most popular curved shell elements are semi-loof elements. The formulation of this element is complex and rarely understood by engineers. This element has general applicability and produces accurate results. It can be applied to thin shells and thick shells and is included in most FEM packages.

Axisymmetric shell elements can be used to model shells of revolution. The simplest axisymmetric shell is a conical frustum, which is represented by a straight line element. Curved axisymmetric shell elements can be used to describe the surface more accurately and are represented by a curved line element. Due to the fact that only line or curve line elements are needed to model the whole shell of revolution the analysis does not use much memory and is therefore rather quick.

As axisymmetric shell elements are used for the finite element analysis that was used in this thesis, a detailed description of a simple axisymmetric element is given in the next section.

2.4.2. The Axisymmetric Shell Element

Axisymmetric shell elements were developed in the area of aeronautical engineering, as a form that often appears in aerospace structures is a thin shell of revolution (e.g. the body of a rocket). A simple axisymmetric element can be constructed as follows:

The axisymmetric shell element is a conical frustum which is represented by a straight line element (Figure 2.7).

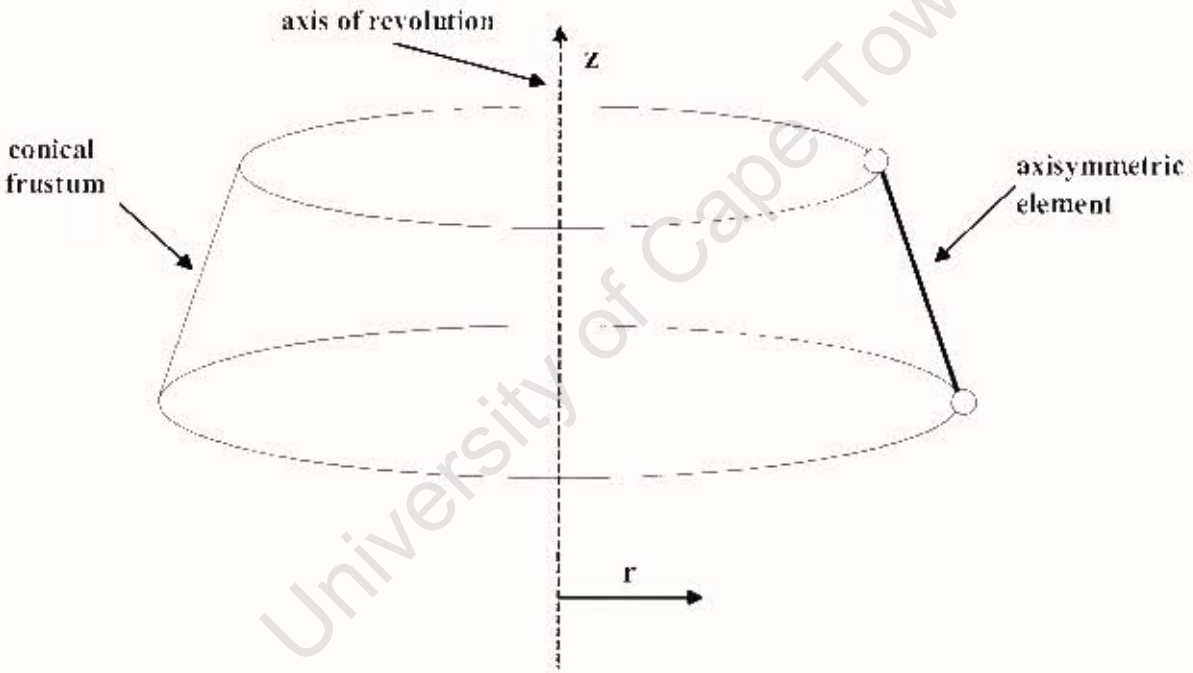

Fig. 2.7: Axisymmetric shell element

The element is considered in the *global r-z* plane and has a *local* coordinate system defined by the *s-t* axes, which is inclined at an angle α, to the global coordinate system. The local coordinate system is used to describe the in-plane and the normal displacement of the element (Figure 2.8). The element has two nodes *i* and *j*, with three degrees of freedom (DOF) associated with it. These are the two displacement components u and w and a rotation component β (Figure 2.8), corresponding to the three local load components P_r, P_Z and M. $\underline{u}$ and $\underline{w}$ are the corresponding global displacement components.

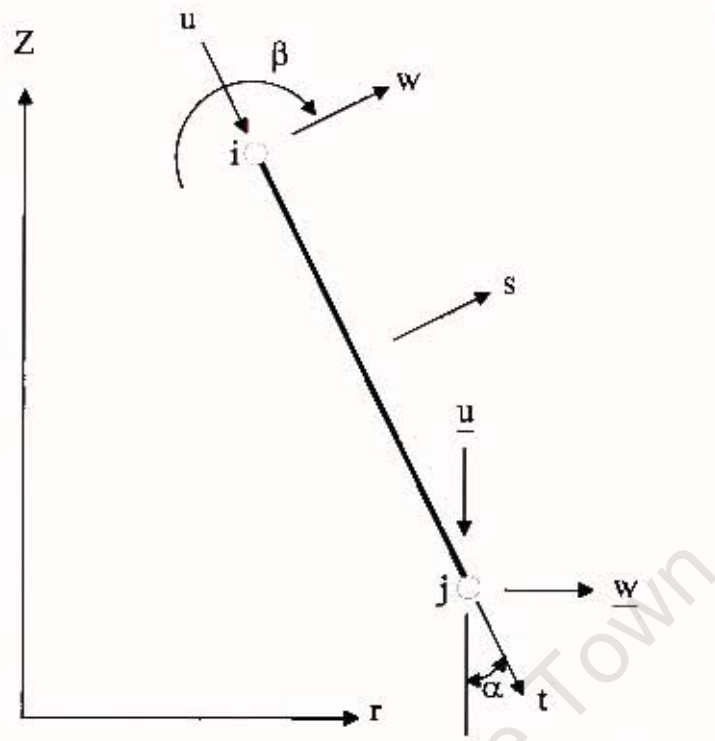

Fig. 2.8: Local coordinate system of the element

The element has a total of four strain components, two membrane (in-plane) and two bending (out-of-plane) strains. There are direct strains and hoop strains present in the element as well.

The strain components for the membrane strain (Figure 2.9) are

$$\varepsilon_{i_m} \quad \frac{du}{ds} \tag{2.34}$$

for the membrane strain and,

$$\varepsilon_{i_{\alpha_m}} = \frac{u \cdot \sin\alpha - w \cdot \cos\alpha}{r} \tag{2.35}$$

for the hoop strain.

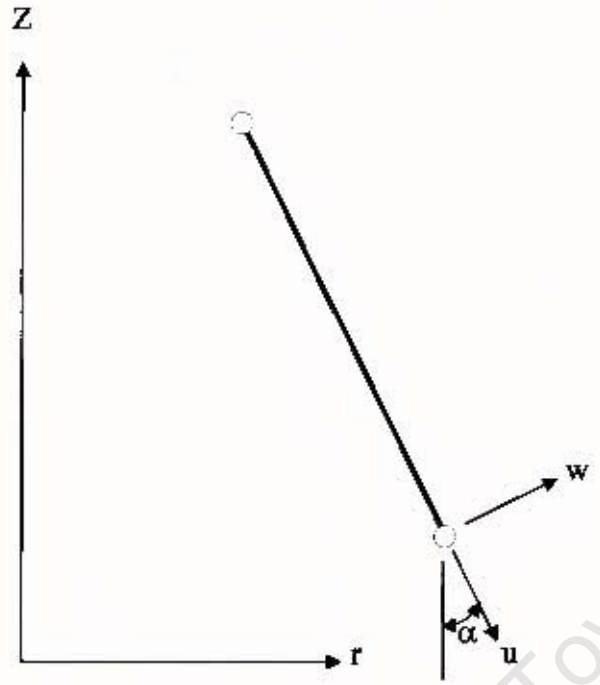

Fig. 2.9: Membrane strain components

Referring to Figure 2.10 the membrane strain component due to bending is given by:

$$\varepsilon_{t_b} = \frac{du}{dt} = \frac{d}{dt}\left(-\frac{h}{2}\cdot\frac{dw}{dt}\right) = -\frac{h}{2}\cdot\frac{d^2w}{dt^2} \qquad (2.36)$$

and the hoop strain component is given by:

$$\varepsilon_{\alpha_b} = -\frac{h}{2}\cdot\frac{dw}{ds}\cdot\frac{\cos\alpha}{r} \qquad (2.37)$$

with h being the thickness of the element as shown in Figure 2.10

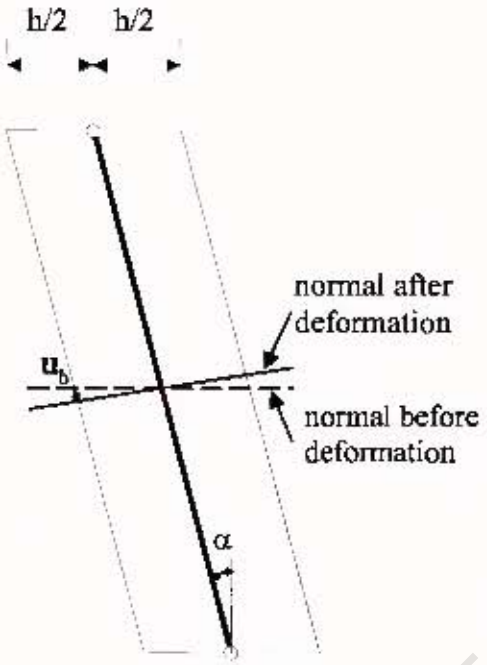

Fig. 2.10: Bending strain component

The displacement vector for the element is defined as:

$$\{u\}^T = \begin{bmatrix} u_1 & w_1 & \frac{dw_1}{dt} & \dots & u_n & w_n & \frac{dw_n}{dt} \end{bmatrix} \tag{2.38}$$

The shape functions for the element are Lagrangian in form, as only the displacement u is required and none of it's derivations:

$$u = \sum_{i=1}^{e} N_i(\xi) \cdot u_i \tag{2.39}$$

where for a linear element:

$$N_1 = 1 - \xi$$
$$N_2 = \xi$$

and

$$\xi = \frac{t - t_i}{L} \tag{2.40}$$

with

L = element length

For the displacement w a Hermitian shape function is required as, in addition to the displacement, the first derivative is also needed. The displacement can be written in terms of the shape function and the nodal displacement as:

$$w = \sum_{i=1}^{n} \left(w_i \cdot g_i + \frac{dw}{dt} h_i \right) \tag{2.41}$$

where:

$$g_i = H_i^{1,0}(n,\xi) \tag{2.42}$$
$$h_i = L \cdot H_i^{1,1}(n,\xi)$$

where, for $H_i^{1,0}$ the subscript i refers to the node number and the superscript $1,0$ refers to the displacement.

The strain-displacement relationships can be written in matrix form as follows:

$$\{\varepsilon\}_m = [B_m] \cdot \{u\} \tag{2.43}$$
$$\{\varepsilon\}_b \quad [B_b] \cdot \{u\}$$

where:

$$[B_m] = [b_1 \quad b_2 \quad \dots \quad b_n] \tag{2.44}$$

with:

$$[b_i] = \begin{bmatrix} \frac{1}{L} \cdot N_i & 0 & 0 \\ \left(\frac{\sin\alpha}{r}\right) \cdot N_i & \left(\frac{\cos\alpha}{r}\right) \cdot g_i & \left(\frac{\cos\alpha}{r}\right) \cdot g_i \end{bmatrix} \tag{2.45}$$

and also:

$$[B_b] = [b_1 \quad b_2 \quad \dots \quad b_n] \tag{2.46}$$

where:

$$[b_i] = \begin{bmatrix} 0 & -\left(\frac{h}{2 \cdot L^2}\right) \cdot \frac{d^2 g_i}{d\xi^2} & -\left(\frac{h}{2 \cdot L^2}\right) \cdot \frac{d^2 h_i}{d\xi^2} \\ 0 & -\left(\frac{h \cdot \sin\alpha}{2 \cdot r \cdot L}\right) \cdot \frac{dg_i}{d\xi} & -\left(\frac{h \cdot \sin\alpha}{2 \cdot r \cdot L}\right) \cdot \frac{dh_i}{d\xi} \end{bmatrix} \tag{2.47}$$

With:

$$\frac{dw}{d\xi} = \frac{dw}{dt} \cdot \frac{dt}{d\xi} = L \cdot \frac{dw}{dt} \tag{2.48}$$

it can be found that:

$$\frac{dw}{dt} = \frac{1}{L} \cdot \frac{dw}{d\xi} \tag{2.49}$$

and it can also be found that:

$$\frac{d^2w}{dt^2} = \frac{1}{L^2} \cdot \frac{dw}{d\xi} \tag{2.50}$$

The stress can be written in terms of the strain as follows:

$$\{\sigma_m\} = [D] \cdot \{\varepsilon_m\} \tag{2.51}$$
$$\{\sigma_b\} = [D] \cdot \{\varepsilon_b\}$$

where:

$$[D] = \frac{E}{1-\nu^2}\begin{bmatrix} 1 & \nu \\ \nu & 1 \end{bmatrix} \tag{2.52}$$

with:

E = Young's modulus
υ = Poisson's ratio

Hence, the strain energy for this element can be written as:

$$U = \{a\}^T \cdot \left[\int_{Vol} [B_m]^T \cdot [D] \cdot [B_m] dVol + \int_{Vol} [B_b]^T \cdot [D] \cdot [B_b] dVol \right] \cdot \{a\} \tag{2.53}$$

Differentiating with respect to the displacement vector $\{a\}$ and equating to zero leads to the *element stiffness matrix* for the membrane stiffness as follows:

$$[K]_m = \int_r \int_z [B_m]^T \cdot [D] \cdot [B_m] \cdot t \cdot dz dr \qquad (2.54)$$

and for the bending stiffness as follows:

$$[K]_b = \int_r \int_z \left[\int_{-\frac{t}{2}}^{\frac{t}{2}} [B_b]^T \cdot [D] \cdot [B_b] ds \right] dz dr \qquad (2.55)$$

The rotation matrix to convert the local element coordinate system to the global coordinate system is given by:

$$[T] = \begin{bmatrix} \cos\alpha & \sin\alpha & 0 \\ \sin\alpha & \cos\alpha & 0 \\ 0 & 0 & 1 \end{bmatrix} \qquad (2.56)$$

Thus it can be deduced that the *global stiffness matrix* can be expressed as:

$$[K]_g = [T]^T \cdot [K]_l \cdot [T] \qquad (2.57)$$

where the subscript g refers to the global coordinate system and *l* to the local coordinate system.

Chapter 3

Buckling Analysis with FEM

3.1. Introduction

Buckling analysis of complex (shell) structures provides a constant challenge for engineers. Only buckling problems with a simple geometric shape and loading can be solved by the analytical methods mentioned in chapter 1, as the formulation and solution of the differential equations are complex. Hence, finite element methods (FEM) are widely used to calculate the critical buckling load of structures. There are two different methods of calculating the critical buckling load with finite element methods:

- linear (eigenvalue) buckling analysis
- nonlinear buckling analysis

3.2. Eigenvalue Buckling Analysis with FEM

Eigenvalue buckling with finite element methods involves calculating the point at which the structure's primary load deflection path is bifurcated by a secondary load deflection path, similar to the classical buckling theory mentioned in 1.3.1. This requires an eigenvalue extraction and the governing equation is given by:

$$\left([K] + \lambda_i \cdot [K_g]\right) \cdot \{u\}_i = 0 \qquad (3.1)$$

where:

$[K]$ = linear stiffness matrix

$[K]_g$ = geometric stiffness matrix

λ_i = i^{th} eigenvalue or the multiplier to the load from which $[K]_g$ is calculated

$\{u\}_i$ = displacement eigenvector or mode shape

The geometric stiffness matrix $[K]_g$ is given by:

$$[K]_g = \int_V [B]_{nl}^T \cdot [\hat{S}] \cdot [B]_{nl} \cdot dV \tag{3.2}$$

where $[B]_{nl}$ is the nonlinear strain-displacement transformation matrix:

$$[B]_{nl} = \left[\cdots \begin{bmatrix} N_{k,1} & 0 & 0 \\ N_{k,2} & 0 & 0 \\ N_{k,3} & 0 & 0 \\ 0 & N_{k,1} & 0 \\ 0 & N_{k,2} & 0 \\ 0 & N_{k,3} & 0 \\ 0 & 0 & N_{k,1} \\ 0 & 0 & N_{k,2} \\ 0 & 0 & N_{k,3} \end{bmatrix} \cdots \right] \tag{3.3}$$

with k being a typical node and:

$$N_{k,i} = \frac{\partial N_k}{\partial x_i} \tag{3.4}$$

The stress matrix $[\hat{S}]$ is defined by:

$$[\hat{S}] = \begin{bmatrix} S & O & O \\ O & S & O \\ O & O & S \end{bmatrix} \tag{3.5}$$

where S is the second Piola-Kirchoff stress tensor:

$$S = \begin{bmatrix} S_{11} & S_{12} & S_{13} \\ S_{21} & S_{22} & S_{23} \\ S_{31} & S_{32} & S_{33} \end{bmatrix} \tag{3.6}$$

and O a 3x3 zero matrix.

Buckling analysis with FEM is a two-pass analysis. The first pass is a linear static analysis which determines the stress for a given reference of loads. The second pass is an eigenvalue analysis which first computes the geometric stiffness matrix. The stresses in equation (3.2) will be based on the results of the linear static analysis. The second pass results are in terms of load factors and mode shape.

As this method is based on the same theory described in 1.3.1. it should be noted that this type of buckling analysis takes no initial imperfections into account. It provides no information about post-buckling behaviour and is limited to cases with no large displacement effects (e.g. follower loading). Such cases are very rare in practical application. The results for this type of buckling analysis therefore often over-estimate the critical buckling load and should therefore be interpreted carefully. An application of an appropriate "knock-down" factor is necessary in order to render a practical and secure critical buckling load.

3.3. Nonlinear Buckling with FEM

In order to do a thorough buckling and post-buckling analysis a full incremental nonlinear static analysis with FEM can be performed. Initial imperfections and residual stress can be taken into account in this type of analysis as well as plasticity effects.

As large deformations occur during this analysis, the updated Lagrangian formulation (see 2.3.2.4.) should be used in order to avoid mesh distortion. Another problem is to overcome the singularity of the incremental tangent stiffness matrix when the structure reaches its stability limit. This problem can be solved by using the Arc-Length solution scheme described in 2.3.3.3. together with the full Newton-Raphson method (see 2.3.3.2.).

The main problem is to find the shape and amplitude of the applied imperfection. The best way of solving this problem would be the establishment of a statistically based imperfection model for a particular class of shell structure, fabricated by the same process, based on extensive measurement of real geometric imperfections on full scale structures. Such an imperfection model must distinguish between high and low quality shell structures. While the approach is rational, its establishment relies on extensive measurement data, which are currently not available.

A method by Speicher and Saal (1991) describes a way to find an appropriate imperfection shape if no information regarding the real imperfection shape is available. They proposed an equivalent imperfection shape of the same shape as the first bifurcation mode to be used and have also deduced the required magnitude of this imperfection in order to produce a safe design. However, this method has only been verified for cylindrical shells and has still to be verified first for other shell structures.

3.4. Comparison of Linear and Nonlinear Buckling with FEM

Even if linear buckling analysis with FEM is not as accurate as nonlinear buckling analysis with FEM, it is widely used in engineering practice. One reason is the computational cost of the analysis. A linear buckling analysis requires less time to perform, while a nonlinear analysis needs a longer time due to its nature. Another reason is the fact that the critical buckling load calculated by the linear analysis can be easily combined with most design standards (e.g. DIN 18800 T4), because they are based on the linear buckling theory. The main reason why the nonlinear buckling theory is not widely used is the difficulty to find an appropriate initial imperfection shape for the analysis. For this reason this method has not been incorporated in most design standards.

Nonlinear buckling analysis, on the other hand, provides the only possible way to calculate a more realistic critical buckling load, as it can include initial imperfections as well as residual stress and plasticity. The effect of deformation dependent force (e.g. following pressure) can only be calculated by this method. It also provides a good opportunity in recalculating the buckling strength of an existing shell structure by measuring the imperfection shape and using this shape for a nonlinear buckling analysis. A nonlinear buckling analysis is thus the only way of calculating the post-buckling behaviour of a structure, which can be of interest as some shell structures can reach a stable post-buckling state instead of total failure.

Chapter 4

Bifurcation Analysis of a Spherical Cap

4.1. Introduction

The finite element method (FEM) is used to investigate the buckling behaviour of a hinged and clamped spherical cap subjected to radial uniform pressure.

A bifurcation (eigenvalue) analysis with FEM (see 3.2.) is carried out. The results are then compared with the theoretical solution described in 1.4.2..

4.2. Description of the Geometry and Loading

The geometry of the investigated spherical cap is described as part of a whole sphere (Figure 4.1).

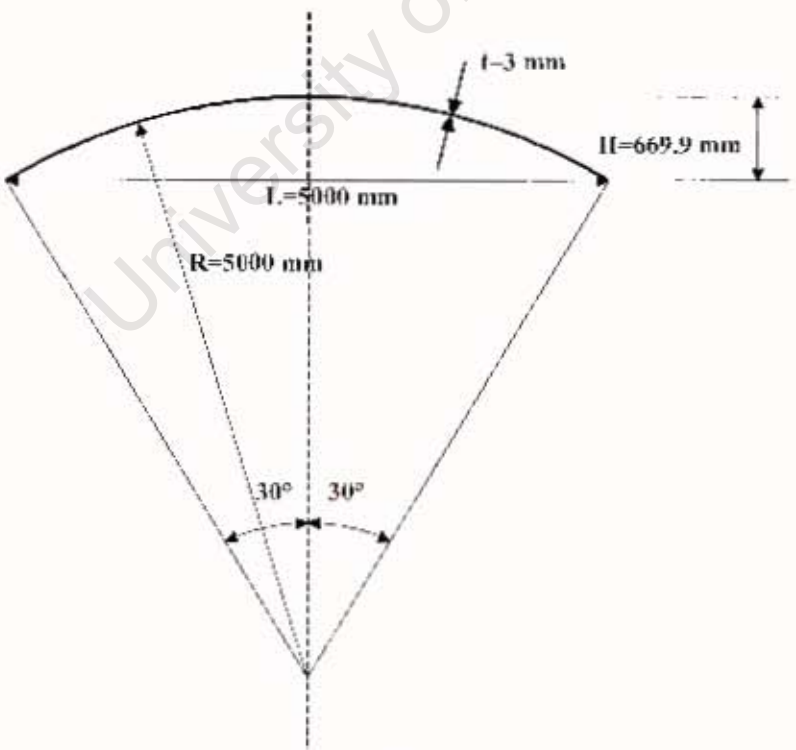

Fig. 4.1: Geometry of the investigated spherical cap

The investigated spherical cap has a radius R of 5000 mm and the thickness t is 3 mm which leads to a R/t-ratio of 1666.7. The angle φ_0 (Figure 1.7) referring to the axis of revolution of 30° leads to a height H of 669.9 mm and a diameter L at the base of 5000 mm. The cap material is steel with a Young's modulus E of 200000 N/mm² and a Poisson's ratio υ of 0.3.

The cap is loaded with uniform radial pressure acting towards the centre of the cap. The supporting edge of the cap is either clamped (Figure 1.9) or hinged (Figure 1.10).

4.3. Discretization with FEM and Solution

The spherical cap is modelled using the general purpose finite element package MSC.MARC/ Mentat 2000. As the geometry and loading is axisymmetric, an axisymmetric shell element (MSC.MARC type 1) is used with the x-axis being the axis of revolution (Figure 4.2). The buckling modes are assumed to be axisymmetric.

A linear-elastic material-law is used for this analysis. The pressure is applied with a value of 1, as a uniform load over the elements, acting perpendicular to the outer surface of the cap (Figure 4.2)

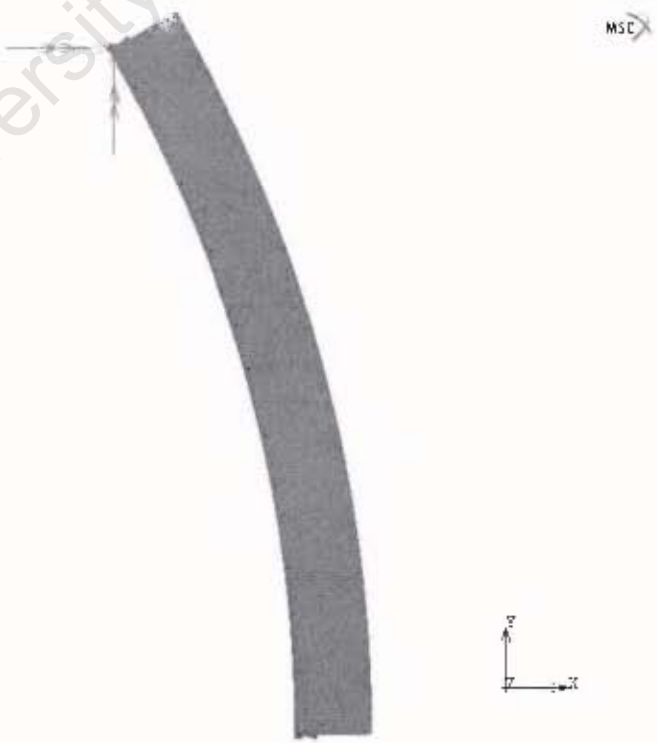

Fig. 4.2: Axisymmetric model of the spherical cap

The mesh is very fine, as it will also be used for the subsequent analyse (see Chapter 5). Each element has a length of 0.52 mm.

A bifurcation analysis is performed. The theoretical background to this analysis is described in 3.2.. The first 15 eigenmode are extracted by the "inverse power sweep" method and the load factor λ_i are printed for every eigenmode.

The applied pressure was chosen as a value of 1 so the load factor has the same value as the critical buckling load.

4.4. Results

4.4.1. Clamped Spherical Cap

The lowest critical pressure obtained from this analysis for the clamped spherical cap is 0.08775 N/mm². The corresponding eigenmode is plotted in Figure 4.3.

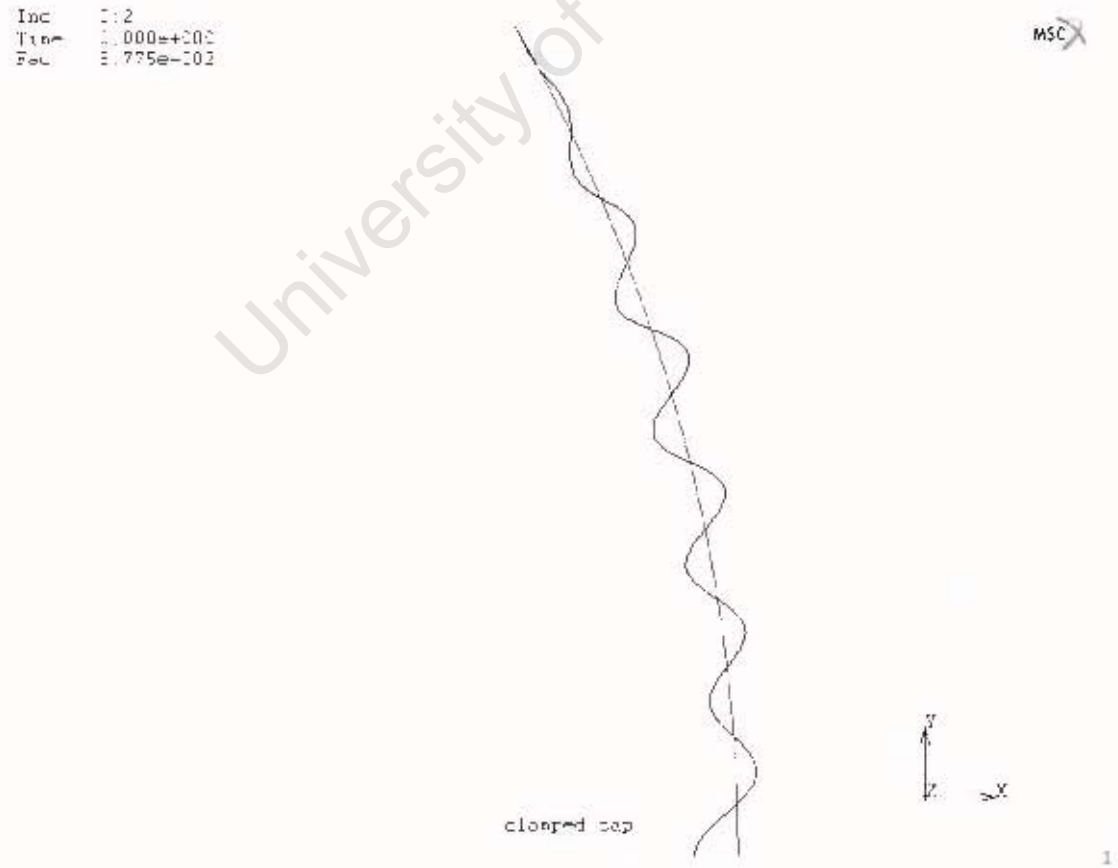

Fig. 4.3: Clamped cap, eigenmode 2, critical pressure 0.08775 N/mm²

The number of waves n over the arc is 11.5. The chosen mesh was fine enough to describe the buckling modes accurately. No curvature change reversals in a single element or discontinuities in the shape were found. All calculated eigenmodes, together with their corresponding critical pressure, can be found in Appendix A.

4.4.2. Hinged Spherical Cap

The lowest critical pressure obtained from this analysis for the hinged spherical cap is 0.08751 N/mm². The corresponding eigenmode is plotted in Figure 4.4.

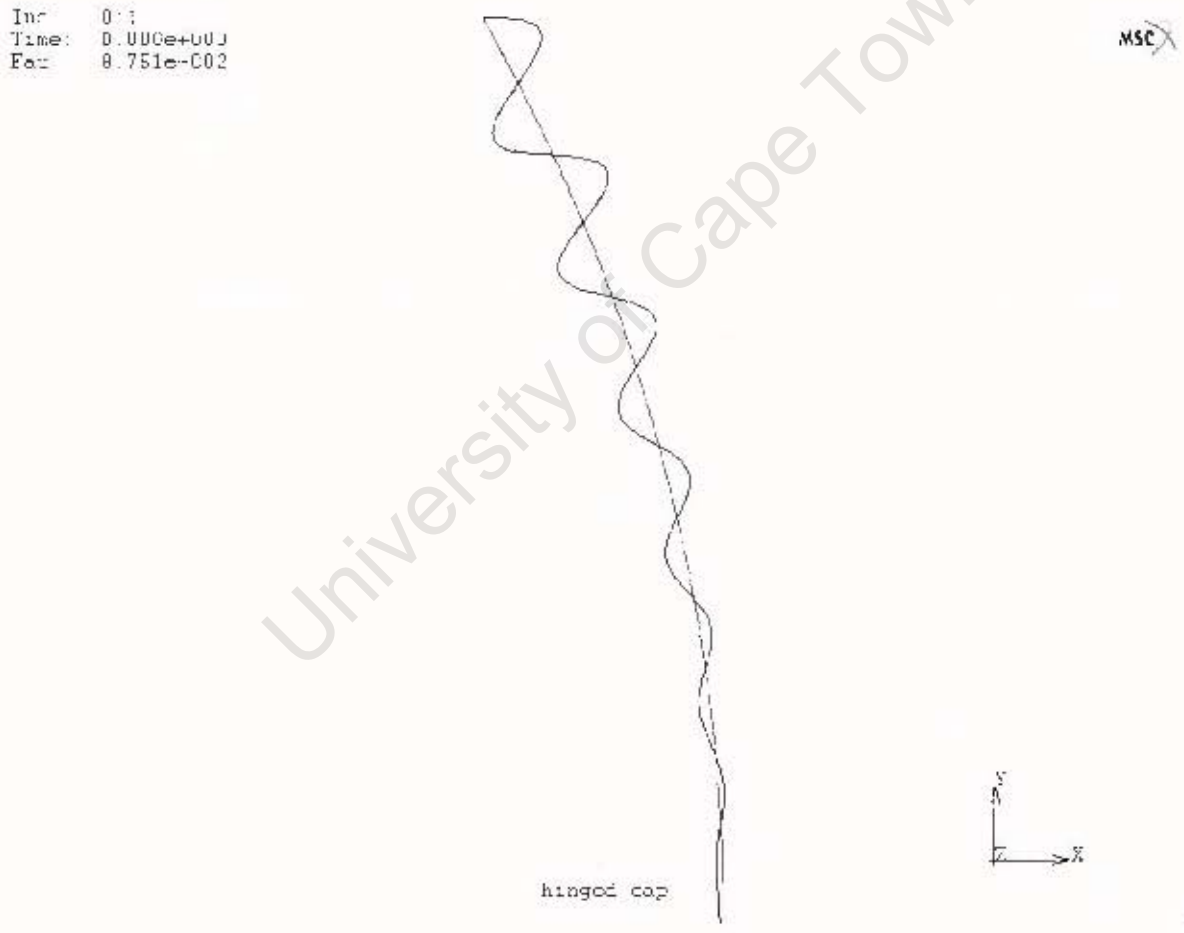

Fig. 4.4: Hinged cap, eigenmode 1, critical pressure 0.08751 N/mm²

The number of waves n over the arc is 12. The chosen mesh was fine enough to describe the buckling modes accurately. No curvature change reversals in a single element or

discontinuities in the shape were found. All calculated eigenmodes, together with their corresponding critical pressure, are shown in Appendix B.

4.5. Conclusions

A linear bifurcation analysis with finite element methods for a spherical cap with a fully clamped and hinged edge was performed.

The theoretical solution described in 1.4.2. for a spherical cap subjected to radial uniform pressure leads to:

$$p_{cr,sph}^{lin} = \frac{2}{\sqrt{3(1-\upsilon^2)}} E \frac{t^2}{R^2} = \frac{2}{\sqrt{3(1-0.3^2)}} \cdot 2000000 \cdot \frac{3^2}{5000^2} = 0.08715 N/mm^2 \qquad (4.1)$$

Comparing this value with the value for the clamped and hinged spherical cap obtained from the analysis shows a difference of 0.68 % for the clamped and a difference of 0.41% for the hinged cap. The clamped cap can carry a slightly higher pressure before buckling occurs due to the larger stiffness of the structure. The difference between the clamped and hinged cap is 0.27% (Table 1).

	clamped cap (FEM)	hinged cap (FEM)	theoretical solution
critical pressure [N/mm²]	0.08775	0.08751	0.08715

Table 1: Comparison of results

There is good consistency between the numerical (FEM) and the theoretical solution. The linear buckling analysis with FEM provides a good method for calculating the linear critical buckling load for these types of shell structure. The obtained value can be easily combined with existing design standards (e.g. DIN 18800 T4) as they are based on the same theoretical background. The computer cost of this analysis is relatively cheap. The computation time on a normal personal computer was less than one minute for a model of 5000 elements.
It should be noticed that the obtained results are "theoretical" buckling loads which may differ from the real buckling load (see 3.2.).

Chapter 5

Effect of a Circumferential Weld On the Buckling Behaviour of a Spherical Cap

5.1. Introduction

Metal shell structures are often constructed by welding curved plates together. Due to the cooling process shrinkage occurs parallel and perpendicular to the weld (see 1.5.3). The shrinkage of the cooling weld imposes a radial inward force on the shell of revolution. This leads to a geometric imperfection and to residual stress in the shell. It appears that the influence of this imperfection on the buckling behaviour has only been investigated on cylindrical and conical shells of revolution (see 1.5.4.1.). In this chapter a nonlinear finite element analysis is carried out to investigate the buckling behaviour of a spherical cap with a circumferential weld depression.

5.2 Description of the Geometry and Loading

The same geometry and loading described in Chapter 4 is again used for this investigation. The geometry of the investigated spherical cap is described as part of a whole sphere (Figure 5.1).

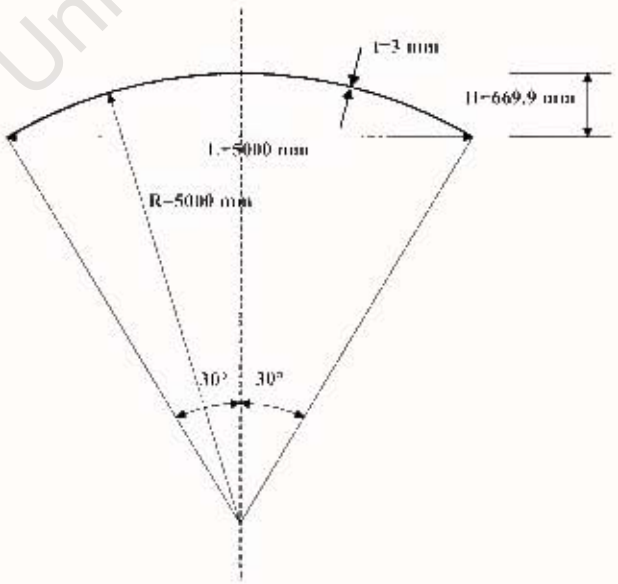

Fig. 5.1: Geometry of the investigated spherical cap

The spherical cap has a radius R of 5000 mm and the thickness t is 3 mm which leads to a R/t-ratio of 1666.7. The angle φ_0 (Figure 1.7) referring to the axis of revolution of 30° leads to a height H of 669.9 mm and a diameter L at the base of 5000 mm.

The steel material used in the test (S235JRG2) has a Young's modulus E of 210000 N/mm² and a Poisson's ratio υ of 0.3. The characteristic yielding stress $\sigma_{y,c}$ for the used material is 240 N/mm².

The cap is loaded with an uniform radial pressure acting towards the centre of the cap. The supporting edge of the cap is either clamped (Figure 1.9) or hinged (Figure 1.10).

5.2.1. Description of the Circumferential Weld

A circumferential weld is applied uniform around the spherical shell. The location of the weld is described by the angle β referring to the axis of revolution (Figure 5.2).

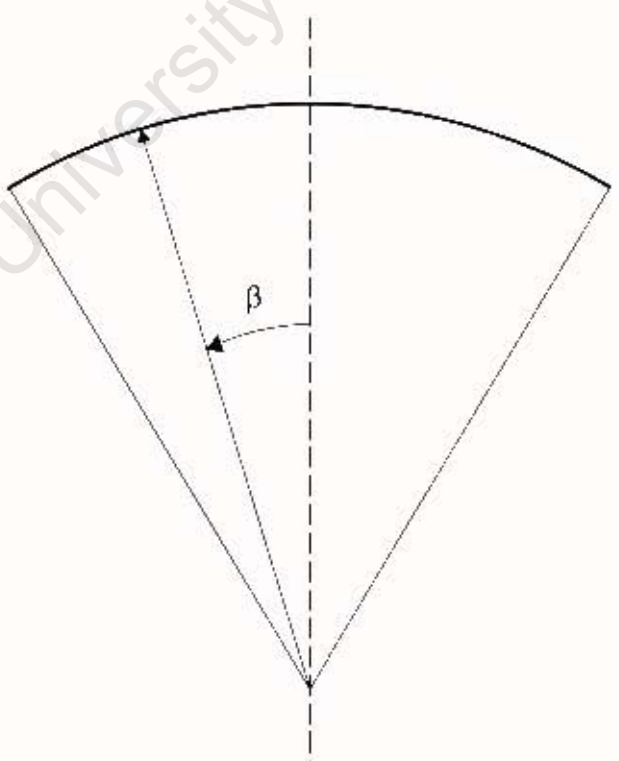

Fig. 5.2: Location of the circumferential weld

Welded samples were examined in order to measure the size of the area that was melted during the welding process, as this is the area where shrinkage due to cooling will occur. This area can be easily identified by looking at the microstructure of the material. The welding samples were cut perpendicular to the weld. The cut surfaces were polished and pictures of the microstructure were taken. Figure 5.3 shows the microstructure of a normal steel before welding.

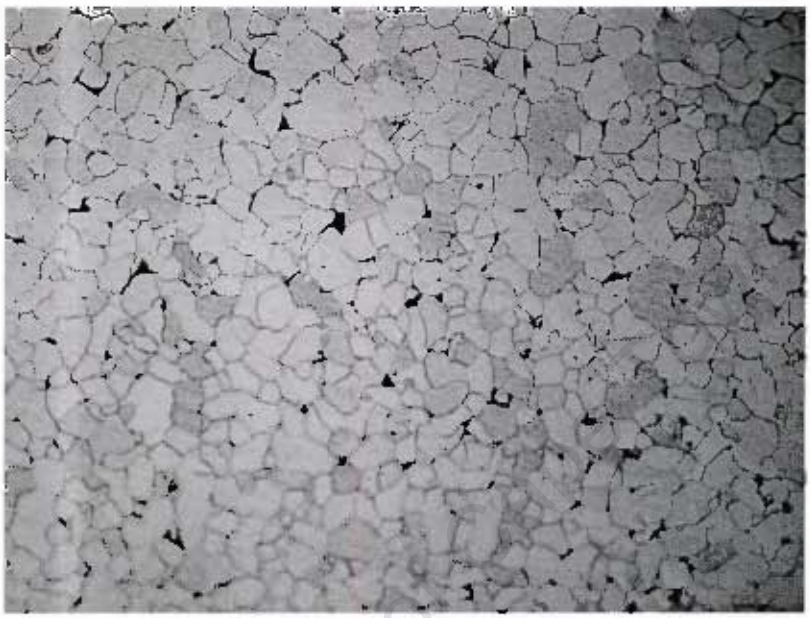

Fig. 5.3: Microstructure of normal steel

The microstructure in the middle of the weld is shown in Figure 5.4.

Fig. 5.4: Microstructure of the weld

The zone next to the welded material is called the "heat influence zone". The change between the weld into this zone can be seen in Figure 5.5. The left side of the picture shows the microstructure of the weld and the right side the microstructure of the heat influence zone.

Fig. 5.5: Change welded material – heat influence zone

Another change in the microstructure can be seen when the heat influence material changes back to the normal material (Figure 5.6).

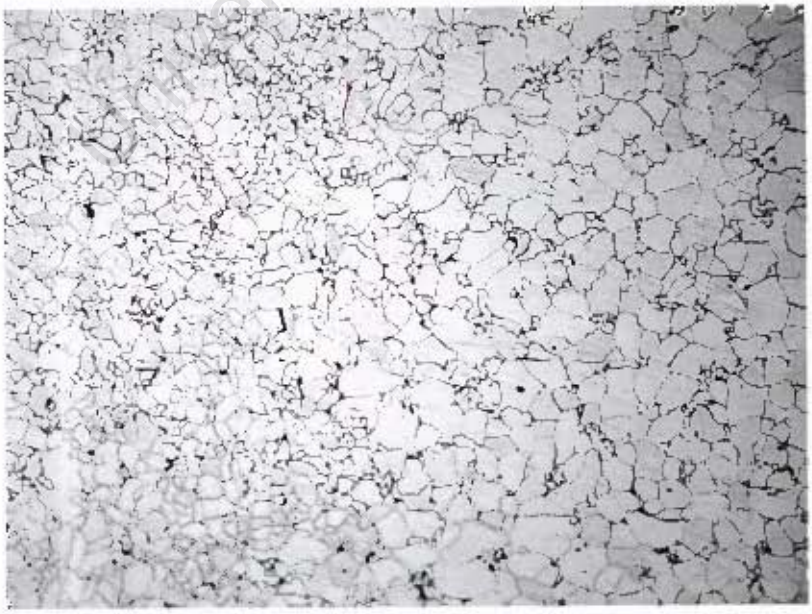

Fig. 5.6: Change heat influence zone – normal material

The microstructure of the heat influence zone can be seen on the left side and the microstructure of the normal material on the right side.

Melting of the material and therefore shrinkage due to the cooling process occurred in the zone of the welded material and in the heat influence zone. The length $l_{heating\beta}$ of these two zones, perpendicular to the weld (Figure 5.7), is measured in order to model the shrinkage in the finite element model.

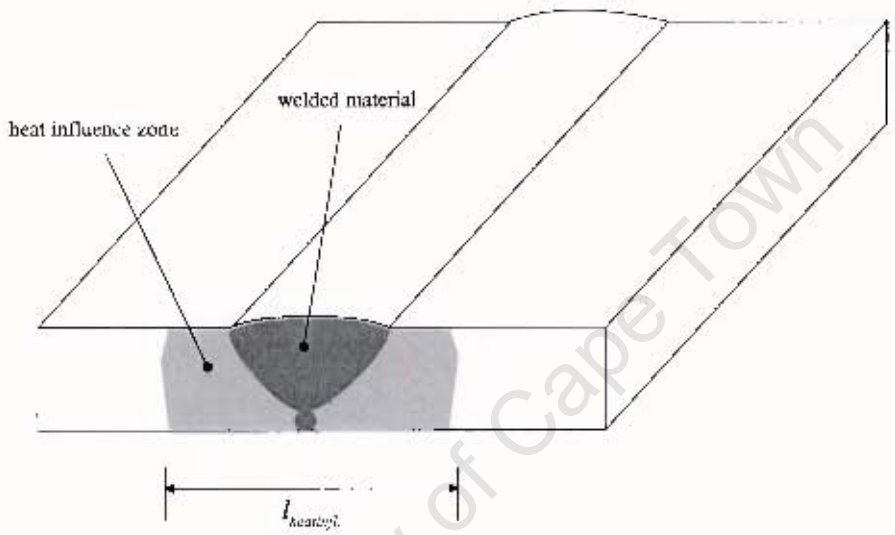

Fig. 5.7: Measurement of $l_{heating\beta}$

Changes in material characteristics due to the welding process (e.g. ductility of the material) are not taken into account in the analysis. The weld is assumed to be fully elastic during the cooling process.

5.3. Discretization with FEM

The general purpose finite element package MSC.MARC/Mentat is used to carry out a nonlinear finite element analysis. The same finite element mesh and boundary conditions used in chapter 4 are again used for this analysis. A linear-elastic material-law is used.

The approximation of the weld distortion is based on the assumption that a constant circumferential tensile stress σ_0 acts as in a circumferential strip of $l_{heating\beta}$.

In a conservative approach, σ_0 can be estimated by

$$\sigma_0 = \sigma_{y,c} \tag{5.1}$$

with $\sigma_{y,c}$ being the lower value of the characteristic yield stress of the welding material or the structural material.

Pre-stressed elements with a value of σ_0 are used to model the distortion due to the welding process using the finite element model. The number of pre-stressed elements n can be easily calculated since a uniform element length over the half arc is used by

$$n = \frac{I_{\text{Segment}}}{\left(\frac{\pi \cdot R \cdot \varphi}{m \cdot 180°}\right)} \tag{5.2}$$

with m being the total number of elements used in the finite element model.

A radial uniform pressure with the magnitude of the critical classical buckling load (see 1.4.2.) for the structure is applied (Figure 5.8).

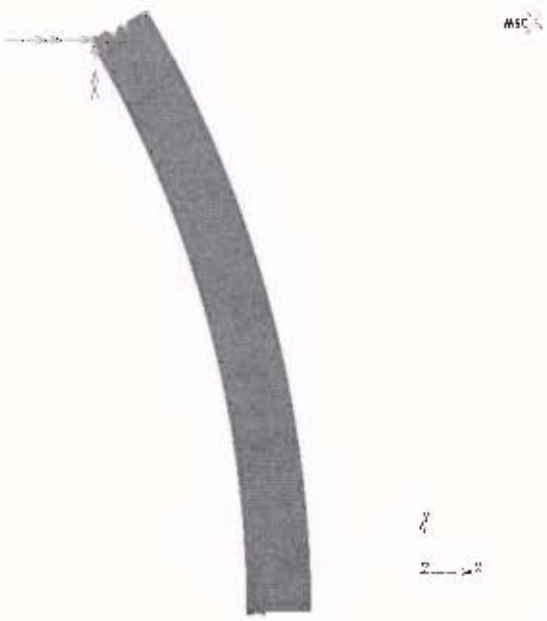

Fig. 5.8: Axisymmetric model of the spherical cap with loading

5.4. Solution Procedure with FEM

A two step solution procedure is applied to solve the described problem with the finite element method.

The first step is to apply the pre-stress σ_0 on the selected elements. The system is then solved without any additional load. This procedure ensures that the applied stresses form an equilibrium.

A sample deformed shape after this procedure can be seen in Figure 5.9.

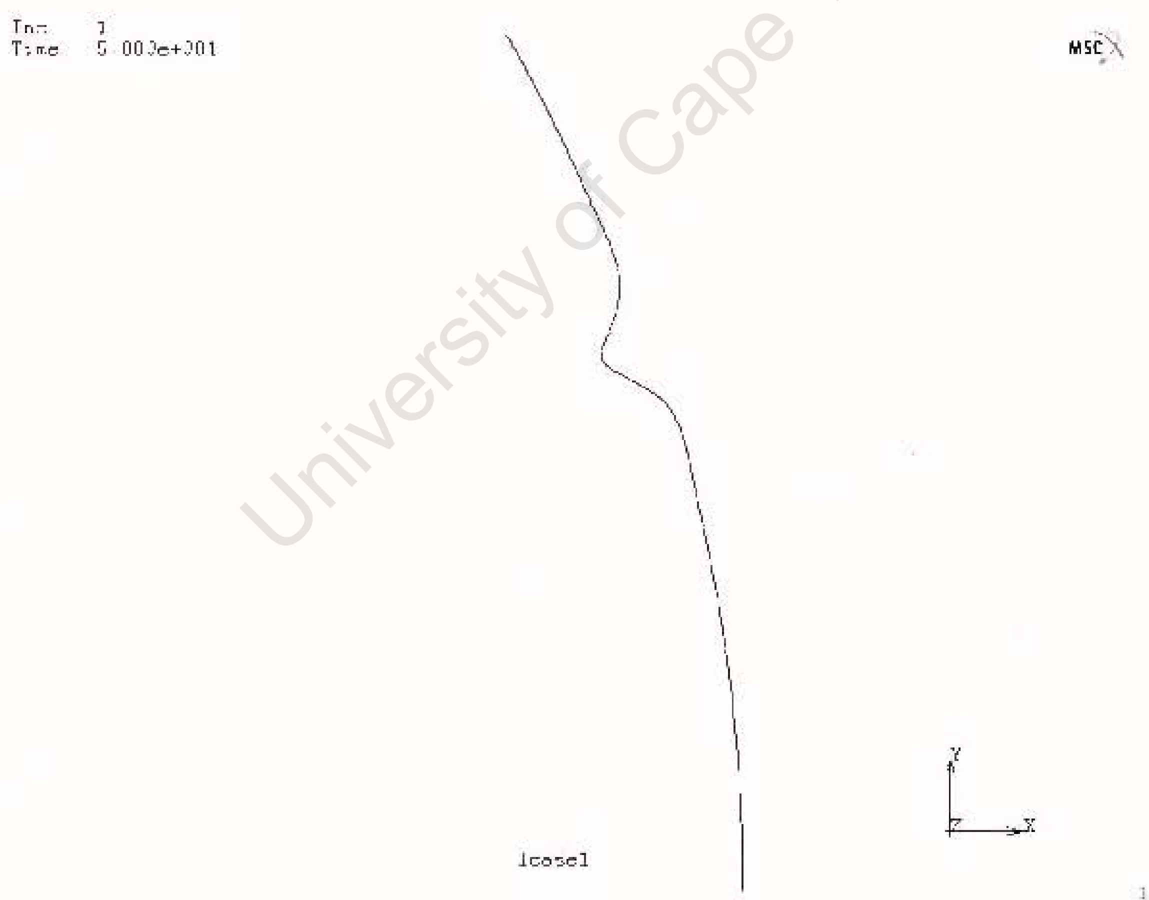

Fig. 5.9: Assumed imperfection shape after solution step 1

The second step is to apply the radial uniform pressure (Figure 5.8). The major difficulty for this type of analysis is to overcome the singularity of the incremental tangent stiffness matrix when the structure reaches its stability limit. The arc length method (see 2.3.3.3.) together with the updated Lagrangian formulation (see 2.3.2.4.) is therefore used to apply the load step-wise for this nonlinear analysis.

5.5. Results

The effect of a circumferential weld depression on the buckling behaviour of a fully clamped cap was investigated for $\beta = 10°$, $\beta = 15°$ and $\beta = 20°$ (Figure 5.2).

The hinged and clamped cap were loaded with a radial uniform pressure of the same magnitude as the classical buckling load according to 1.4.2.:

$$p_{cr,cap}^{lin} = \frac{2}{\sqrt{3(1-\upsilon^2)}} E \frac{t^2}{R^2} = \frac{2}{\sqrt{3(1-0.3^2)}} \cdot 2100000 \cdot \frac{3^2}{5000^2} = \underline{\underline{0.09151 N/mm^2}} \qquad (5.3)$$

σ_0 was chosen to be the characteristic yielding stress of the structural material (S235JRG2) throughout the analysis (see 5.4):

$$\sigma_0 = \sigma_{y,k} = 240 N/mm^2 \qquad (5.4)$$

$l_{heating}$ was set to 13 mm based on the measurement of welding samples (see 5.2.1).
This leads to (see equation (5.2))

$$n = \frac{l_{heating}}{\left(\frac{\pi \cdot R \cdot \varphi}{m \cdot 180°}\right)} \qquad \frac{13}{\frac{\pi \cdot 5000 \cdot 30°}{5000 \cdot 180°}} \approx 25 \qquad (5.5)$$

pre-stressed elements.

5.5.1. Clamped Spherical Cap

The clamped spherical cap with a circumferential weld depression under the angle $\beta = 10°$ shows a reduction in the buckling strength of 65% compared to the classical buckling strength of a spherical cap. The applied weld depression initiates the buckling deformation. Local buckling occurs mainly in the area between the weld depression and the top of the cap (Figure 5.10). The post-buckling stiffness of the analysed structure can be described as very weak. Snap-through of the hole cap occurs after the critical load is reached.

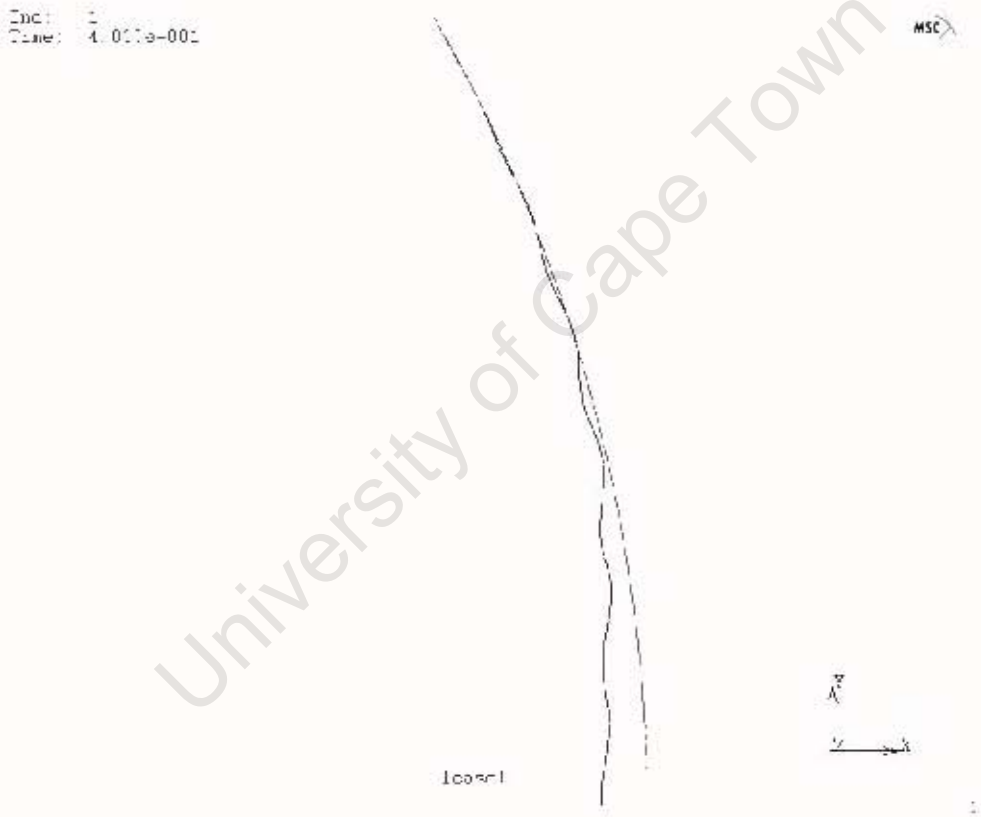

Fig. 5.10: Buckling deformation for $\beta = 10°$ (clamped cap)

The clamped spherical cap with a circumferential weld depression under the angle β =15° shows a similar buckling and post-buckling behaviour. The buckling strength has decreased by 60% compared to the classical buckling strength. The buckling deformation can be seen in Figure 5.11.

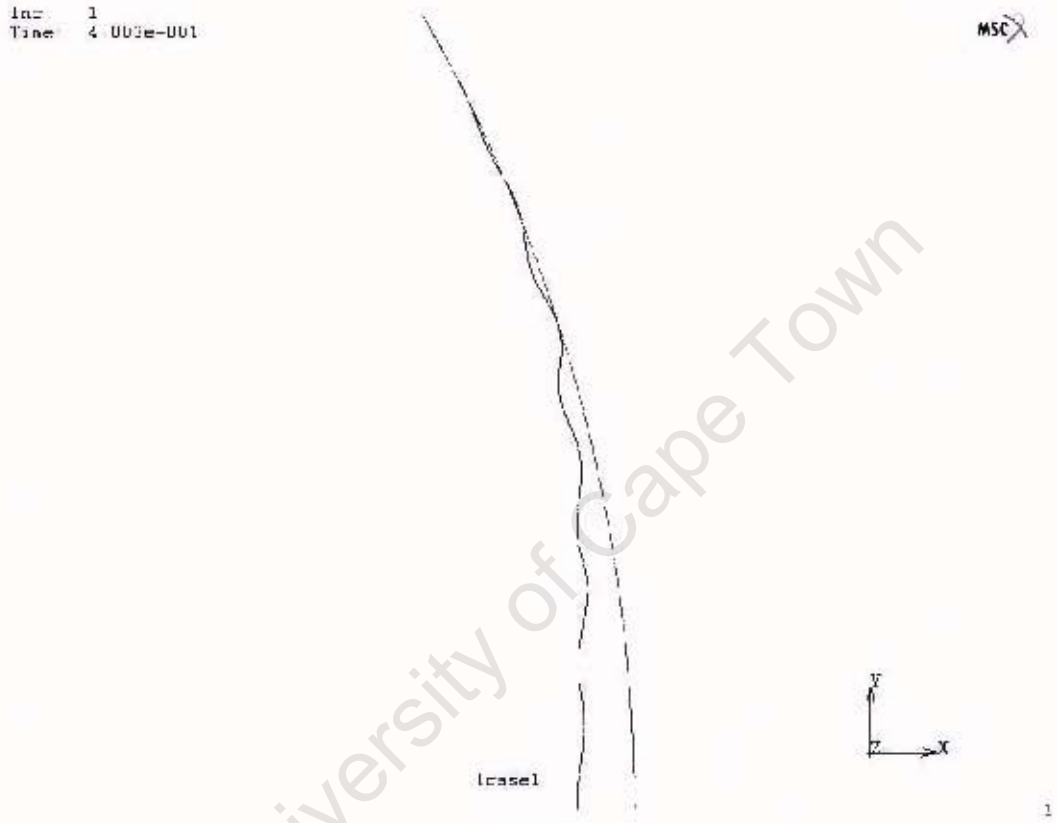

Fig. 5.11: Buckling deformation for β =15° (clamped cap)

For β =20° a decrease of 55% in the buckling strength can be found. The cap shows the same buckling and post-buckling behaviour as the caps with weld depression under the angle β =10° and β = 15°. The buckling deformation can be seen in Figure 5.12.

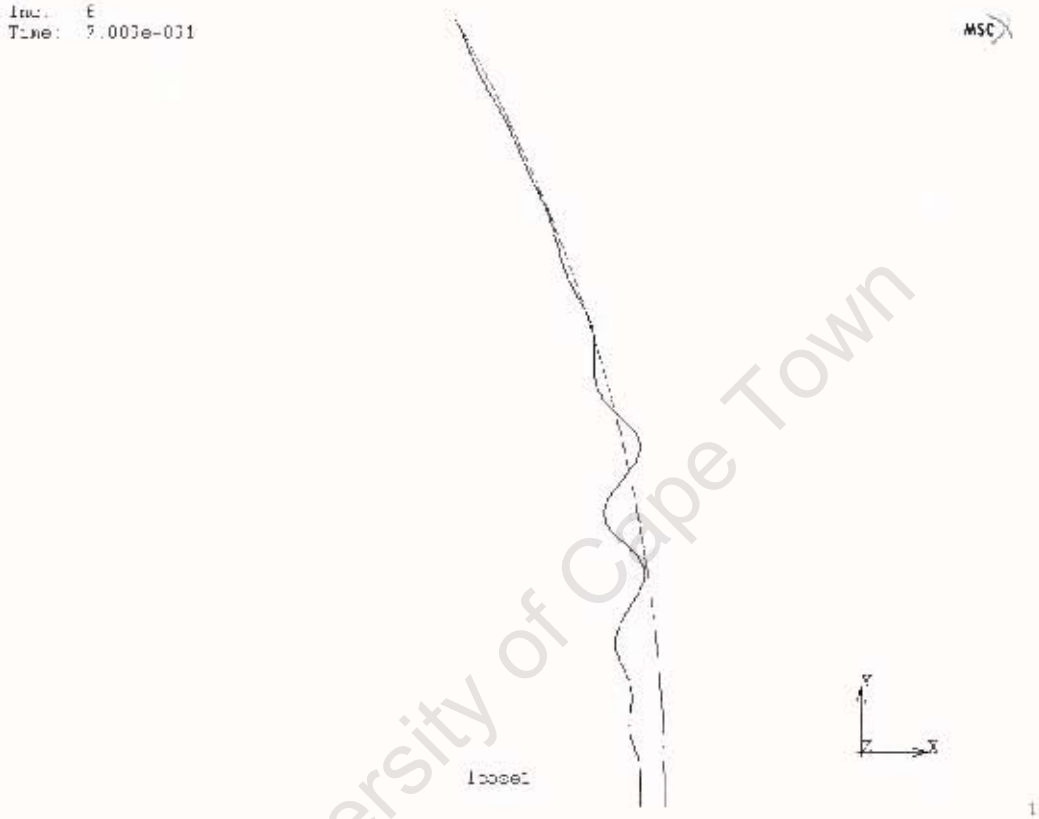

Fig. 5.12: Buckling deformation for β =20° (clamped cap)

The circumferential weld depression leads to a decrease in the buckling strength for the clamped spherical cap in the area of 60% . The buckling strength increases towards the edge of the investigated spherical cap. All results are listed for comparison in Table 5.1.

β	10°	15°	20°
[%] of the classical buckling load	35	40	45

Table 5.1: Results for the clamped cap

5.5.2. Hinged Spherical Cap

The hinged spherical cap with a circumferential weld depression under the angle $\beta = 10°$ shows a 65% decrease in the buckling strength compared to the classical buckling strength of a spherical cap.

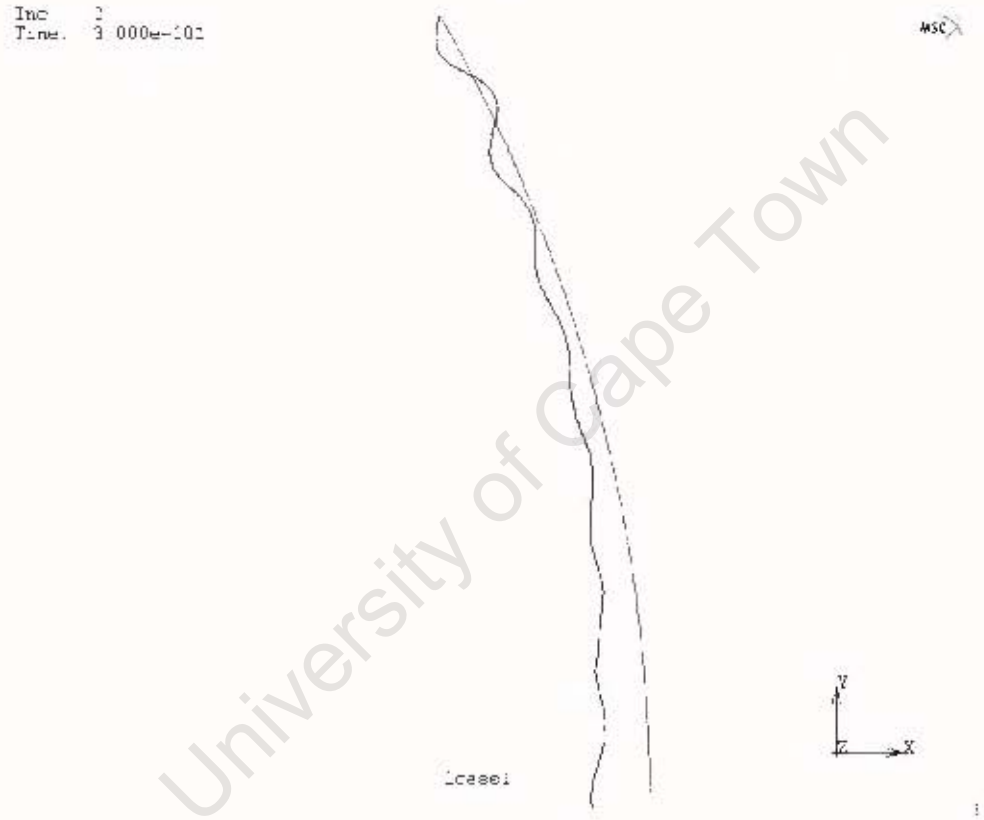

Fig. 5.13: Buckling deformation for $\beta = 10°$ (hinged cap)

The applied weld depression initiates the buckling deformation (Figure 5.13). Local buckling occurs mainly in the area between the edge of the cap and the weld depression. The post-buckling stiffness of the analysed structure can be described as very weak. Snap-through occurs after the critical load is reached (Figure 5.14).

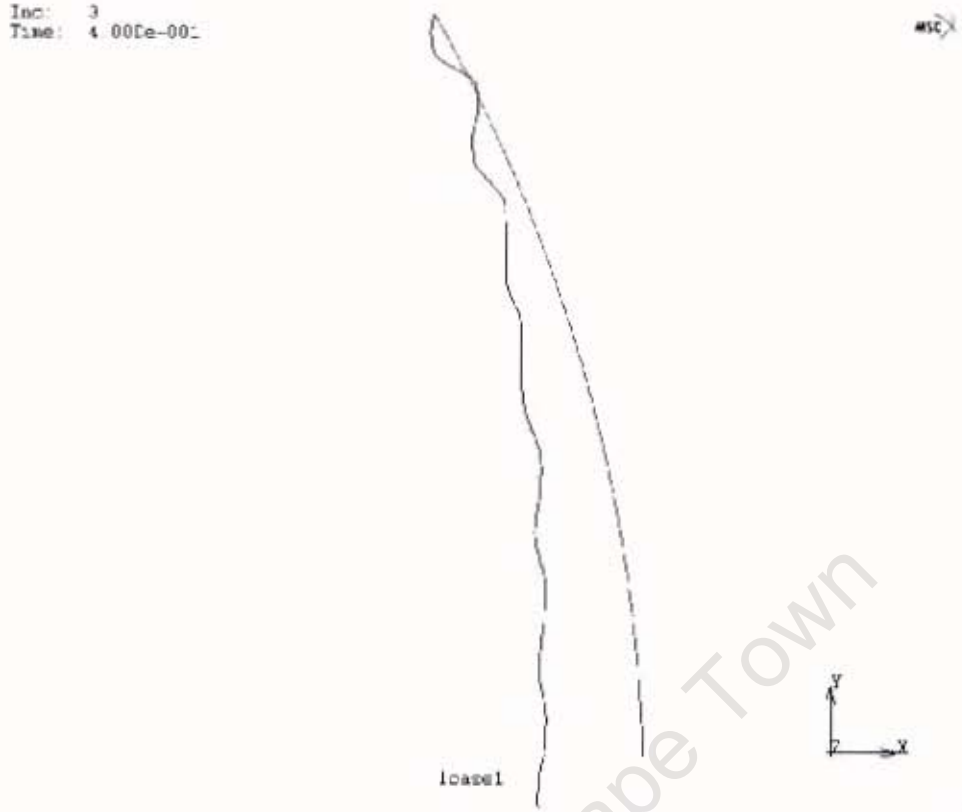

Fig. 5.14: Post-buckling deformation of the hinged cap

The clamped spherical cap with a circumferential weld depression under the angle $\beta = 15°$ shows a similar buckling and post-buckling behaviour. The buckling strength is decreased by 70% compared to the classical buckling strength. The buckling deformation can be seen in Figure 5.15.

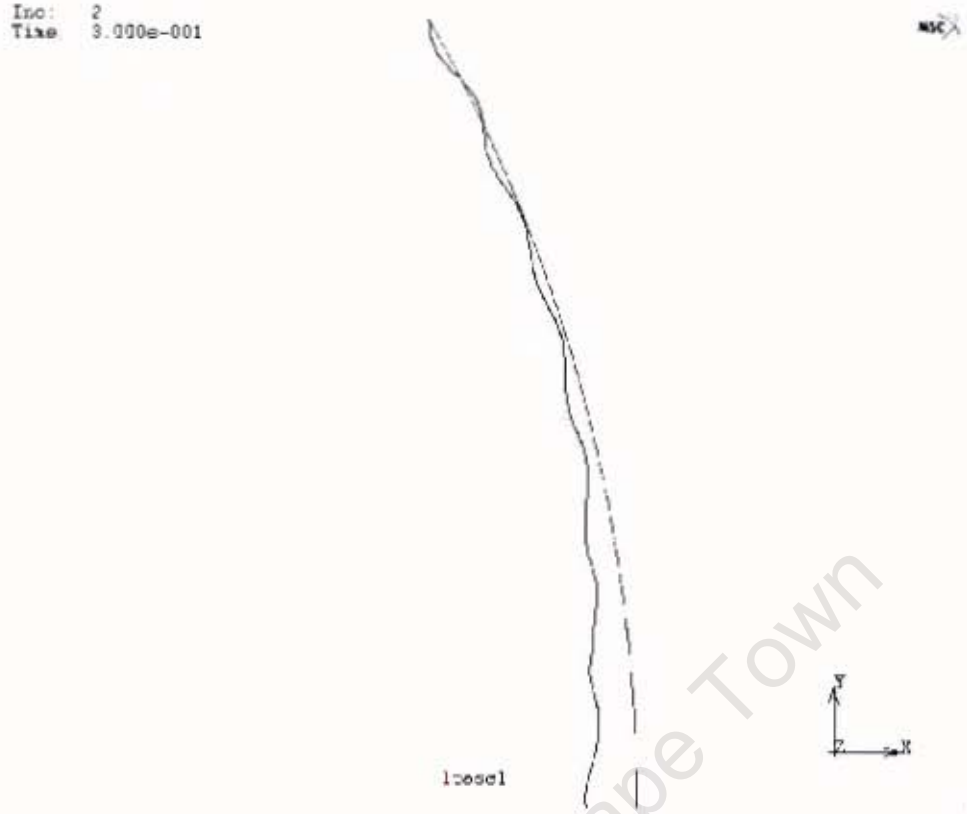

Fig. 5.15: Buckling deformation for β =15° (hinged cap)

For β =20° a decrease of 75% in the buckling strength can be found. The cap shows the same buckling and post-buckling behaviour as the caps with weld depression under the angle β =10° and β =15° respectively. The buckling deformation can be seen in Figure 5.16.

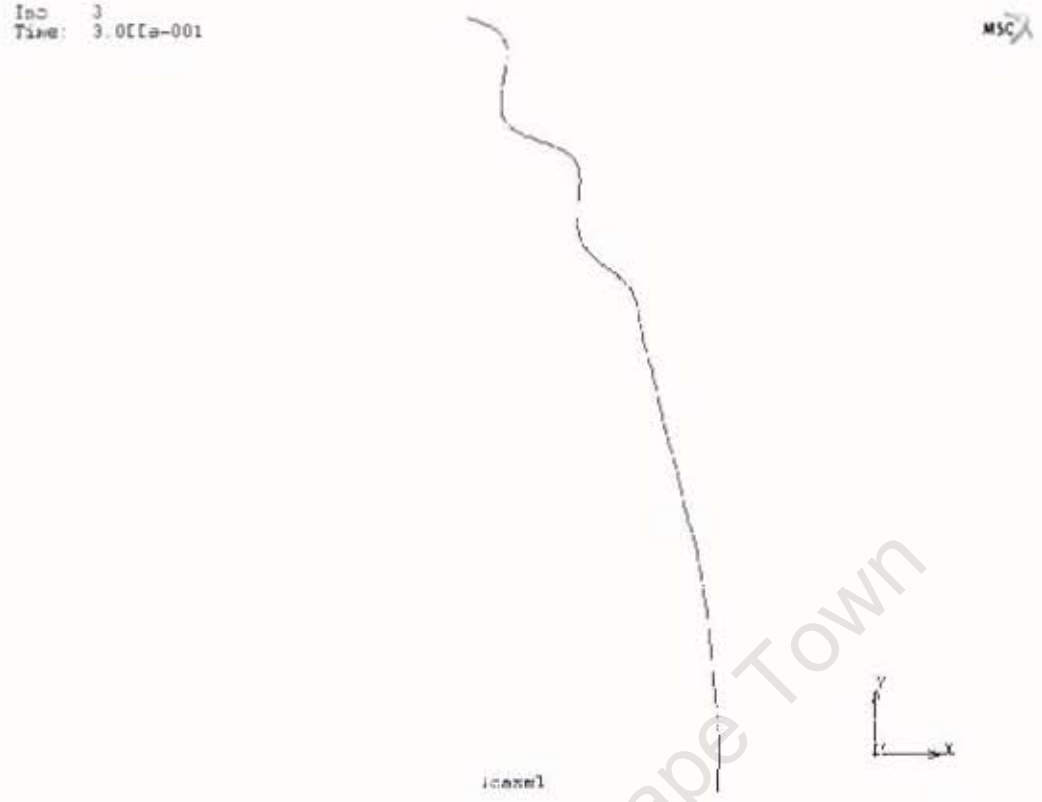

Fig. 5.16: Buckling deformation for β =20° (hinged cap)

The circumferential weld depression leads to a decrease in the area of 30% in the buckling strength of the hinged spherical cap. The buckling strength decreases towards the edge of the investigated spherical cap. All results are listed for comparison in Table 5.2.

β	10°	15°	20°
[%] of the classical buckling load	25	30	35

Table 5.2: Results for the hinged cap

5.5.3. Comparison of Clamped and Hinged Spherical Cap

The results for the clamped and hinged spherical cap with a circumferential weld depression are compared in Figure 5.17.

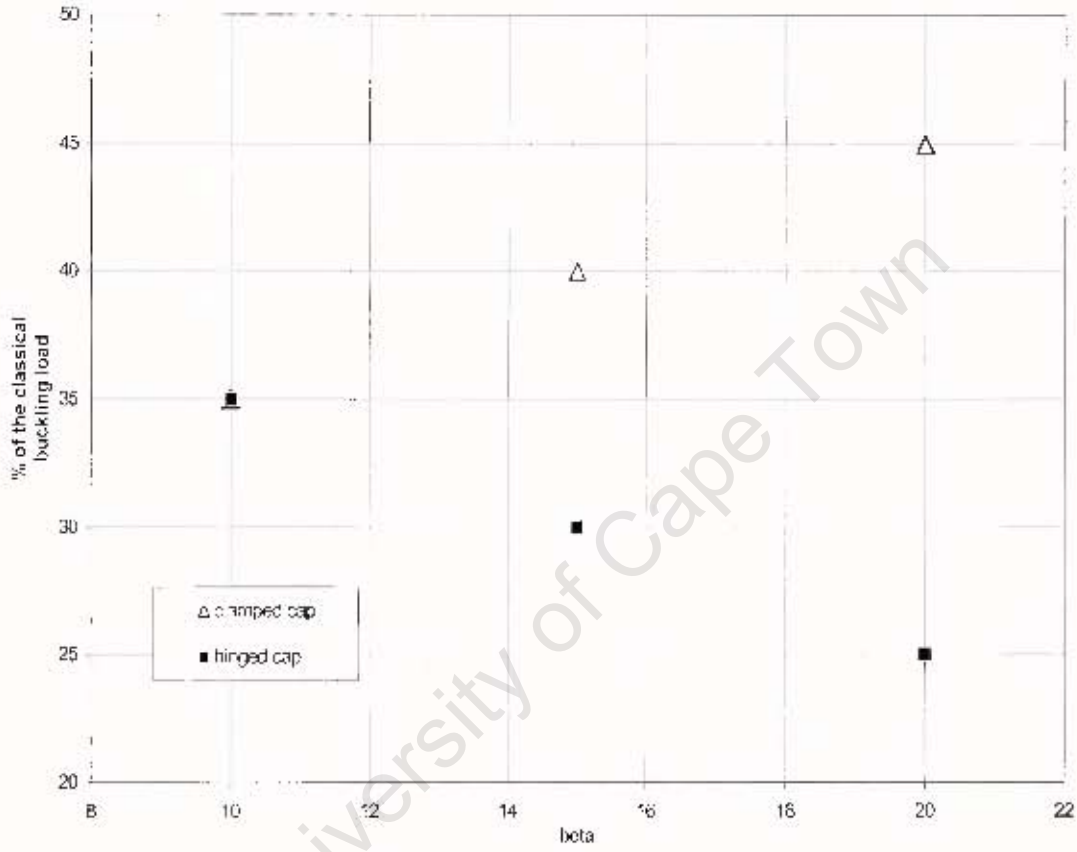

Fig. 5.17: Comparison of results for different edge conditions

The buckling strength of the investigated cap depends on its boundary conditions. The clamped spherical cap shows an increase of 35% in the buckling strength compared to the classical buckling strength for β =10° and an increase of up to 45% for β =20°. The hinged cap exhibits an opposite behaviour. The buckling strength decreases from 35% for β =10° to 25% for β =20°.

Both structures show a similar post-buckling behaviour. The post-buckling stiffness of both structures can be described as weak. Snap-through occurs in both cases after the critical load has been reached.

5.5.4. Discussion of Results

The hinged and the clamped spherical cap under uniform external pressure with a circumferential weld depression show a decrease of a similar magnitude in the buckling strength compared to investigations on cylindrical shells under axial loading (see 1.5.4.1.). This behavior agrees with the well-known similarities in the buckling behaviour of cylindrical shells under axial loading and spherical shell under uniform external pressure. Both groups of structures show a multi-mode buckling behaviour, which makes them very sensitive to initial imperfections.

Hutchison (1967) (see 1.5.3.) showed that an imperfection of the same shape of the eigenmode shape leads to the greatest reduction in the buckling strength of a spherical cap. The shape of the circumferential weld depression is similar to the eigenmode shapes of the spherical cap (see chapter 4 and appendix A, B), which explains the low buckling loads obtained by the analysis carried out. The postbuckling deformations shown have a very similar shape compared to the eigenmode shapes, which supports to this idea.

The clamped and the hinged spherical cap show the same reduction in the buckling strength if the weld is located near the top of the cap. The boundary conditions have no significant influence if the weld is located near the top of the cap

The increase in buckling strength with the weld closer to the edge of the clamped cap can be explained by the larger stiffness of the cap in this area due to the clamped edge of the cap. The hinged cap an the other hand is less stiff closer to the edge of the cap, which explains a decrease in the buckling strength compared to the case where the weld depression is located closer to the top of the cap

Chapter 6
Conclusions and
Recommendations for Further Investigation

The calculation of the stability load of shell structures provides an unlimited range of challenges for engineers. This thesis has provided a literature review in the area of shell stability with a special focus on spherical shells and the effects of imperfections due to the manufacturing process.

An introduction into linear and nonlinear finite element analysis was also provided. Different types of buckling analysis with finite element methods were discussed.

A bifurcation analysis of a pressure loaded spherical cap with FEM was carried out. Good consistency between the theoretical and the numerical solution was found. Bifurcation analysis with FEM provides a good method to calculate the classical buckling load. It can be easily combined with existing design standards because of the same theoretical background.

The effect of a circumferential weld depression on the buckling behaviour of a rather thin ($R/t=1667$) clamped and hinged spherical cap subjected to radial uniform pressure was investigated by using nonlinear finite element methods. The modelling of the weld depression was described in detail. The results show a significant decrease in the buckling strength due to the circumferential weld depression.

The clamped spherical cap shows a decrease of between 65% and 55% (mean 60%) and the hinged spherical cap a decrease of between 75% and 65% (mean 70%) depending on the location of the weld depression.

Comparison of the results, together with the results of investigation on the effect of a circumferential weld depression on the buckling behaviour of cylindrical shells, subjected to axial loading (see 5.5.4.), shows a decrease in the buckling strength of a similar magnitude.

It has been shown that the boundary conditions of the edge have an influence on the buckling strength of the spherical cap with a circumferential weld depression. The clamped spherical cap shows a decrease in the buckling strength if the weld is located near the top of the cap, while the hinged spherical cap shows an opposite behaviour with regards to the buckling strength.

The effect of a circumferential weld depression was modelled by assuming a relatively simple imperfection shape. Measurement of real imperfection shapes due to welding should be on full-scale structures to improve the accuracy of this analysis. Nevertheless, the described method provides a good way to investigate the effect of weld depressions under different conditions and can be applied to all kinds of shells of revolution.

The given numerical results obtained from the analysis can only give an estimate about the decrease in the buckling strength and it must be verified with experimental results.

List of References

Arbocz, J. (1982): "The Imperfection Data Bank, a Mean to Obtain Realistic Buckling Loads",
Buckling of Shells, Springer Verlag Berlin, p. 535-567

Arbocz, J. (1991): "Towards an Improved Design Procedure for Buckling Critical Structures",
Buckling of Shell Structures on Land, in the Sea and in the Air, Elsevier Applied Science, London, p. 270-276

Arbocz, J. and Babcock, C.D. (1981): "Computerised Stability Analysis Using Measured Initial Imperfections",
Proc. of 12th Congress of Int. Council of Aeronaut Sci., Oct 12-17, München, p. 688-701

Arbocz, J. and Holl, J.M.A.M. (1991): "Collapse of Axially Compressed Cylindrical Shells with Random Imperfections",
AIAA Journ., No. 29(12), p. 2247-2256

Bornscheuer, F. W. ; Hafner, L. and Ramm, E. (1983): "Zur Stabilität eines Kreiszylinders mit einer Rundschweißnaht unter Axialbelastung" (in German),
Der Stahlbau 52, Heft 11

Bornscheuer, F. W. and Hafner, L. (1983): "The Influence of an Imperfect Circumferential Weld on the Buckling Strength of Axially Loaded Circular Cylindrical Shells",
Proc. 3rd Int. Colloquium on the Stability of Metal Structures, p. 407-414

Budiansky, B. (1960): "Buckling of Clamped Shallow Spherical Shells",
Proc. Symp. Theory Thin Elastic Shells, Delf, The Netherlands

Budiansky, B. and Hutchison, J.W. (1966): "A Survey of Some Buckling Problems"
AIAA Journ., Vol. 4 (9), p. 1505

Calladine, C.R. (1983): "Theory of Shell Structures ",
Cambridge University Press, Cambridge

Calladine, C.R. (1995): "Understanding Imperfectionsensitivity in the Buckling of Thin-Walled Shells",
Thin-Walled-Structures, No. 23(14), p. 215-235

Citerley, R.L. (1982): "Imperfection Sensitivity and Post-Buckling Behaviour of Shells",
Pressure Vessels and Piping: Design Technology 1982, ASME, New York, p. 27-45

Clarke, M.J. and Rotter, J.M. (1988): "A Technique for the Measurement of Imperfections in Prototype Silos and Tanks",
Research Report R565, Univ. of Sydney, Australia

Ding, X. (1995): "Surface Profiling Systems for Measurement of Large Scaled Steel Silos",
PhD thesis, School of Civ. Eng. , Univ. of Sydney, Australia

Ding, X., Coleman, R. and Rotter, J.M. (1996): "Technique for Precise Measurement of Large-Scale Silos and Tanks",
Journ. Surv. Eng. 122, No. 1, p. 14-25

Donnel, L.H. (1934): "A New Theory for the Buckling of Thin Cylinders under Axial Compression",
Trans ASME, No. 56, p. 795-800

Dostanova, S. and Raizer, V. (1973): "Issledovanie ustoichivosti pologih obolochek polozhitel´noi krivinzny metodom lokal´nykh varitsii" (in Russian),
Stroit Mekh. i. Rasch Sooruzh., p. 34-39

El Damatty, A.A.; Korol, R.M. and Mirza, F.A. (1997): "Stability of Imperfect Steel Conical Tanks under Hydrostatic Load",
Journ. of Struc. Eng. 123, No. 6, p. 703-712

Elishakoff, I; Manen, S.; Vermeulen, P.G. and Arbocz, J. (1987): "First Order Second-Moment Analysis of the Buckling of Shells with Random Imperfections".
AIAA Journ., No. 25(8), p. 1113-1117

Ethrog, U. (1986): "Measuring the Deformation of Storage Tanks",
Photogrammetria 40, p. 299-310

Fischer, E. (1989): "Zur Bestimmung von Kreisdeformationen" (in German),
Vermessungstechnik 3, Heft 37, p. 89-91

Flügge, W. (1932): "Die Stabilität der Kreiszylinderschalen" (in German),
Ing.-Archiv 3, p. 463-506

Flügge, W. (1973): "Stresses in Shells",
second edition, Springer-Verlag Berlin

Gocalves, P. and Croll, J. (1992): "Axisymmetric Buckling of Pressure-Loaded Spherical Caps",
Journ. of Struct. Eng. 118, No.4, p. 970-985

Goldberg, J.E.; Korman, T. and Baluch, M.H. (1974): "On the Use of various shell Theories in the Analysis of axisymmetrically loaded circular cylinders",
Nucl. Engng Des., No. 30, p. 88-92

Huang, N.C. (1964): "Unsymmetrical Buckling of Thin Shallow Spherical Shells",
Journ. Appl. Mech. 31, p. 447-457

Hoff, N.J.; Madsen, W.R. and Mayers, J. (1966): "The Postbuckling Equilibrium of Axially Compressed Circular Cylindrical Shells",
AIAA Journ., No. 4, p. 126-133

Hutchison, J.W. (1967): "Imperfection Sensitivity of Externally Pressurised Spherical Shells",
Journ. Applied Mechanics, March 1967, p. 49-55

Hutchison, J.W. and Koiter, W.T. (1970): "Postbuckling Theory",
Applied Mech Review, Vol. 23, p. 1353-1366

Kármán, T. and Tsien, H.S. (1939): "The Buckling of Spherical Shells by External Pressure",
Journ. Aeronautic Sci. 7, p. 43

Kármán, T. and Tsien, H.S. (1941): "The Buckling of Thin Cylindrical Shells Under Axial Compression",
Journ. Aeronautic Sci. 8, p. 303

Kármán, T.; Dunn, L.G. and Tsien, H.S. (1940): "The Influence of Curvature on the Buckling Characteristics of Structures",
Journ. Aeronautic Sci. 7, p. 276

Kempner, J. (1954): "Postbuckling Behaviour of Thin Cylindrical Shells",
Journ. Aero. Sci., No. 21(5), p. 329-334

Koiter, W.T. (1945): "On the Stability of an Elastic Equilibrium",
thesis, Delf, The Netherlands

Koiter, W.T. (1963): "Elastic Stability and Post-Buckling Behaviour",
Proceedings Symposium on Nonlinear Problems,
University of Wisconsin Press, Madison, p. 257

Kollár, L. and Dulácska E. (1984): "Schalenbeulen, Theorie und Ergebnisse der Stabilität gekrümmter Flächentragwerke" (in German),
Werner-Verlag, Düsseldorf

Krenzke, M. and Kierman, T.J. (1963): "Elastic Stability of Near-Perfect Shallow Spherical Shells",
AIAA Journ. 1, p. 2855-2857

Krysik, R. and Schmidt, H. (1990): "Beulversuche an längsnahtgeschweißten stählernen Kreiszylinder- und Kegelstumpfschalen im elastisch-plastischen Bereich unter Meridiandruck- und Innendruckbelastung" (in German),
Forschungsbericht 51 Univ. GH Essen, Germany

Kunieda, H. (1992): "Classical Buckling Loads of Spherical Shell under Uniform Pressure",
Journ. of Eng. Mech. 118, p. 1513-1525

Lacher, G. and Haspel, H. (1980): "Baustellenmaßnahmen zur Erzielung der Maßhaltigkeit bei einem großen Zementklinkersilo" (in German),
Der Stahlbau, Berlin, p. 65-69

Leggett, D.M.A. and Jones, R.P.N. (1942): "The Behaviour of Cylindrical Shells under Axial Loading when the Buckling Load has Been Exceeded",
ARC Rep. and Memorandum no. 2190

Loo, T.T. (1954): "Effects of Large Deflections and Imperfections on the Elastic Buckling of Cylinders under Torsion and Axial Compression",
Proceedings of the 2nd US Congress of Applied Mechanics, Lansing MI. p. 345-346

Lorenz, Z. (1908): "Achsensymetrische Verzerrung in dünnwandigen Hohlzylindern" (in German),
Z. ver. deut. Ing. 52, p. 1766-1793

Lundquist, E. (1933): "Strength Test of Thin-Walled Duralumin Cylinders in Compression",
NACA Tech. Note, No. 523

Marguerre, K. (1938): "Zur Theorie der gekrümmten Platte großer Formänderung",
Proc. 5th Int. Congr. of Applied Mechanics, Cambridge MA, p.93-101

Mark, J., Holst F.G. and Calladine C.R. (1999): "Imperfections in Cylindrical Shells Resulting from Fabrication Misfits",
Journ. of Eng. Mech 4. vol. 125, p. 410-418

Michielsen, H.F. (1948): "The Behaviour of Thin Cylindrical Shells after Buckling under Axial Pressure",
Journ. Aero Sci, No. 15 (12), p. 739-744

Mises, von , R. (1923): "Über die Stabilitätsprobleme der Elastitzitätstheorie" (in German),
Z. angew. Mathe. Mech. 3, p. 406

Moss, M (1990): "Light Measurement – for More Accurate Tank Calibration",
Pet. Rev. (April), p. 174-178

MSC.Marc User's Guide (2000), Version 2000, MSC.Software Corporation
http:// www.marc.com

Narasimhan, K.Y. and Hoff, N.J. (1971): "Snapping of Imperfect Thin-Walled Circular Cylindrical Shells of Finite Length",
Journ. Applied Sc., No. 38(1), p. 162-171

Neut, van der, A. (1932): "The Elastic Stability of the Thin-Walled Sphere",
thesis, Delf, The Netherlands

Pian, T.H.H. (1964): "Derivation of Element Stiffness Matrices by Assumed Stress – distribution",
AIAA Journ., No. 2, p. 1333-1336

Papo, H. and Shmutter, B. (1978): "Tank Calibration by Stereophotogrammetry",
Photogrammetria 34, p. 101-109

Pflüger, A. (1981): "Elementare Schalenstatik" (in German),
5. Aufl., Springer-Verlag, Berlin

Pircher, M. and Bridge, R. (2001): "The Influence of Circumferential Weld-Induced Imperfections on the Buckling of Silos and Tanks",
Journ. of Constructional Steel Research, Vol. 57, p.569-580

Rammerstorfer, F.G. and Skrna-Jakl, I. (1991): "The Influence of Welding Stresses and Distortions on the Stability of Shells of Revolution",
in Mechanical Effects of Welding, IUTAM Symposium, Luleaa, Schweden, p. 239-259

Reisner, E. (1950): "On Axisymmetrical Deformations of Thin Shells of Revolution",
Proceedings of Symposia in Applied Mathematics
*(McGraw-Hill Book, New York), Vol. 3*p. 27-52

Robertson, A. (1929): "The Strength of Tubular Structures",
ARC Report and Memorandum No. 1185

Rotter, M.J. and Teng, J.G. (1989): "Elastic Stability of Cylindrical Shells with Weld Depressions",
Journ. of Struc. Eng. 115. No 5, p. 1244-1263

Schmidt, H. and Stracke, M (1986): "Belastungs- und Beulversuche an axialsymmetrisch belasteten Rotationsschalen aus Metall im elastisch plastischen Bereich zur Überprüfung nichtlinearer Rechenprogramme" (in German),
Forschungsbericht 38, Univ. GH Essen, Germany

Singer, J. (1982): " The Status of Experimental Buckling Investigations of Shells",
Buckling of Shells, Springer Verlag, Berlin, p. 501-534

Speicher, G. and Saal, H. (1991): "Numerical Calculation of Limit Loads for Shells of Revolution with Particular Regard to the Applying Equivalent Initial Imperfection",
Buckling of Shell Structures, on Land, in the Sea and in the Air.
Elsevier Appl. Sci. London, p. 466-475

Shmutter, B. and Ethrog, U. (1971): "Calibration of Storage Tanks",
Photogrammetric Engrg. 37, p. 261-266

Tillman, S.C. (1970): "On the Buckling Behaviour of Shallow Spherical Caps Under Uniform Pressure",
Int. Journ. of Solids and Structures, Vol. 6 (1), p.37-52

Thurston, G.A. (1961): "A Numerical Solution of the Nonlinear Equations for Axisymmetric Bending of Shallow Spherical Shells",
Journ. of Appl. Mech. 28, p. 557-568

Thurston, G.A. and Penning, F.A. (1966): "Effect of Axisymmetric Imperfections on the Buckling of Spherical Caps under Uniform Pressure",
AIAA Journ. 4 p. 319-327

Timoshenko, S.P. (1953): "History of Strength of Materials",
McGraw-Hill. New York

Truesdell, C. (1977): "First Course in Rational Continuum Mechanics – Vol. I",
Academic Press, New York

Tsien, H.S. (1941): "Theory of Buckling of Thin Shells",
Journ. of Aeronautic Sci. 9, p. 373-384

Tvergaard, V. (1976): "Buckling Behaviour of Plate and Shell Structures"
Theoretical and Applied Mechanics, ed. W.T. Koiter, Holland. p. 233-247

Vlasov, V. (1944): "Basic Differential Equations in General Theory of Elastic Shells" (English translation),
NACA Tech. Memorandum, No. 1241,NACA Washington (1951)

Washizu, K. (1982): "Variational Methods in Elasticity and Plasticity",
3rd edition, Pergamon Press

Weinitschke, H.J. (1965): "On Asymmetric Buckling of Shallow Spherical Shells",
Journ. Math. Phy. 44, p. 141-163

Wlassow, W. (1958): "Allgemeine Schalentheorie und ihre Anwendung in der Technik" (in German),
Akademi-Verlag, Berlin

Yoshimura, Y (1955): "On the Mechanism of Buckling of a Circular Cylindrical Shell under Axial Loading",
NACA TM No. 1390

Zienkiewicz, O.C. and Taylor, R.L. (1991): "The Finite Element Method: Basic Formulation and Linear Problems",
Vol. II, McGraw-Hill, London

Zingoni, A. (1997): "Shell Structures in Civil and Mechanical Engineering",
Thomas Telford, London

Zoelly, R. (1915): "Über ein Knickproblem an Kugelschale" (in German),
Thesis Zürich, Switzerland

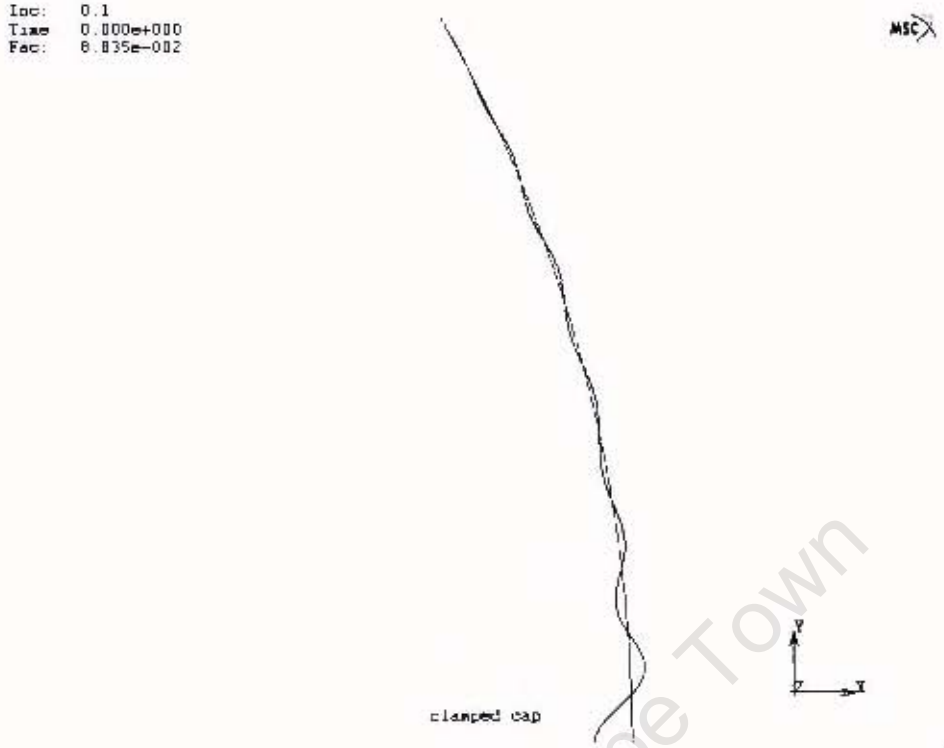

Figure 1: clamped cap, eigenmode 1, critical pressure 0.08835 N/mm²

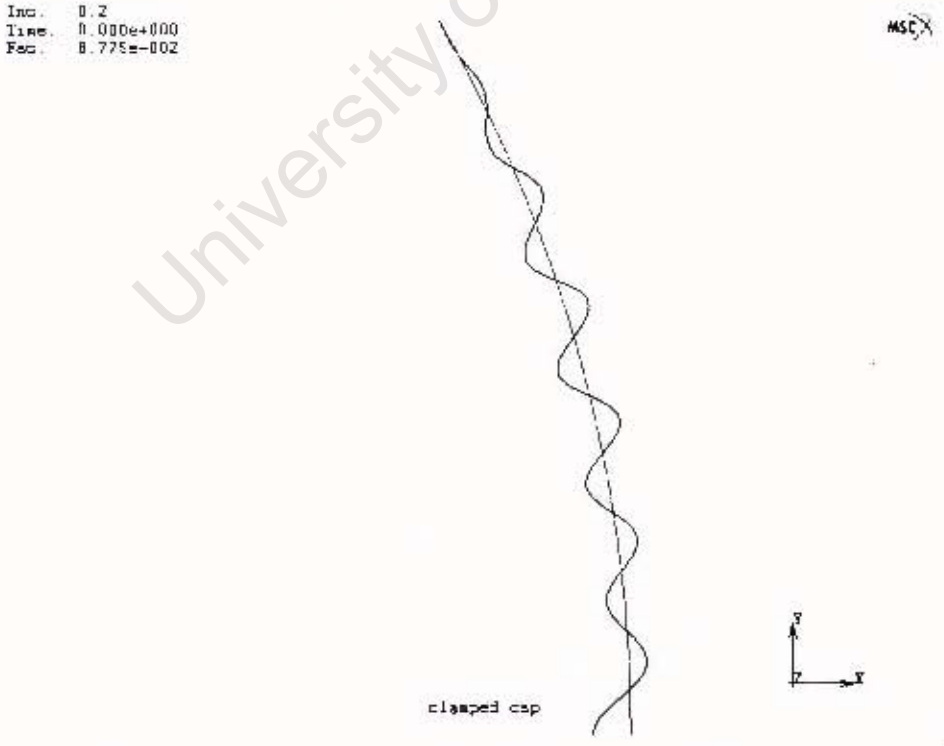

Figure 2: clamped cap, eigenmode 2, critical pressure 0.08775 N/mm²

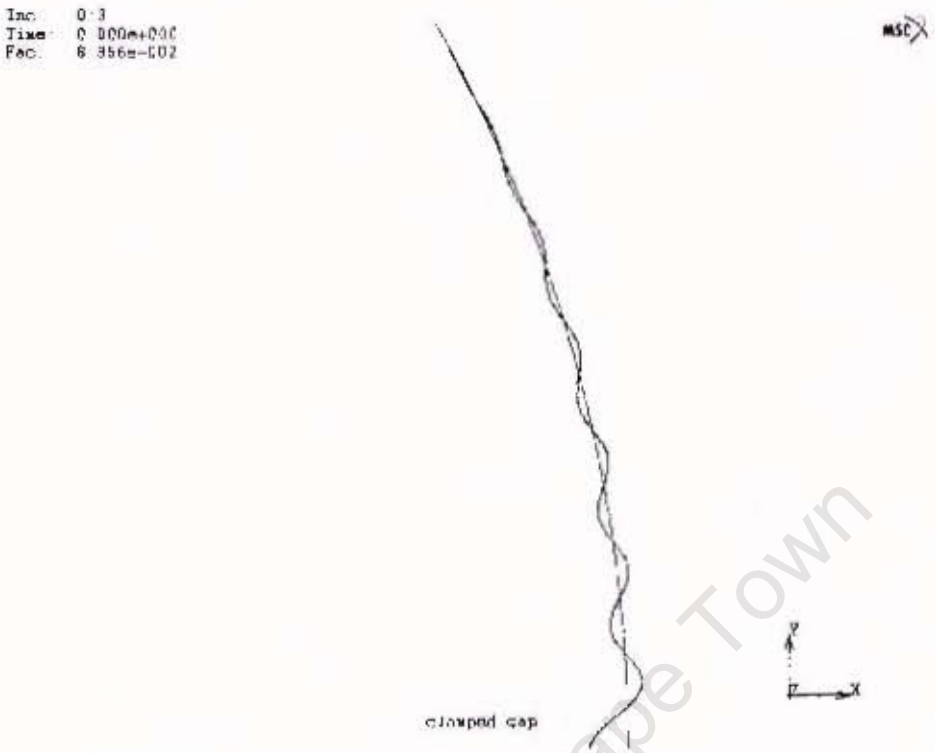

Figure 3: clamped cap, eigenmode 3, critical pressure 0.08856 N/mm²

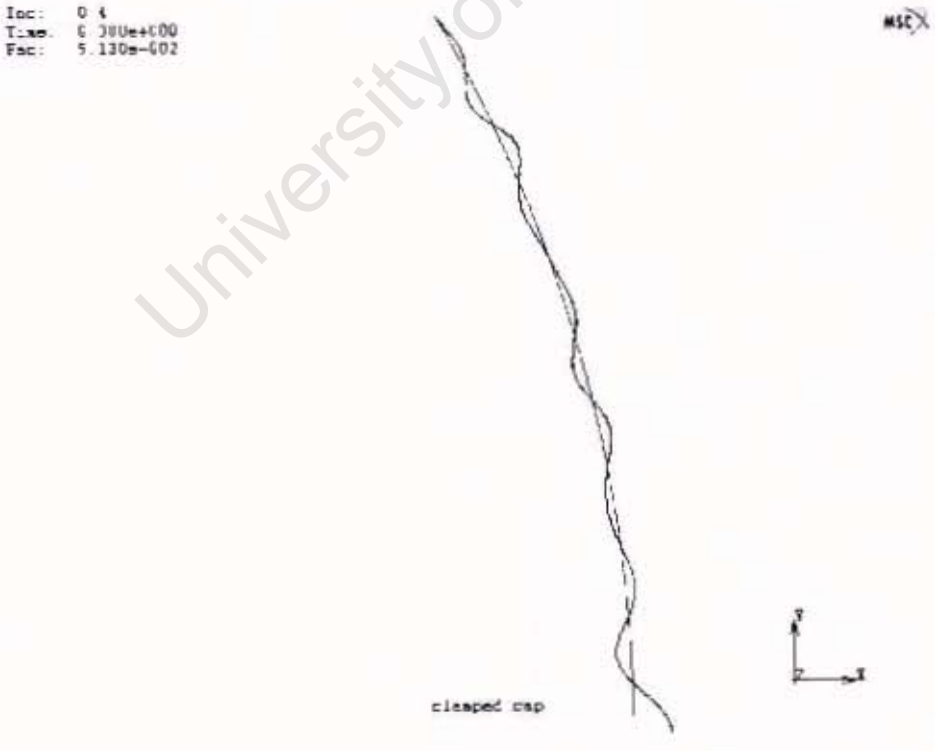

Figure 4: clamped cap, eigenmode 4, critical pressure 0.09130 N/mm²

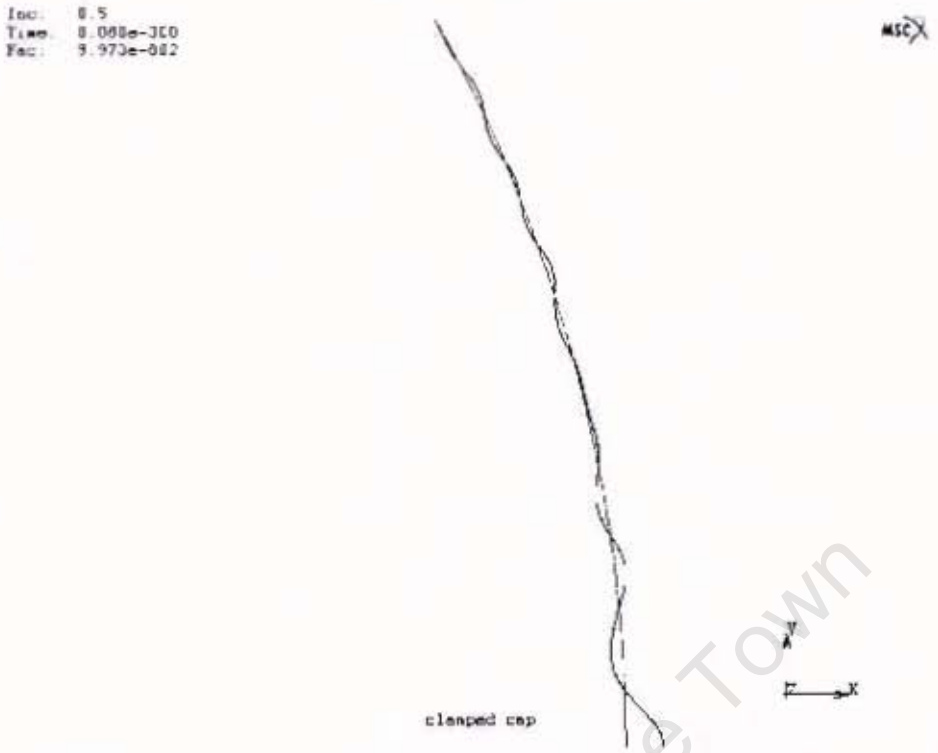

Figure 5: clamped cap, eigenmode 5, critical pressure 0.09970 N/mm²

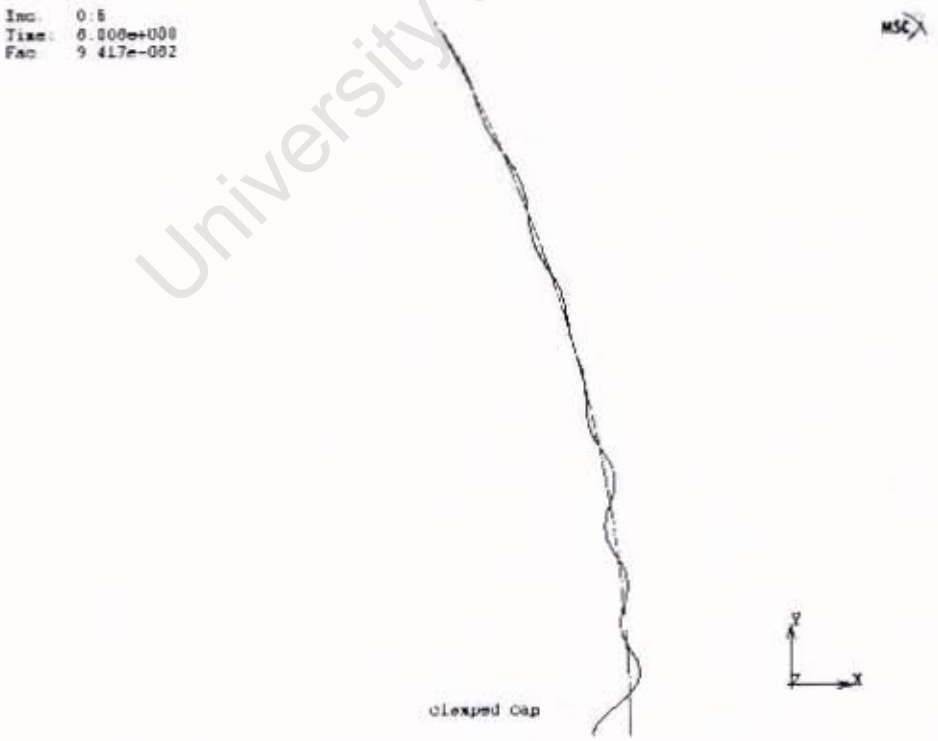

Figure 6: clamped cap, eigenmode 6, critical pressure 0.09417N/mm²

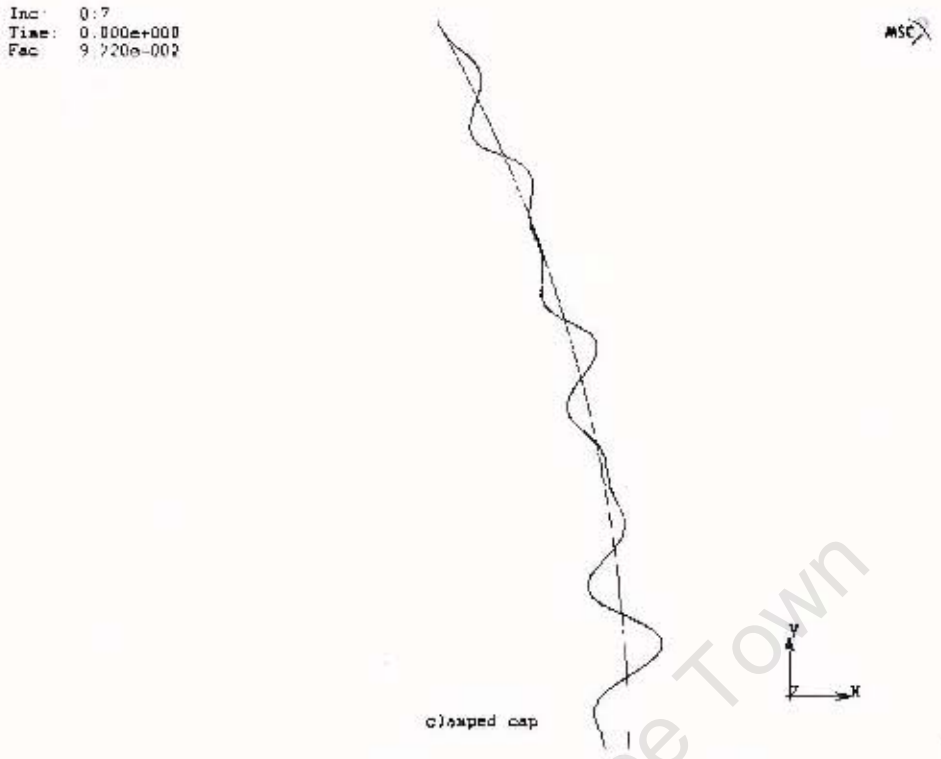

Figure 7: clamped cap, eigenmode 7, critical pressure 0.09720 N/mm²

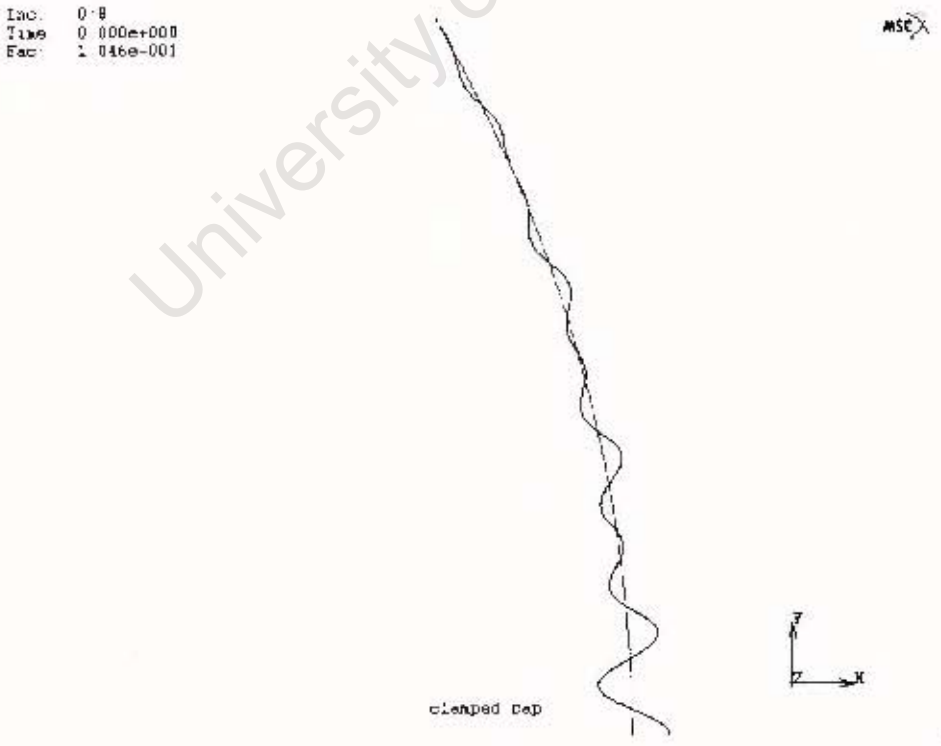

Figure 8: clamped cap, eigenmode 8, critical pressure 0.1046N/mm²

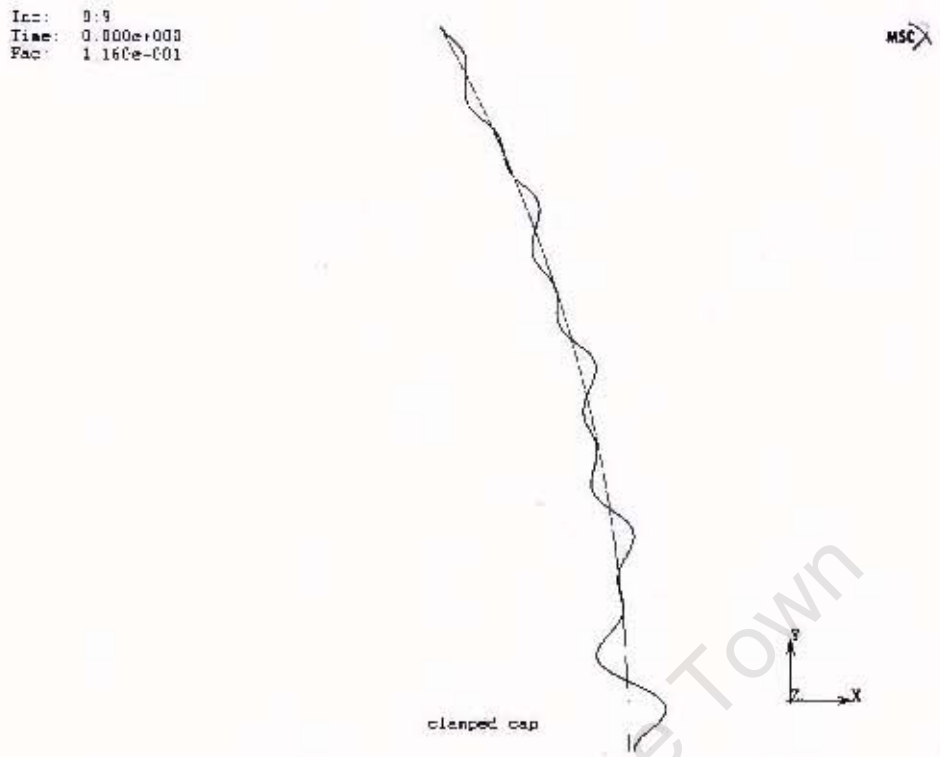

Figure 9: clamped cap, eigenmode 9, critical pressure 0.1160 N/mm²

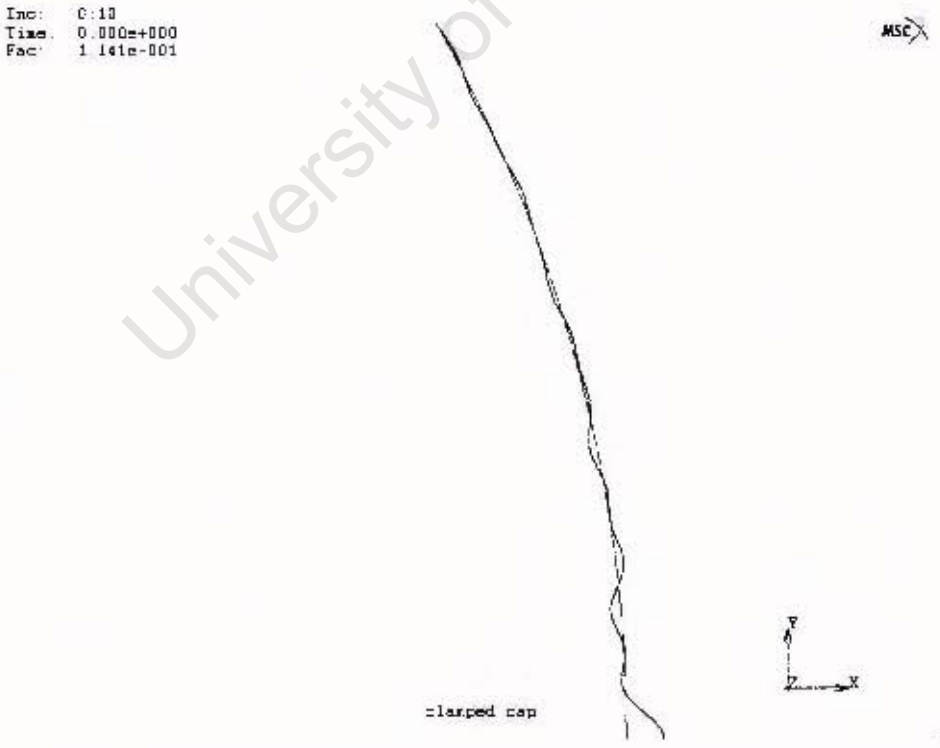

Figure 10: clamped cap, eigenmode 10, critical pressure 0.1141 N/mm²

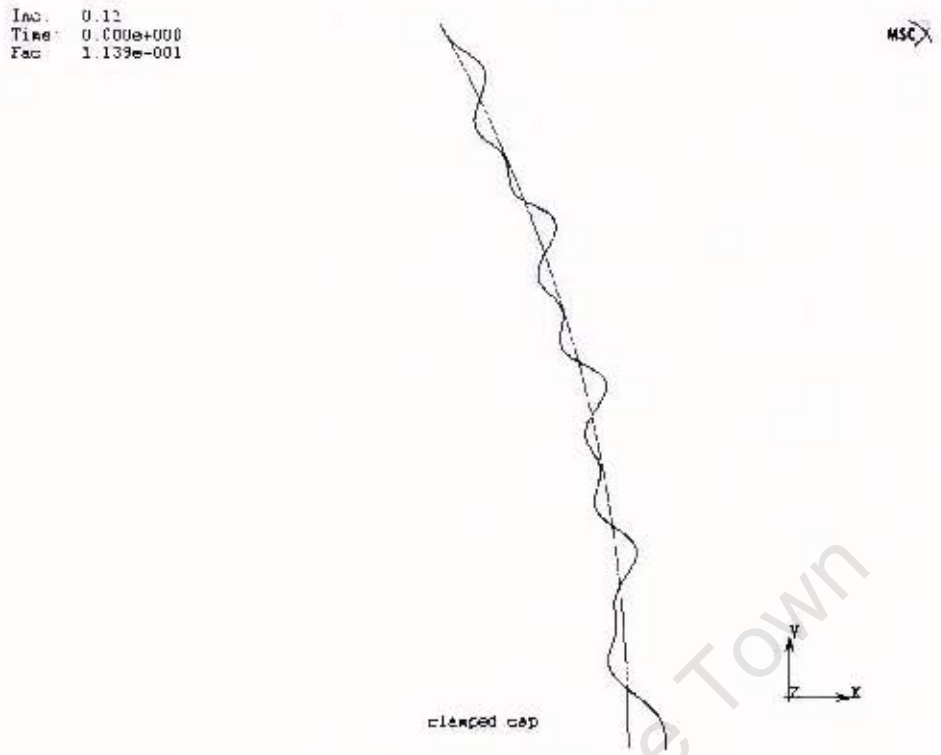

Figure 11: clamped cap, eigenmode 11, critical pressure 0.1139 N/mm²

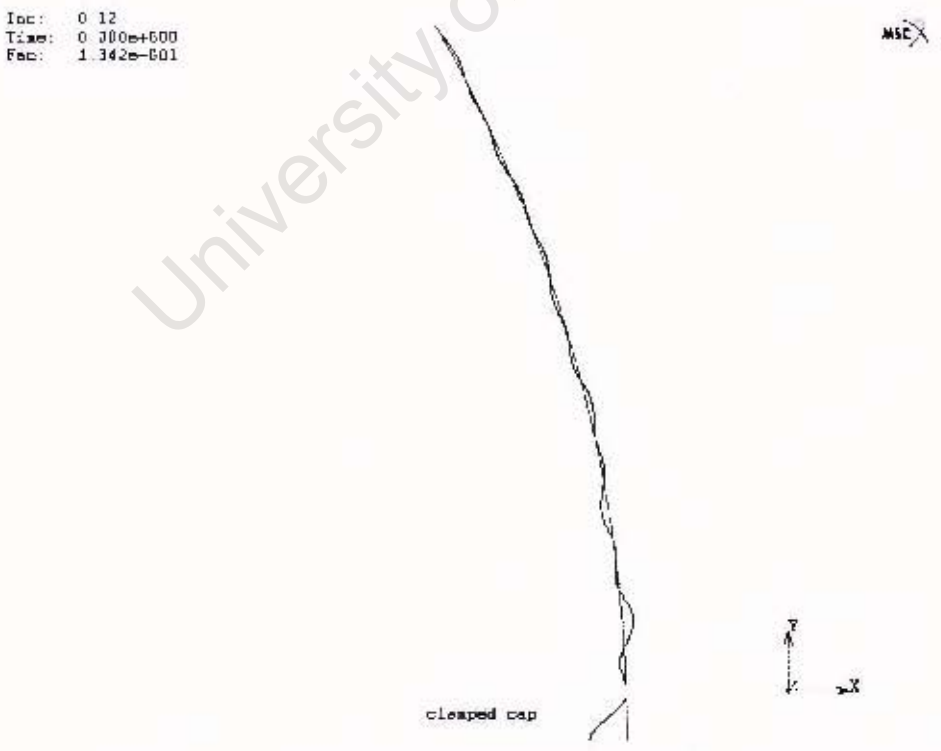

Figure 12: clamped cap, eigenmode 12, critical pressure 0.1342 N/mm²

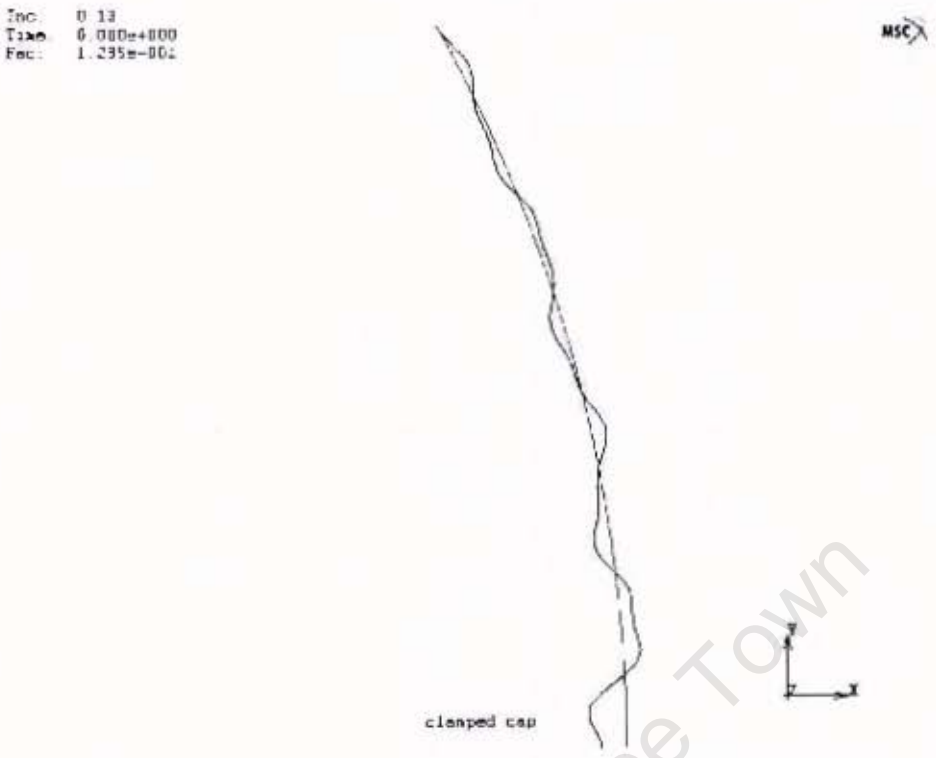

Figure 13: clamped cap, eigenmode 13, critical pressure 0.1285 N/mm²

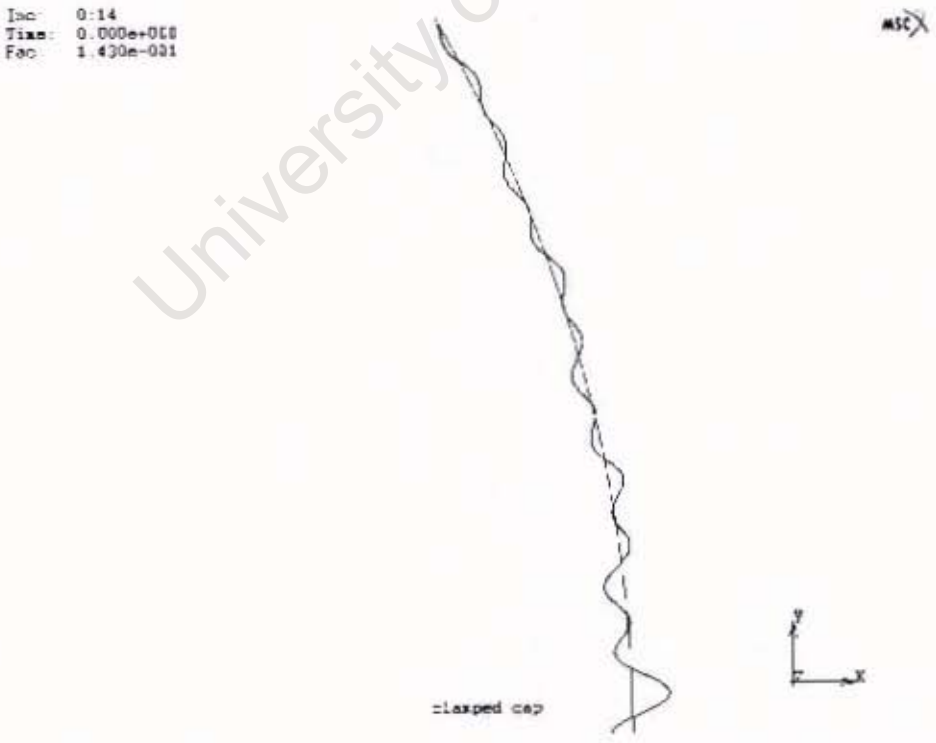

Figure 14: clamped cap, eigenmode 14, critical pressure 0.1430 N/mm²

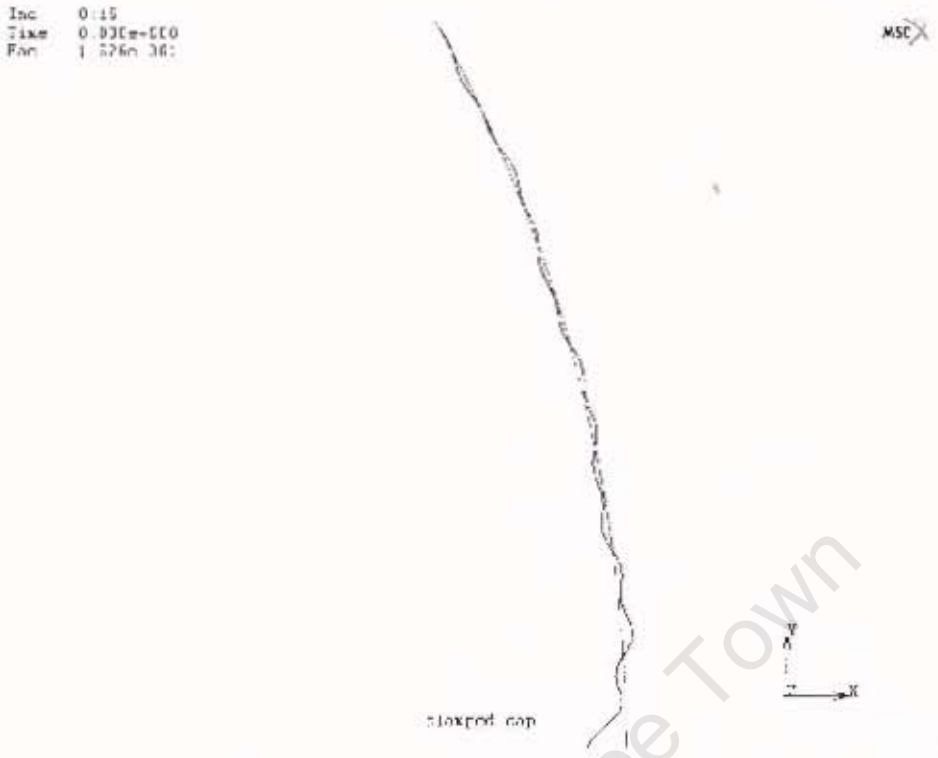

Figure 15: clamped cap, eigenmode 15, critical pressure 0.1526 N/mm²

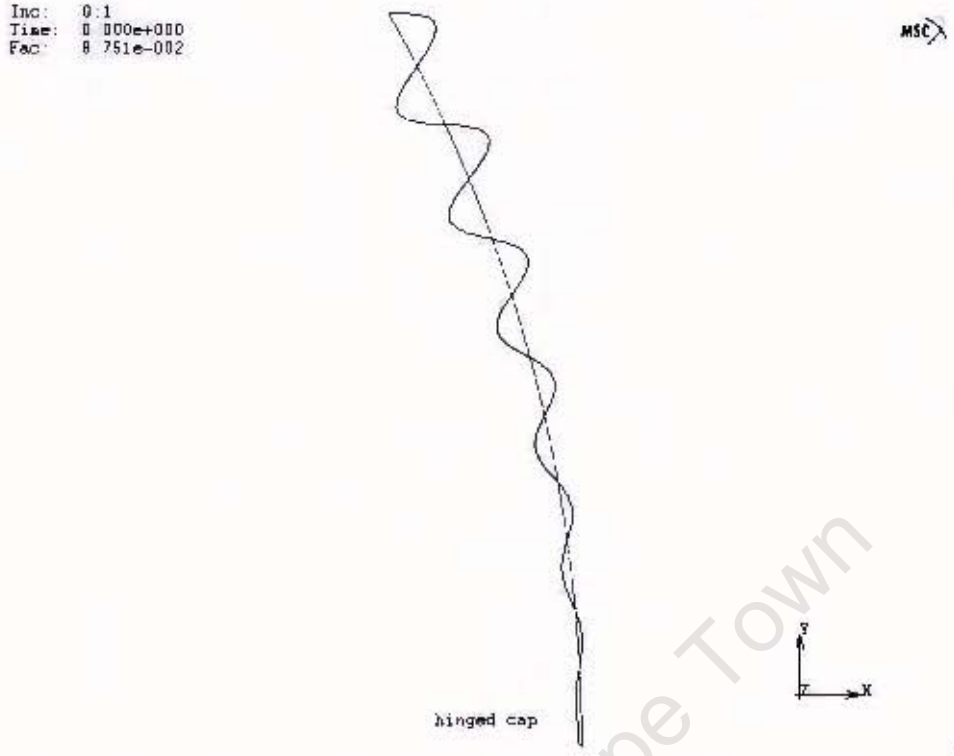

Figure 1: hinged cap, eigenmode 1, critical pressure 0.08751 N/mm²

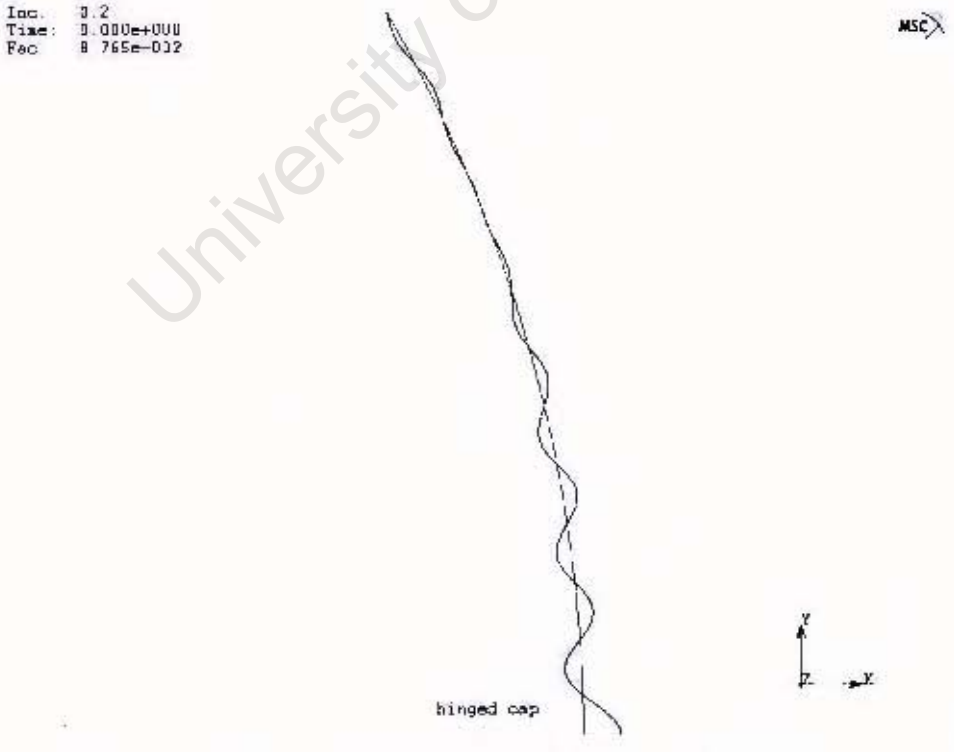

Figure 2: hinged cap, eigenmode 2, critical pressure 0.08765 N/mm²

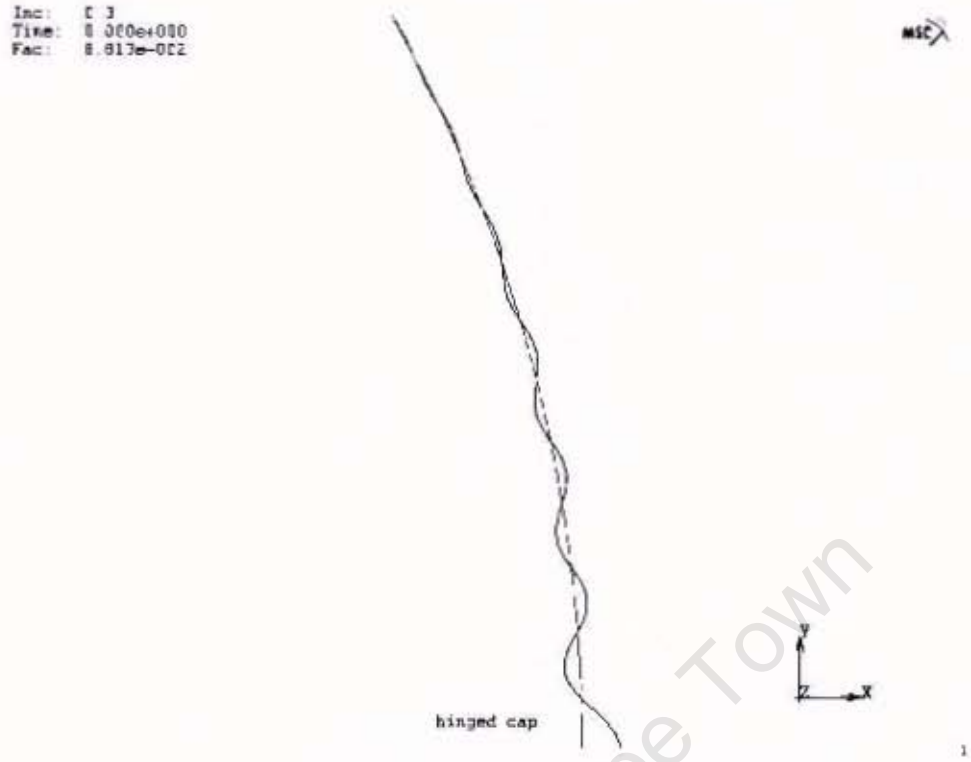

Figure 3: hinged cap, eigenmode 3, critical pressure 0.08813 N/mm²

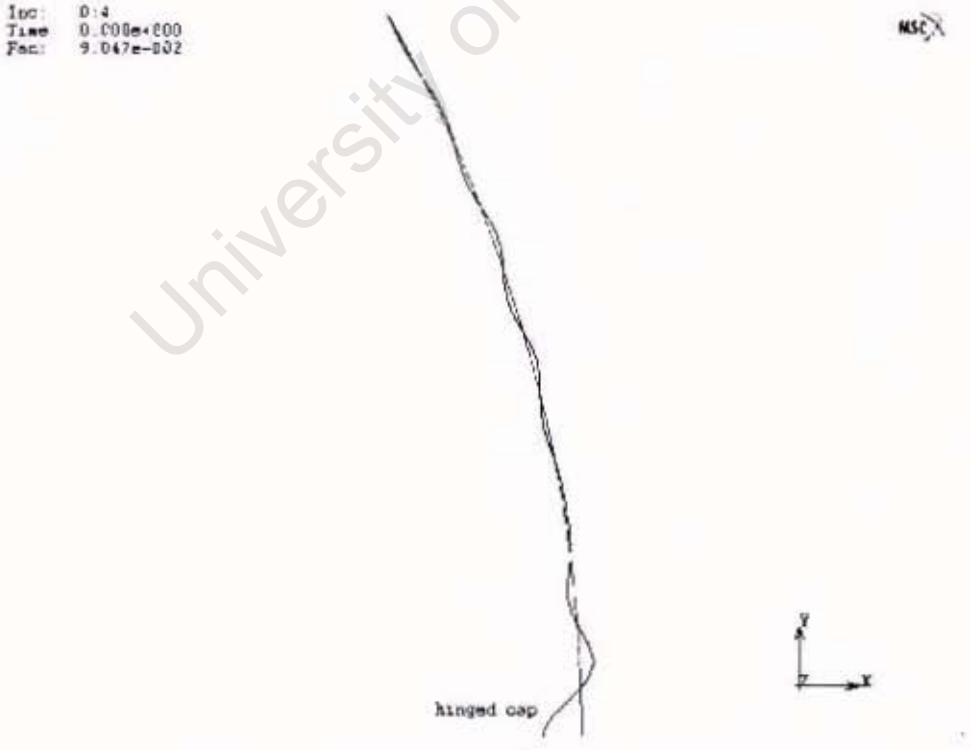

Figure 4: hinged cap, eigenmode 4, critical pressure 0.09047 N/mm²

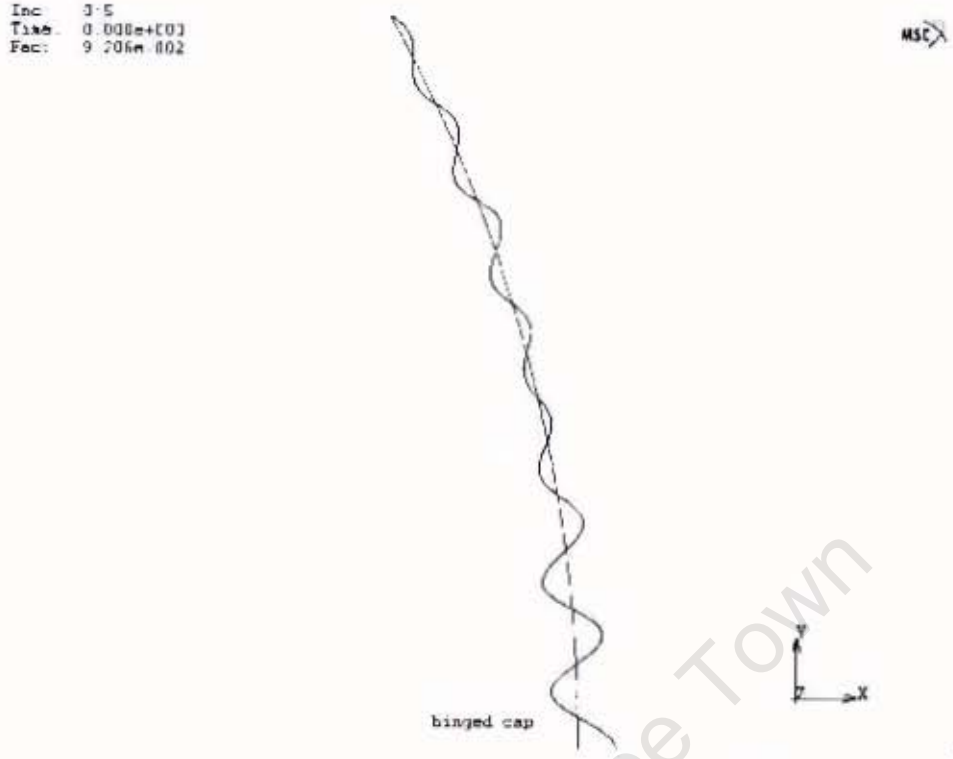

Figure 5: hinged cap, eigenmode 5, critical pressure 0.09206 N/mm²

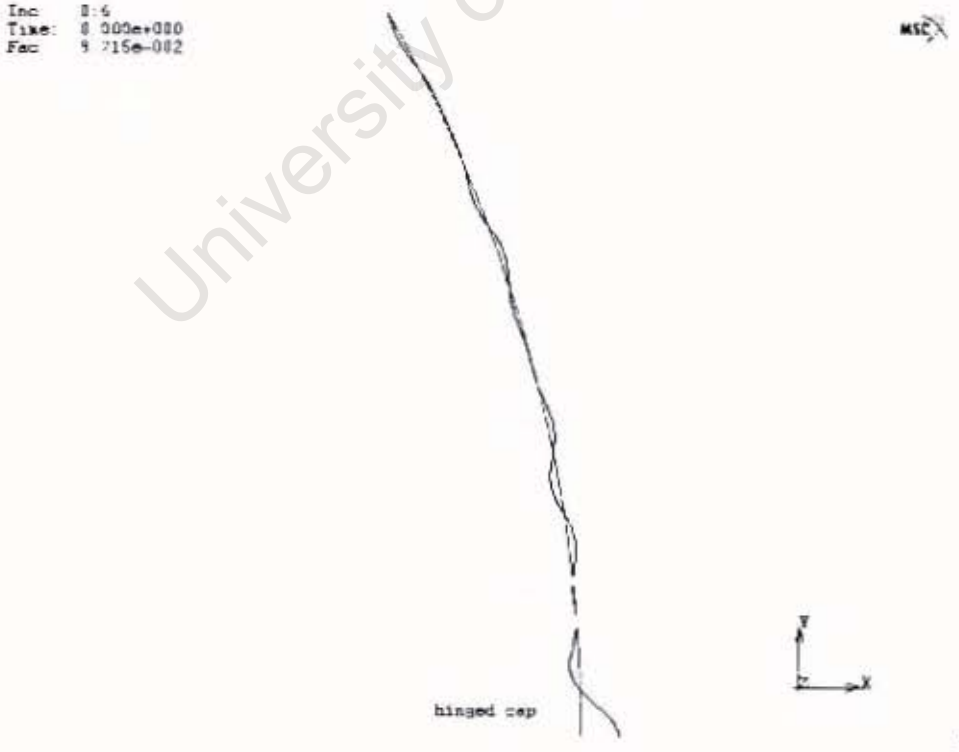

Figure 6: hinged cap, eigenmode 6, critical pressure 0.09715 N/mm²

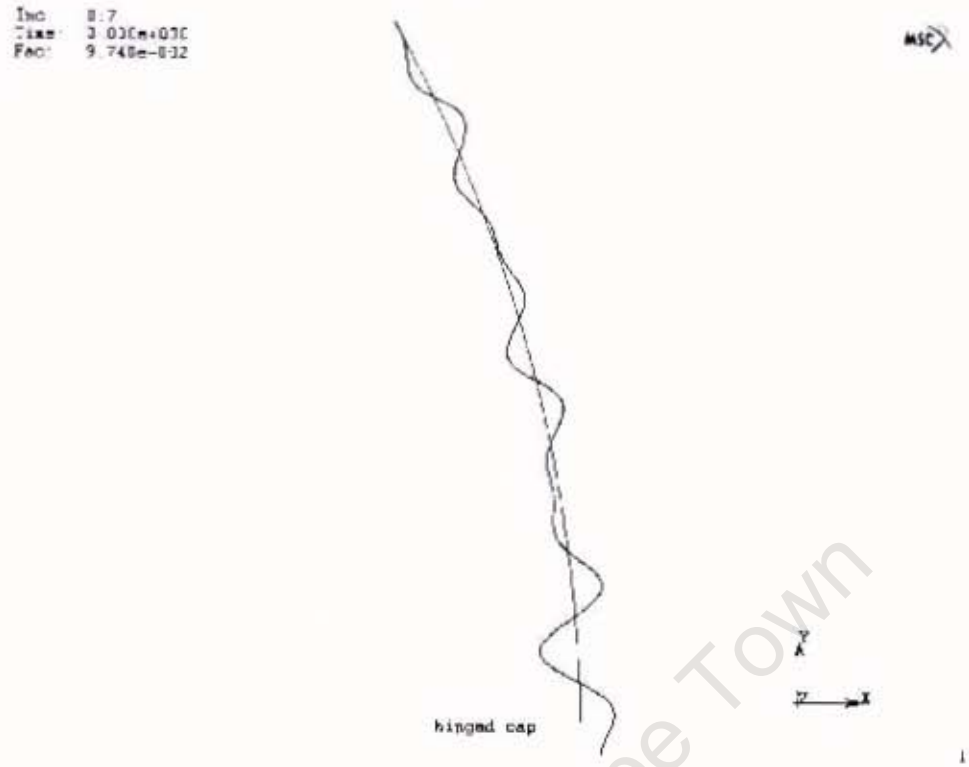

Figure 7: hinged cap, eigenmode 7, critical pressure 0.09740 N/mm²

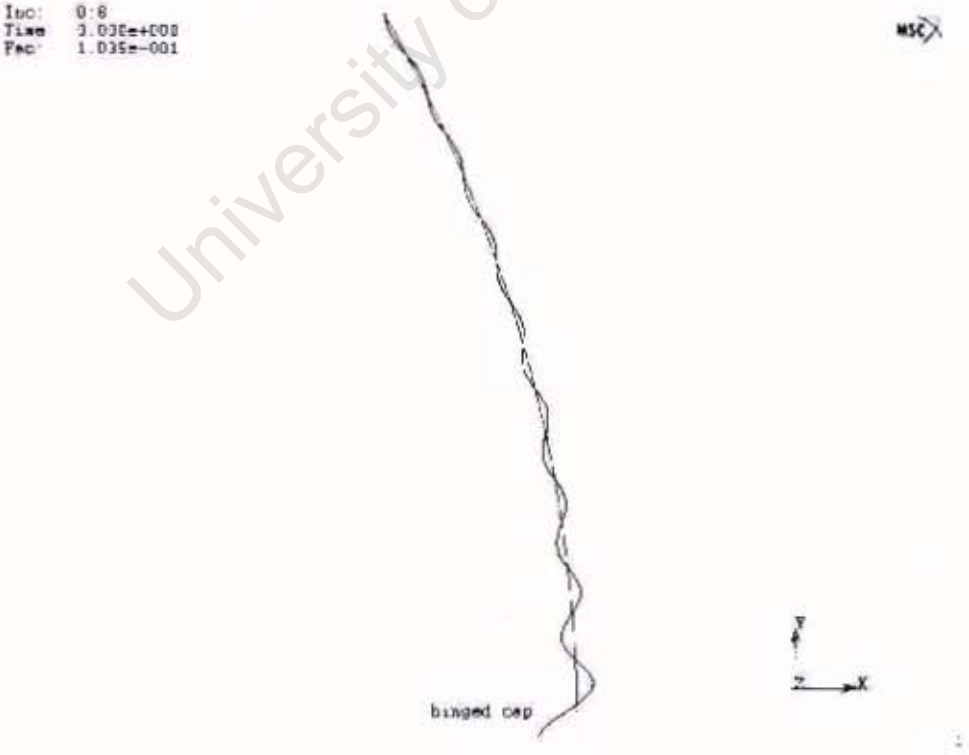

Figure 8: hinged cap, eigenmode 8, critical pressure 0.1035 N/mm²

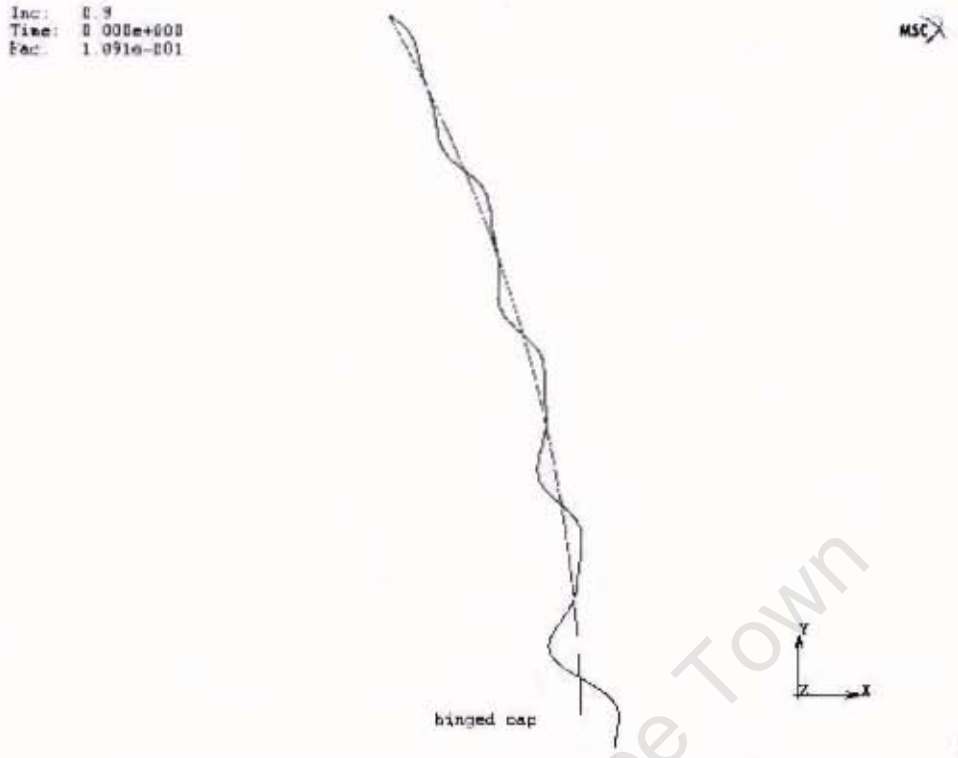

Figure 9: hinged cap, eigenmode 9, critical pressure 0.1091 N/mm²

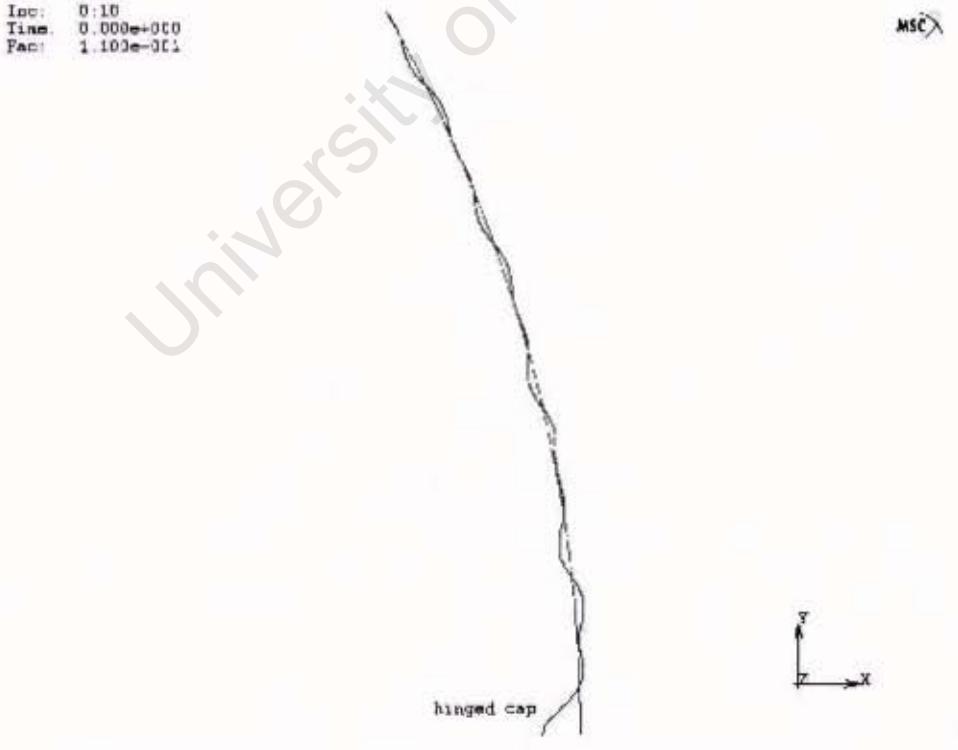

Figure 10: hinged cap, eigenmode 10, critical pressure 0.1100 N/mm²

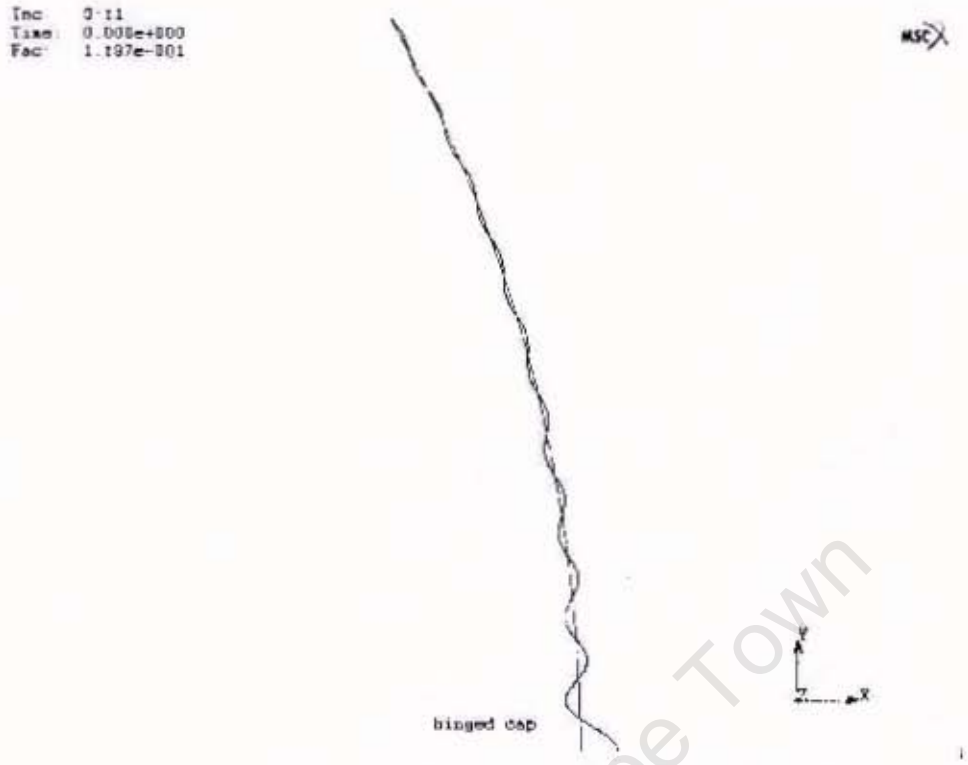

Figure 11: hinged cap, eigenmode 11, critical pressure 0.1187 N/mm²

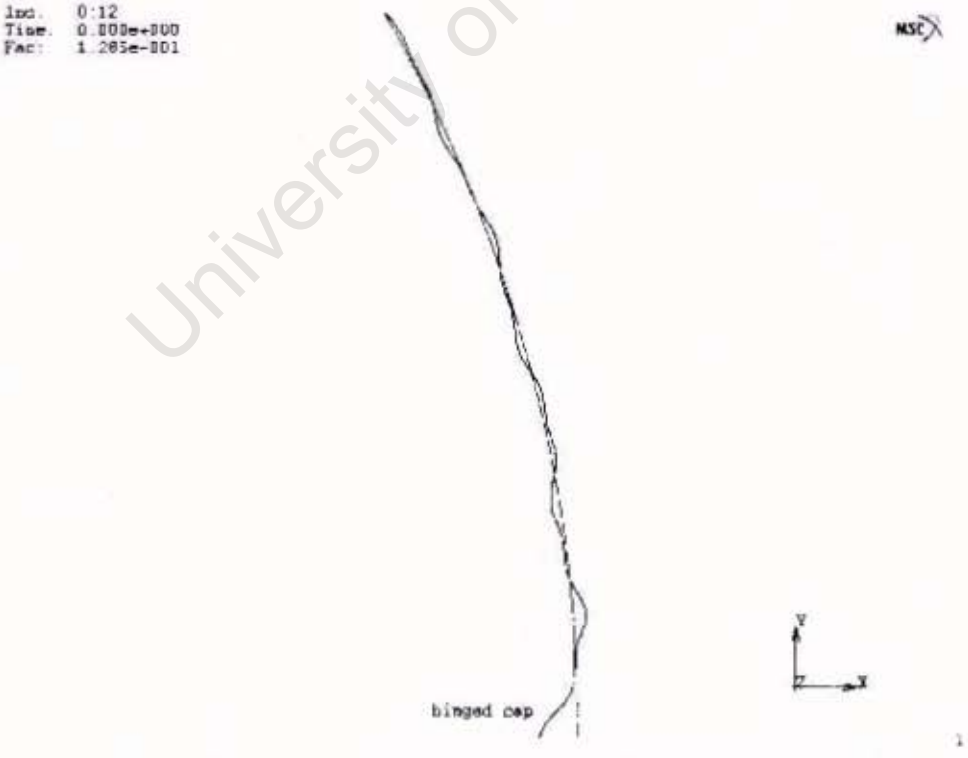

Figure 12: hinged cap, eigenmode 12, critical pressure 0.1285 N/mm²

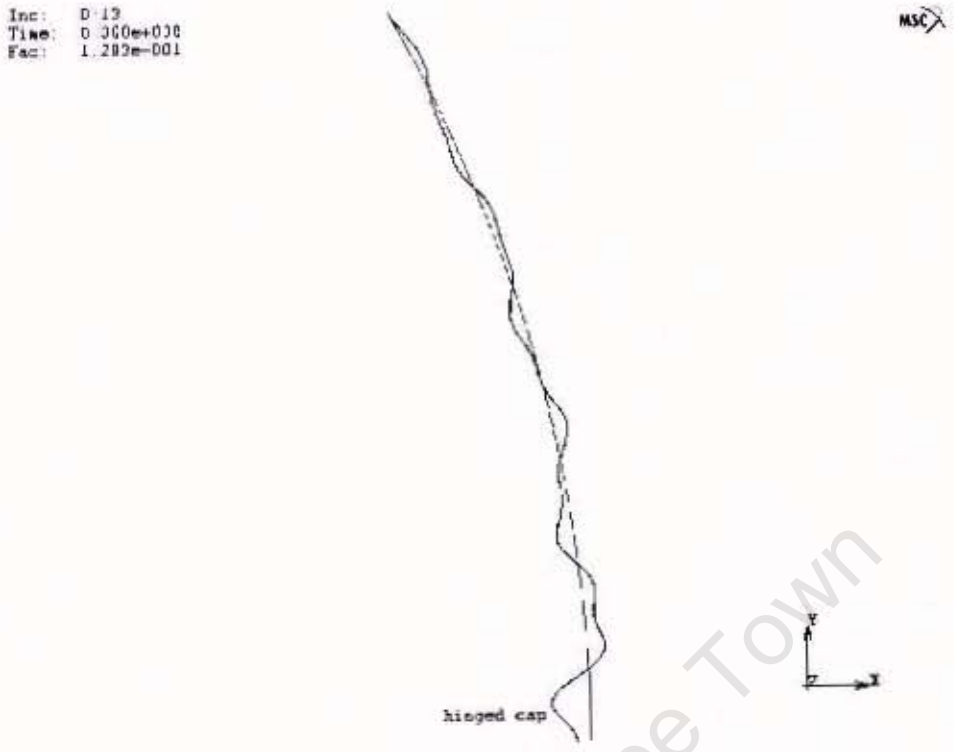

Figure 13: hinged cap, eigenmode 13, critical pressure 0.1283 N/mm²

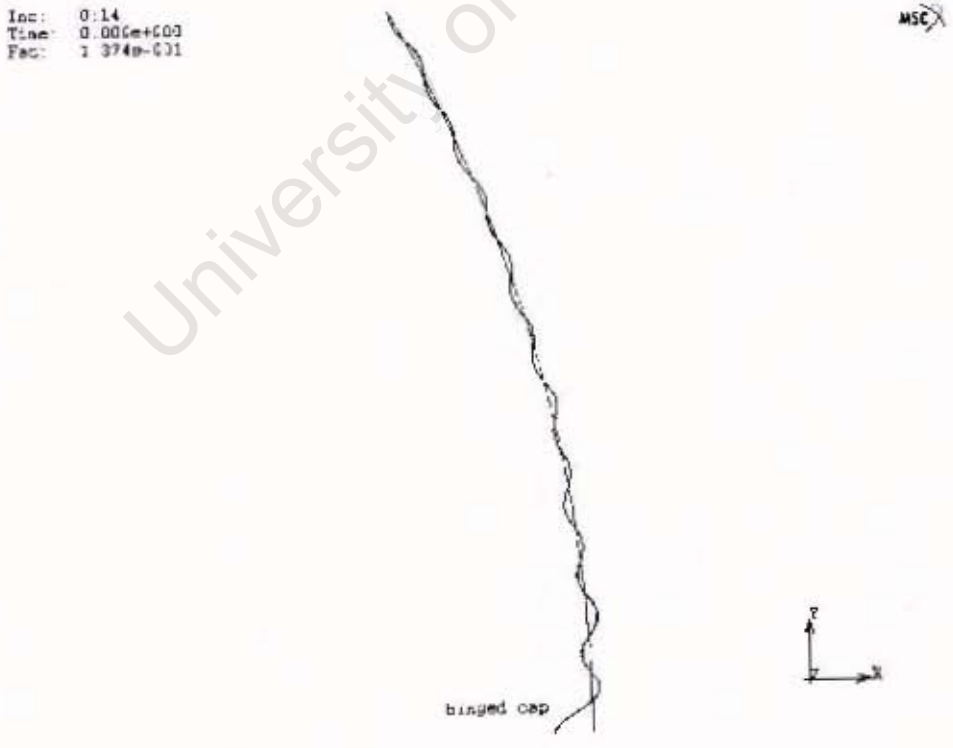

Figure 14: hinged cap, eigenmode 14, critical pressure 0.1374 N/mm²

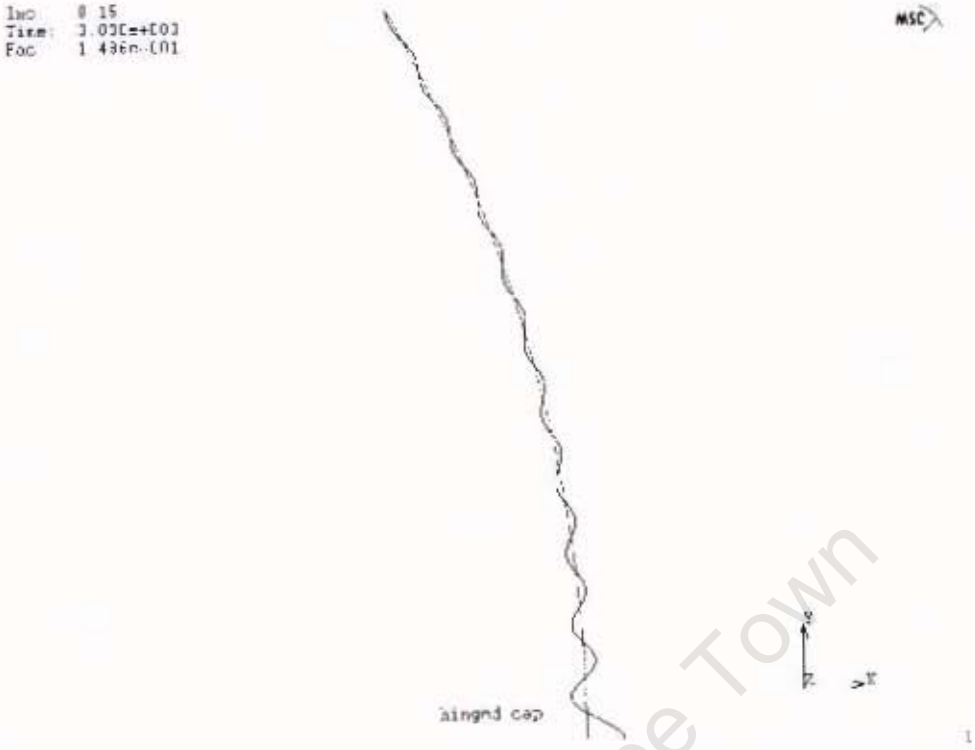

Figure 15: hinged cap, eigenmode 15, critical pressure 0.1486 N/mm²